Transverse-Plane Ankle Rotation for Lower-Limb Amputees Using Two Novel Prostheses

Nathan M. Olson

A dissertation
submitted in partial fulfillment of the
requirements for the degree of

Doctor of Philosophy

University of Washington

2016

Reading Committee:

Glenn Klute, Chair

Santosh Devasia

Vipin Kumar

Katherine Steele

Program Authorized to Offer Degree:
Mechanical Engineering

University of Washington

Abstract

Transverse-Plane Ankle Rotation for Lower-Limb Amputees Using Two Novel Prostheses

Nathan M. Olson

Chair of the Supervisory Committee:
Dr. Glenn Klute
Mechanical Engineering

Lower-limb amputees often suffer from pain and discomfort caused by prosthesis use. Problems include musculoskeletal issues caused by compensatory gait patterns and skin injuries caused by shear stress at the interface between the residual limb and the socket. Torsion adapters have been shown to relieve these skin problems, but are not commonly prescribed due to a perceived decrease in stability. This study describes the Torsionally Active Prosthesis (TAP), a novel prosthesis that aims to provide the same reduction in shear stress as a torsion adapter without the accompanying decrease in stability. The work consists of four parts. First, a powered prosthesis capable of general motion in the transverse plane was developed. Second, exploratory human subject testing was performed to identify a pattern of motion that reduces transverse-plane torque at the socket without reducing torsional stiffness. The results indicate that this can be achieved by coupling transverse-plane ankle rotation with sagittal-plane ankle rotation. Third, the powered prosthesis was configured to perform this axis coupling and human subject testing was performed to determine its efficacy. Three subjects wore the prosthesis and walked at their self-selected speed in straight lines and clockwise and counterclockwise circles with at least three levels of axis coupling, including zero coupling. The subjects showed a trend toward decreased socket torque with increased axis coupling. Finally, the Pivot-Flex Foot (PFF), an unpowered prosthesis that could provide axis coupling was designed, built, and bench-tested. The PFF demonstrated

a linear coupling between transverse-plane ankle rotation and sagittal-plane ankle rotation during bench testing.

TABLE OF CONTENTS

LIST OF FIGURES

LIST OF TABLES

ACKNOWLEDGMENTS

I would like to thank my advisor, Glenn, who got me started and provided just the right amount of management. Thanks to Vipin Kumar for providing my first UW home in the Microcellular Plastics Lab, and letting me keep my space even when I was working on prosthetic legs. Andrei and Huimin made the Microcellular Plastics Lab a welcoming environment and spent many hours discussing ideas with me. Jonathan, Jonethan, Corey, and Kyle helped me develop ideas and refine my presentations. Special thanks to Luck who set up the electronics station at the VA and got me started with PIC programming.

I built several devices for this research, and it wouldn't have been possible without assistance from the ME staff. Bill helped me with strain gauges and loaned me an oscilloscope on a semi-permanent basis. Eamon and Reggie helped me release parts from the blocks of metal they were trapped inside of. Michelle helped me with the composite parts.

At the VA, I couldn't have performed my bench tests or human subject tests without help from the staff. Jan recruited subjects for me. Ava helped develop and run tests and assisted with link model development. Rose and Krista helped run tests and process motion-capture data. Matt ran the RGS for me.

I would like to thank my family for their love in support. Jolina in particular has been a constant companion and friend and has brightened my days.

This research was funded by the Department of Veterans Affairs, Rehabilitation Research and Development Service (grants I21 RX001933, A9243C, and A9248-S).

DEDICATION

To my grandparents.

Chapter 1

INTRODUCTION

1.1 Importance of Transverse Plane Rotation

In a study of 78 long-term lower-limb prosthesis users with trauma-related amputations, only 43% reported being satisfied with their prostheses [18]. Twenty-four percent reported wounds or skin irritation caused by the prosthesis. In a survey of 935 amputees, nearly one third expressed dissatisfaction with prosthesis comfort and 24.3% expressed overall dissatisfaction with their prostheses [67]. In a survey of 255 lower-limb amputees, 74% reported residual limb pain, and 33% of those described it as severely bothersome [22]. In a survey of 97 transfemoral amputees, 62% reported sores or skin irritation from the socket, 51% reported residual limb pain, and 46% reported pain in the intact leg [34]. Amputees ranked the avoidance of blisters or sores on the residual limb as in issue of importance in uses and design of prostheses [48]. In a survey of 109 amputees, 57% reported experiencing moderate to severe pain most of the time while wearing a prosthesis [61].

One source of pain and discomfort is epidermoid cysts which occur where the skin of the residual limb rubs against the brim of the socket [53]. These cysts often develop over years of prosthesis use, and can become painful enough to prevent use of the prosthesis [54]. These and other skin problems are attributed to the shear stress and humidity seen by the skin of the residual limb of lower-limb prosthesis users [20, 59]. Shear stress has been shown experimentally to cause blisters [60], and is a primary cause of callosities and trophic ulcers [90]. According to Levy, the most promising approach to dealing with epidermoid cysts caused by prosthesis use is "improvement in prosthetic fit with reduction of shearing forces" [54].

A major source of shear stress on the residual limb of amputees is transverse-plane torque

[94]. Transverse-plane torque is a normal part of walking in non-amputees and increases in the inside leg of a turn [26]. Turning steps compose a large fraction of the steps of daily living [76, 29]. In non-amputees, transverse-plane torque is transmitted from the ground to the trunk through the bones and muscles of the leg. In amputees, the torque is transmitted from the prosthetic socket to the skin of the residual limb. Amputees experience less transverse-plane torque during walking than non-amputees [80, 78], due to compensatory gait patterns.

Prosthetic legs for transtibial amputees typically consist of a prosthetic foot which is connected by a rigid pylon to the socket which interfaces with the residual limb. Because rotation is not allowed between the foot and the socket, any rotation between the foot and the knee must occur at the knee or between the residual limb and the socket. Thus amputees must either adopt a compensatory gait pattern with reduced tranverse-plane rotation or accept sliding between the residual limb and the socket. To avoid these unattractive alternatives, the development of prosthetic devices to allow greater transverse-plane rotation was recommended by the 1947 report on fundamental studies of human locomotion by the University of California Prosthetic Devices Research Project [95].

1.2 Musculoskeletal Problems Associated with Prosthesis Use

In addition to skin problems at the interface between the residual limb and the socket, prosthesis users also suffer from increased rates of musculoskeletal problems such as osteoarthritis and chronic back pain compared with nonamputees. Melzer et al. found a higher rate of osteoarthritis in the intact-limb knee in a group of transtibial and transfemoral amputees than in the general population [58]. Lemaire and Fisher found higher joint forces and a higher rate of osteoarthritis in the intact-limb knee in elderly transtibial amputees [51]. In the prosthetic-side knee, Burke et al. found a lower rate of osteoarthritis in transtibial amputees than in the general population [9]. Together, these findings suggest that asymmetrical loading on the intact and prosthetic sides puts the intact limb at an increased risk of developing osteoarthritis. Improving prosthesis comfort during walking could lead to a more symmetric weight distribution and decreased risk of osteoarthritis.

Studies have found a higher prevalence of back pain in lower limb amputees (52%-71% [9, 87, 23]) and transtibial amputees (62% [46]) compared with the general population(10%-45% [68]). Together with a high prevalence of back pain, Burke et al. found a high prevalence of scoliosis (64%) in lower limb amputees, which "suggests that mechanical factors consequent on the amputation may be responsible for the back symptoms" [9]. Amputees compensate for reduced ankle power by increasing hip power on the amputated side in both straight-line walking [102, 83, 75] and turning [98].

1.3 The Role of Shank Torque in Human Walking

In straight-line gait in both transtibial amputees and non-amputees, whole-body transverse-plane angular momentum varies periodically with the gait cycle [84]. Shank torque is near zero until midstance, at which point it rises rapidly to its maximum value before falling to zero at the end of stance [78]. During this period the shank torque opposes the body's transverse-plane angular momentum, and thus serves as a brake to keep the body from over-rotating.

During circular walking, the center of mass is shifted toward the inside of the circle [64]. This changes the moment arm of the propulsive forces about the center of mass. Compared with straight-line walking, torque is lower in the outer shank as propulsive forces opposing the body's transverse-plane angular momentum act on a longer moment arm. Conversely, torque is higher in the inner shank as propulsive forces opposing the body's transverse-plane angular momentum act on a shorter moment arm. As in straight line gait, shank torque acts as a brake on whole-body angular momentum during circular walking.

1.4 Torsion Adapters

Until now, attempts to allow greater transverse-plane rotation in prosthetic legs have used torsion adapters, which are torsional springs placed in series with the rigid pylon. An early torsion adapter, the UC-BL shank axial rotation device, was described in 1978 [47]. The design used ball bearings to support axial load and bending moments and an elastomeric

torsion spring to allow transverse-plane rotation. Modern commercially available torsion adapters also use an elastomeric centering spring, although the stiffness curves vary widely between brands and models [26]. Commercially available torsion adapters typically also contain adjustable or swappable components that provide different stiffness settings.

Several studies have investigated the effect of torsion adapters on amputee gait kinematics and kinetics. Lamoureux and Radcliffe found a large reduction in shank torque during straight walking in two transfemoral amputees wearing a torsion adapter [47]. Van der Linden found an increase in transverse-plane rotation of the socket relative to the foot in one of two transfemoral amputees [97]. Segal et al. found a reduction in transverse-plane torque in unilateral transtibial amputees during straight-line and circular walking [80]. Su et al. investigated gait kinematics in bilateral transtibial amputees and found increased transverse-plane ankle rotation with the use of a torsion adapter [92].

Throughout these gait studies, use of a torsion adapter was found to decrease the magnitudes of transverse-plane joint moments, making them less similar to the higher joint moments exhibited by non-amputees. Conversely, use of a torsion adapter was found to increase the transverse-plane rotation of leg segments, making leg kinematics more similar to non-amputee kinematics. This increased gait symmetry is one of the primary benefits cited by users of torsion adapters [71]. Use of torsion adapters has also been reported to relieve skin abrasions and epidermoid cysts [47], improve socket comfort by reducing irritation and pain [14], and reduce pain interference with daily activites [77].

Despite the reported advantages of torsion adapters, they are still not commonly prescribed. This may be because torsion adapters reduce gait stability during straight-line walking [81]. While the trend toward reduced stability found by Segal et al. was not considered statistically significant ($p = 0.09$) [81], subjective feelings of instability have been referenced by clinicians [71] as a contraindication to the prescription of torsion adapters [92].

1.5 The Human Ankle

In non-amputees, large transverse-plane rotations occur even during straight walking, which has been the focus of most kinematics studies. In an early biomechanics study, Levens et al. measured an average of 19 degrees of rotation at the lower leg during straight walking [52] and concluded that prosthetic legs should provide for transverse rotation. Flick at al. measured transverse-plane rotation of of the foot relative to the knee during straight walking and walking on a 1m-radius circle [26]. The range of motion was found to be 20 degrees for straight walking and 26 degrees on the inside of a turn. This is similar to the sagittal plane rotation seen during walking, which is also around 20 degrees [35]. Lundberg et al. measured a voluntary range of rotation of over 20 degrees in the ankle-foot complex during 30 degrees of lower-limb rotation [57]. This means that most of the transverse-plane rotation is coming from a joint which lower-limb amputees do not have.

The human ankle is a complex mechanism that does not behave like a a simple hinge [21, 107]. Instead, rotations in all three axes are allowed and coupled together [4, 38, 13]. In particular, the axis of rotation of the talo-crural joint during ankle dorsiflexion is inclined downwards and laterally relative to horizontal, and the rotation ranges from 10 to 26 degrees among individuals [56]. This rotation couples dorsiflexion with internal rotation of the shank relative to the foot, a feature which is not replicated in prosthetic feet and ankles.

1.6 The Torsionally Active Prosthesis

While ankle rotation in the transverse plane has the same order of magnitude as rotation in the sagittal plane, lower-limb prosthesis designers have primarily focused on sagittal-plane kinematics [99]. Evaluations of ankle kinematics for biomimetic ankle design have often ignored other planes of motion entirely [72, 35, 36, 86]. While some work has been done on evaluating the behavior of the human ankle in the transverse plane with an eye toward prosthesis design [30], the best design for a prosthetic ankle may not be the closest match to an intact human ankle because of the addition of the socket-residual limb interface.

In particular, powered prosthetic ankles have primarily provided motion in the sagittal plane only [1, 93, 39, 7, 11, 105]. Recently, powered prosthetic compenents have been designed which modulate motion in the coronal [65, 31] and transverse [66] planes. The transverse plane device was only capable of adjusting its torsional stiffness about a fixed equilibrium point, however. A new design is required to provide more general motion in the transverse plane.

A series elastic actuator (SEA) is an actuator with a motor and gearbox whose output is connected to the driven load with a flexible elastic element [69]. SEAs have found widespread use in prostheses [2, 33, 105], orthoses [8, 70], and robots [73, 16, 41]. SEAs have several benefits over traditional stiff actuators. The elastic element filters shock loads applied to the gearbox by the load, which decreases the strength requirement of the gearbox and improves safety during interactions with humans. Series elasticity simplifies force control by turning it into a position control problem. The elastic element also introduces the possibility of energy storage, which can reduce the power requirement of the motor and improve energy efficiency [33]. Figure 1.1 shows the schematic of an SEA.

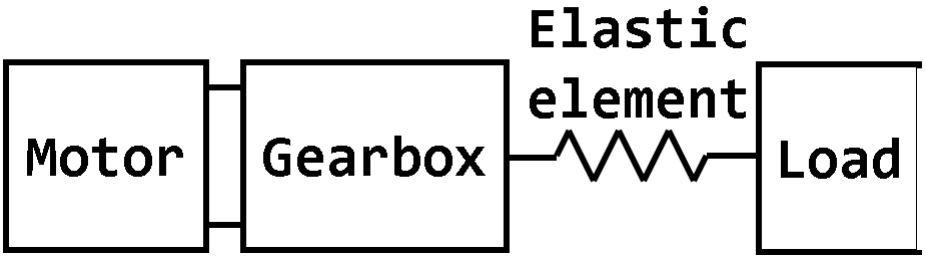

Figure 1.1: Schematic of a series elastic actuator.

A series elastic actuator is an appropriate choice for a prosthesis used to explore transverse plane motion because of its generality. The SEA is capable of providing variable stiffness as well as varying the equilibrium position. Although rotation and torque cannot be set independently, the SEA can provide any desired relationship between rotation and torque within a certain bandwidth. This includes nonlinear stiffness profiles and time-varying equilibrium

positions. In particular, the SEA allows its quasi-stiffness to be distinct from its stiffness, a property that is lacking in passive and semi-active devices [74].

In a lower-limb prosthesis, quasi-stiffness relates torque and rotation throughout the gait cycle, while stiffness describes the position-related component that stores and releases energy. Socket torque can be reduced by reducing the quasi-stiffness of the prosthetic leg. Torsion adapters do this by reducing the stiffness of the prosthetic leg. The stiffness reduction is often accompanied by feeling of instability by the user of the prosthesis [92]. This study investigates whether a prosthesis that reduces the torsional quasi-stiffness without reducing the stiffness can provide the benefits of a torsion adapter and mitigate its disadvantages.

A series elastic actuator with rotation in the transverse plane has been designed to enable this investigation. The device is called the Torsionally Active Prosthesis (TAP). Preliminary human subject tests used an iterative controller to reduce the peak transverse-plane torque during gait. The results suggest that torque reduction can be achieved by a linear coupling between ankle sagittal-plane rotation and transverse-plane rotation. This relationship would be obtainable using a purely passive design, which would increase the chances of its widespread use.

While this study investigates coupling between ankle sagittal-plane rotation and transverse-plane rotation, the TAP could be used for other transverse-plane investigations. For example, it could be configured to act as a torsion adapter with variable stiffness and/or damping. It could also be used to explore different behavior in different conditions, such as standing vs. walking. Or, as one subject suggested, its 360°rotation capability could be used to enable some wicked dance moves.

This dissertation describes the work completed to date on the TAP and its passive successor, the Pivot-Flex Foot (PFF), as well as an outline for future work in this area. It begins with the mechanical design of the TAP, followed by software and control system development. Bench testing results are shown to confirm model predictions and simulate human subject testing. Next, preliminary human subject test results are presented. The results of preliminary human subject testing were used to develop an control strategy that cou-

ples transverse-plane rotation with sagittal-plane ankle rotation. Results are presented from three human subjects who tested the axis-coupling scheme. The design, manufacture, and testing of a passive device designed to have mechanical axis coupling is presented, followed by conclusions and suggestions for future work in this area.

Chapter 2
TAP MECHANICAL DESIGN

This chapter describes the mechanical design of the TAP. The design requirements are presented along with their rationale. A description of the overall system design and component selection is given. The design of the torque transducer is described in detail because of the transducer's pivotal roles. Finally, a simple dynamic model of the system is presented, which is used for control system development.

2.1 Requirements

The TAP was designed for laboratory testing on transtibial amputee subjects. While the TAP should be robust enough to be worn by amputee subjects in the lab, it was not designed to handle real-world use and abuse. The power system was designed for tests on the order of an hour, rather than all day as would be preferred for real-world application.

2.1.1 Axial Loads

In order to allow a wide range of amputee subjects to test the TAP, it was designed to support a 75th percentile male adult (98.9 kg, 218 lb) [27]. The corresponding design axial load was 1200 N.

2.1.2 Torsional Loads and Motion

The transverse-plane kinematics and kinetics of amputee gait were studied by Segal et al. [80, 78]. The maximum average peak ankle torque on the prosthetic limb was 0.23 N-m/kg during circular walking. For a 75th percentile male adult, the average peak torque would be

22.7 N-m. The TAP was designed to generate and measure torque up to 28.5 N-m to allow for significant inter-subject variability.

2.1.3 Bandwidth

The TAP should be able to track nonamputee kinematic trajectories. The power spectrum of the nonamputee ankle during walking is unknown. However, the ankle power spectrum in the sagittal plane has been analyzed during walking, where 99.7% of the power occurs at frequencies under 6 Hz [101]. The TAP should have a bandwidth of at least 10 Hz to allow ankle trajectories similar to those of nonamputees.

2.1.4 Prosthesis Mass

Several research studies have examined the metabolic cost of increasing the mass of the prosthetic limb in transtibial amputees [82]. Gailey et al. found no significant difference in oxygen consumption or heart rate when 907 g was added to the prosthesis [28]. Lin-Chan et al. looked at the effect of adding up to 2.31 kg to the prosthesis on walking at a range of speeds and found that increased mass did not have a significant effect on oxygen consumption or gait efficiency [55]. Lehman et al. found that adding up to 1.5 kg to the prosthesis did not change the metabolic efficiency of walking at self-selected speed or at 2 m/s, nor did it change the self-selected walking speed [49]. However, the placement of the added mass did effect metabolic efficiency, with more proximal mass distribution leading to more efficient gait. The pylon that the TAP replaces typically weighs about 150g. To keep the added mass below 1.5 kg, the TAP should weigh less than 1.65 kg. The completed TAP weighs 1.00 kg without the battery, and places the added mass as proximal as possible by design.

2.1.5 Usability

Prosthesis height directly limits the population of amputees that can use it by setting an upper limit on the length of the residual limb. In order to serve a large fraction of transtibial

amputees, the TAP was kept as short as possible. It can use standard pyramid adapters to interface with prosthetic feet and sockets. With a low profile Vari-Flex (Ossur Americas, Aliso Viejo, CA.) foot, the minimum build height of the prosthesis is 26.0 cm measured from the heel of the cosmesis to the top of the pylon female pyramid adapter. A custom adapter was built to further reduce the minimum build height so that more amputees could use the TAP. The custom adapter replaces the male pyramid adapter of the prosthetic foot. The custom adapter allows adjustment of height and rotation using spacers of different heights. The minimum build height of the TAP using the custom adapter is 22.2 cm. Figure 2.1 shows the custom adapter attaching the TAP to a prosthetic foot.

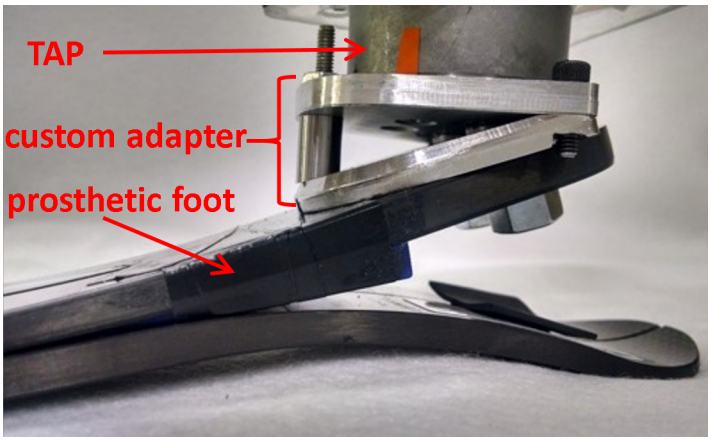

Figure 2.1: The custom adapter used to reduce minimum TAP build height.

To facilitate laboratory testing of overground and treadmill walking, the TAP was designed to be self-contained in terms of sensing, processing, and control. This eliminates the need for an accessory backpack or tether. The TAP was designed with an SD card with up to 4 GB of data storage for data collection during laboratory testing. The SD card was used for data logging and TAP configuration for bench testing and the first human subject trial. After the first human subject test, the SD card was replaced with a Wi-Fi module and data logging was done offboard on a laptop computer.

2.2 System Design

The heart of the TAP is the series elastic actuator, composed of a brushed 60W DC motor (RE30, Maxon Precision Motors, San Mateo, CA), an inline strain wave gearbox(CSF14-2XH-F, Harmonic Drive, Hauppauge, NY), and an aluminum torsion spring that doubles as a torque transducer. The TAP also uses a microprocessor and sensor board(UDB5, SparkFun Electronics, Boulder, CO), a Wi-Fi module(RN-XV, Microchip Technology Inc., Los Gatos, CA), and a motor controller(28v15, Pololu Robotics and Electronics, Las Vegas, NV). A magnetic encoder (Maxon Precision Motors, San Mateo, CA) with 1024 counts per turn is used for monitoring the position of the motor. A string potentiometer is used to measure the distance from the top of the TAP to the toe of the user's shoe in order to provide an estimate of sagittal-plane ankle rotation. The TAP is shown in Figure 2.2.

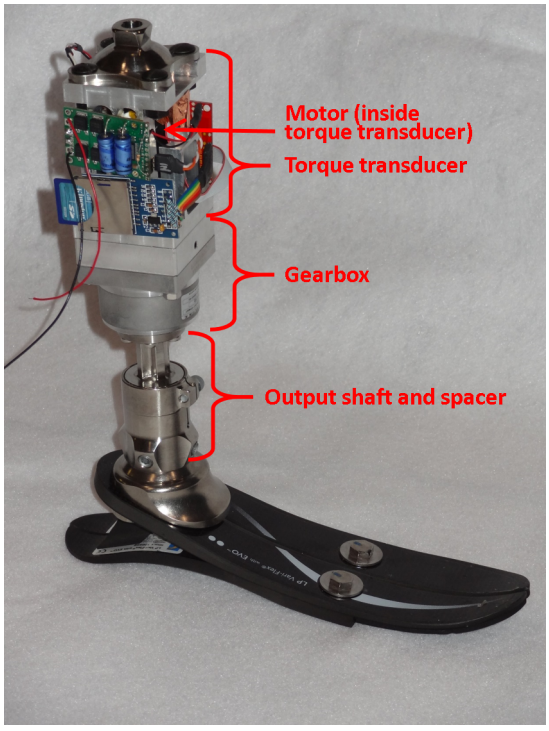

Figure 2.2: The Torsionally Active Prosthesis.

The PIC UAV Development Board (UDB5) was chosen to control the TAP. The UDB5 has a 16-bit dsPIC33F digital signal processing microcontroller operating at 40 million instructions per second and an onboard 3-axis accelerometer and 3-axis gyroscope. The dsPIC33F operates at 3.3V, but has several 5V-tolerant pins, allowing it to interface directly with the 5V motor position encoder and the 5V motor controller.

Two sets of batteries were selected for the TAP. An 11.1V, 4A-hr lithium polymer battery was used for initial human subject tests. The 300g battery was carried on a beltpack and connected to the TAP by a cable that was run down the subject's leg. Only about 30% of the battery's capacity was used during a three-hour human subject test. To reduce battery weight, a set of 11.1V, 1.2A-hr batteries that can be mounted directly on the TAP were selected. This lower-capacity battery weighs 90g. It was estimated that this battery would need to swapped at most once during a three-hour human subject test, but in practice it typically needed to be swapped two or three times per test.

2.3 Torque Transducer Design

There exist commercially available torque transducers in the required torque range. For example, the College Park iPecs system is specifically designed for use with lower-limb prostheses and provides six-axis load measurement. However, any commercially available load cell would have to be placed in series between the prosthesis and socket, significantly increasing the build height. To keep the height and weight of the TAP as low as possible, a custom torque transducer was designed. The torque transducer serves the alternate functions of housing the motor, connecting the gearbox to the socket, and providing rotational compliance. Because the torque transducer is built around the motor, it does not add height to the device overall.

The design of the torque transducer is a modified hollow cruciform shaft. A full Wheatstone bridge with two strain gauges on each of two opposing beams is used for measuring torque. The sensing beams are connected to a double-beam support structure that serves to increase the stiffness of the sensing beams with respect to axial torque while decreasing

their stiffness with respect to bending moments and axial force. Six non-sensing beams are used instead of the traditional two to increase axial and bending stiffness. The transducer is shown in Figure 2.3.

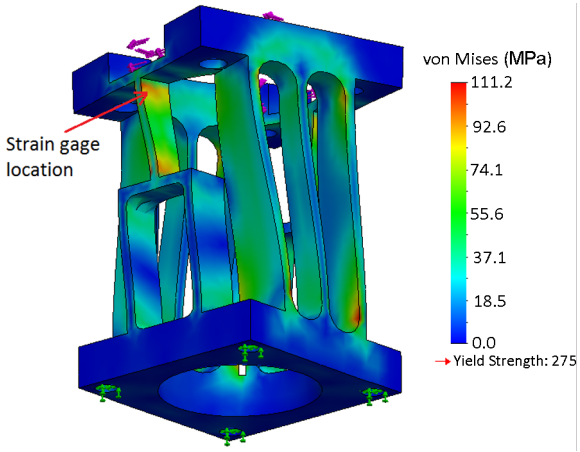

Figure 2.3: FEA model of torque transducer. Color indicates the von Mises stress. Strain gauges are symmetrically placed on the sensing beams as indicated.

The torque transducer must operate in the harsh electromagnetic interference (EMI) environment imposed by the motor and motor controller. To reduce the effect of motor-induced noise, the Wheatstone bridge is driven by a 3.3V square-wave alternating current that is synchronized with the motor pulse-width modulation (PWM). The AC signal is generated by the microcontroller and amplified by a line driver. The Wheatstone bridge voltage is amplified by an instrumentation amplifier. The amplified output is sampled by the microcontroller eight times per half-period of the excitation wave. The torque measurement is obtained by averaging the 16 measurements taken during one period of the excitation wave. A trim potentiometer in the Wheatstone bridge allows the torque sensor output to be zeroed at the sensor. Figure 2.4 shows the torque sensor schematic.

Figure 2.5 shows the physical realization of the excitation and amplification circuit. The entire circuit is housed at the top of the torque transducer in the small space between the top of the motor/encoder assembly and the bottom of the upper pyramid adapter. This

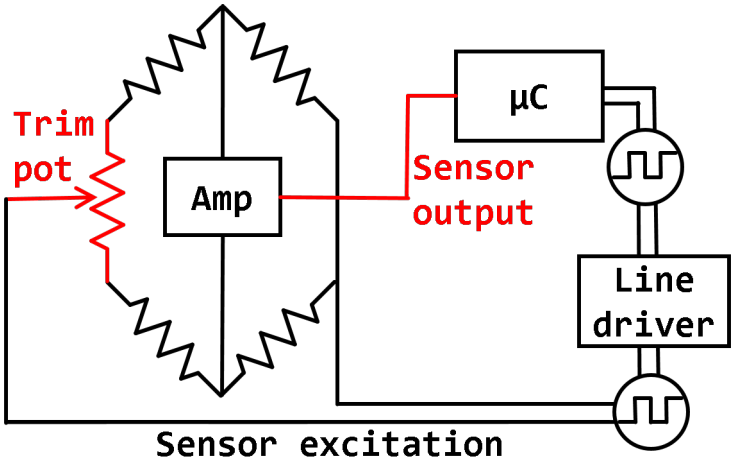

Figure 2.4: Torque sensor excitation, control, and sensing schematic.

location minimizes the length of the strain gauge wires, which helps mitigate EMI from the motor. The strain gauges and the amplifier are also shielded with copper tape.

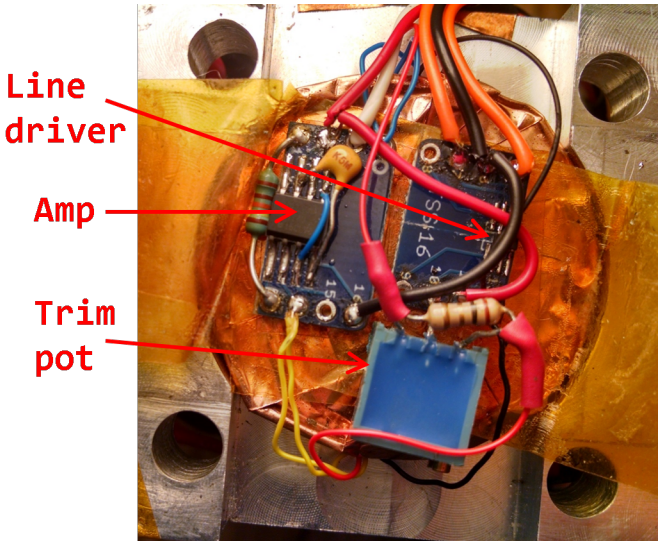

Figure 2.5: Torque sensor excitation and amplification circuit.

2.4 System Dynamics Model

Figure 2.6 shows the simplified system model used for control system development. The rotational inertia of the motor rotor, gearbox, and motor housing are lumped into a single inertia, J. The rotational inertia of the components that rotate with the motor, although small, dominate the effective inertia because their effect is multiplied by 10,000, the square of the gearbox gear ratio [19]. The elastic element is treated as a spring with stiffness k.

$$\frac{d}{dt}\begin{bmatrix}\theta_m \\ \dot{\theta_m} \\ \theta_s\end{bmatrix} = \begin{bmatrix}0 & 1 & 0 \\ -k/J & 0 & k/J \\ 0 & 0 & 0\end{bmatrix}\begin{bmatrix}\theta_m \\ \dot{\theta_m} \\ \theta_s\end{bmatrix} + \begin{bmatrix}0 & 0 \\ 0 & 1/J \\ 1 & 0\end{bmatrix}\begin{bmatrix}\dot{\theta_s} \\ T_m\end{bmatrix} \tag{2.1}$$

In the actual system, the motor current is directly controlled instead of the torque. In a ideal motor, the current and torque are directly proportional. However, the gearbox provides a large amount of damping, so a better model for the relationship between current and torque is

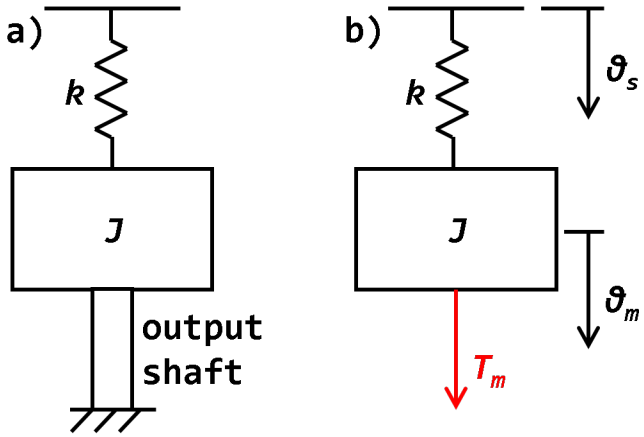

Figure 2.6: a) Diagram of simple system model. b) Model with the output shaft fixed, as in the mechanical test machine or in stance phase of walking.

$$T_m = I/K_Q - c_g\dot{\theta_m} \tag{2.2}$$

where I is the motor current, K_Q is the torque constant of the motor/gearbox combo, and c_g is the damping in the motor and gearbox. Using equation 2.2, equation 2.1 becomes

$$\frac{d}{dt}\begin{bmatrix}\theta_m\\ \dot{\theta_m}\\ \theta_s\end{bmatrix} = \begin{bmatrix}0 & 1 & 0\\ -k/J & -c_g/J & k/J\\ 0 & 0 & 0\end{bmatrix}\begin{bmatrix}\theta_m\\ \dot{\theta_m}\\ \theta_s\end{bmatrix} + \begin{bmatrix}0 & 0\\ 0 & 1/(JK_Q)\\ 1 & 0\end{bmatrix}\begin{bmatrix}\dot{\theta}_s\\ I\end{bmatrix} \tag{2.3}$$

Chapter 3
TAP SOFTWARE AND CONTROL SYSTEM DESIGN

This chapter begins with a description of the software management scheme used to track changes to TAP-related software. The functions and important implementation details of the TAP software are then described. The control system design and analysis are presented, along with the identification of dynamic model parameters. Finally, the iterative controller used for initial human subject testing is presented.

3.1 Software Tracking

The TAP relies on complex software to function. To manage the software throughout its evolution, the version control system Subversion (Apache Software Foundation, Los Angeles, CA) is being used. Using Subversion, changes to the software are periodically "committed" to a repository with comments. This creates a version of the software that can always be recalled or compared to later versions. Subversion has been used to track code for the TAP from a time even before the code compiled or the microprocessor was received (v159), all the way through the most recent human subject test (v715). To date, over 200 code versions related to the TAP have been saved. Subversion is also being used to track changes to the dynamics model, the data processing and analysis routines, and this document.

3.2 Software Components

3.2.1 LegPilot

LegPilot is a dsPIC33F program written in C and compiled using the Microchip XC16 compiler that controls the behavior of the TAP. With the exception of the attitude estimation routine, it is written entirely in fixed-point. The 16-bit dsPIC33F operates at 40 million

instructions per second and has hardware support for division but not for floating point operations. This makes floating-point arithmetic computationally expensive. The application code consists of 17 files with about 1800 lines of code. The application has undergone about 172 revisions since its creation. Table 3.1 shows the operating frequency of different tasks on the dsPIC33F.

Task	Frequency [Hz]
Instruction clock	40,000,000
Torque sensor sampling	333,333
Wi-Fi UART	115,200
Sagittal-plane ankle rotation sensor sampling	104,167
Battery voltage sensor sampling	104,167
Motor PWM	20,833
Torque sensor excitation	10,417
Torque meausurement	10,417
Torque control	10,417
IMU sensor read	200
Sensor averaging	200
Gait event detection	200
Data downlink	200
Encoder	interrupt driven
Settings uplink	interrupt driven

Table 3.1: Operating frequencies of system tasks

Most of the tasks that are performed by the dsPIC33F occur during interrupts. The highest priority interrupt responds to the edge of a motor encoder pulse. The encoder interrupt is given highest priority because it is very important not to miss any encoder

pulses and because accurate time-stamping is important for motor speed estimation. At each encoder pulse, the position counter is either incremented or decremented, and the motor speed is calculated as the inverse of the time between pulses. If no encoder pulse occurs for 6.6 ms, the motor speed is set to zero. The speed of the output shaft of the gearbox must be less than 0.5°/s for this condition to occur.

The motor is controlled in drive/coast fashion by a direction pin and a pulse-width modulation (PWM) pin. The pulse width modulation is performed at 21 kHz. This frequency was chosen because it is above the human audible range. The torque sensor bridge is driven by a square-wave input that is synchronized to the motor PWM and half its frequency. Thus current flows through the bridge one direction during one PWM pulse and the opposite direction during the next pulse. Since both motor pulses are the same, and electromagnetic interference(EMI) induced in the sensor bridge by the motor should have equal and opposite effects durings two successive pulses. In each direction, the torque sensor is sampled 16 times. This sampling occurs without any CPU intervention. The first 8 samples are discarded to reduced switching transients, and the last 8 samples of each direction are averaged with the appropriate sign. The torque computed by this averaging is then used by the inner-loop controller to calculate the PWM for the next pair of PWM pulses. Figure 3.1 shows the PWM and torque sensor timing. There is approximately 0.17 ms delay in the inner-loop torque control.

The string potentiometer that measures sagittal-plane ankle rotation and the battery voltage divider are also sampled synchronously with the motor PWM. However, they are both excited by direct current and therefore more sensitive to EMI. To mitigate this, both values are low-pass filtered in hardware, and only the sample farthest from the start of a motor pulse is used to measure sagittal-plane ankle rotation and battery voltage.

The MPU6000 IMU is configured to output data at 200 Hz. When data is available, it interrupts the dsPIC33F, which reads the data over SPI, calibrates the sensors, updates the gait cycle estimator, and initiates a data packet downlink. Sensor calibration uses a fixed scale factor and a temperature-dependent offset determined using a lookup table. The

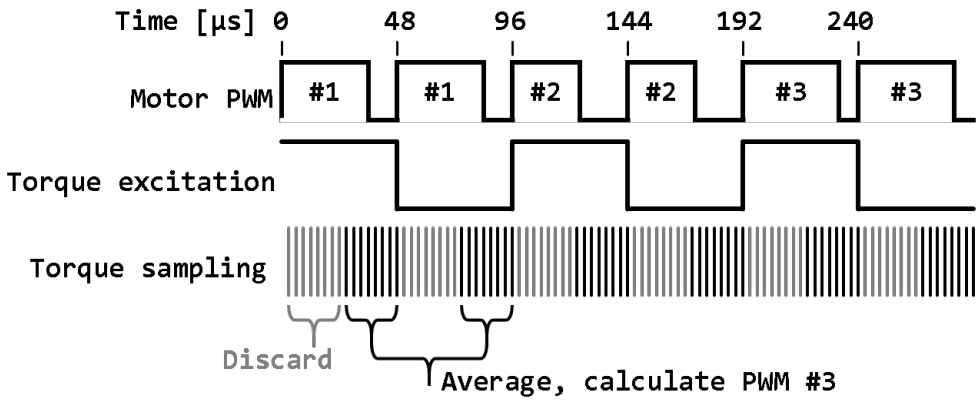

Figure 3.1: Timing diagram for motor control and torque sensing

iterative controller also runs in this interrupt on the transition from stance to swing. Profiling was performed to ensure that this computationally-intensive algorithm was able to complete inside a single cycle of the 200 Hz interrupt.

Data is sent to the WiFly module for downlink at 200 Hz. Each data packet consists of 16 2-byte entries: header, packet length, packet number, rotation, torque, PWM, 3 gyros, IMU temperature, 3 accelerometers, sagittal-plane ankle rotation angle, equilibrium position, and battery voltage. One bit of the battery voltage field is used to report whether the TAP is in stance or swing phase. Computed values such as Euler angles are not downlinked.

In addition to its operational mode, LegPilot also has two simulation modes that can be selected at compile time. In RGS_TEST mode, torque and sagittal-plane ankle rotation sensing and motor control operate normally. Instead of reading data from the IMU, a prerecorded set of data are acted upon. Data playback is initiated by an external synchronization pulse. This mode is useful for testing with the Robotic Gait Simulator (RGS) [3] or the mechanical testing machine. The RGS uses an actuated force plate that moves relative to a rigidly mounted foot to simulate gait kinematics and kinetics. Because the prosthetic leg is fixed, the inertial sensor values need to be spoofed to make them consistent with the leg motion being simulated. In GAIT_SPOOF mode, IMU sensor values come from a prerecorded

data file as well as torque and sagittal-plane ankle rotation sensor values. Motor control is disabled. This mode was particularly useful for developing the LegGUI graphical user interface.

3.2.2 DataParser

DataParser is a PC application written in C++ that converts binary data files into human-readable comma-separated value (.csv) files. The application code consists of a single file with about 250 lines. The application has undergone about 20 revisions since its creation.

3.2.3 LegGUI

LegGUI is a PC application written in C# that provides a realtime interface with the TAP over Wi-Fi. The application code consists of about 1000 lines of manually-written code and 500 lines of auto-generated Designer code. The application has undergone about 30 revisions since its creation. A screenshot of LegGUI is shown in Figure 3.2.

LegGUI runs on a Windows 8.1 laptop computer and uses a Windows Wireless Hosted Network to provide a WPA2-encrypted Wi-Fi access point. When the TAP powers up, it connects to the access point and initiates a TCP connection with LegGUI. TCP is a reliable connection that detects and repairs damaged or missing packets. Once the connection is made, the TAP begins streaming data to the PC. Whenever LegGUI is running, it automatically records all data received from the TAP. This helps avoid the loss of valuable data due to human error. Additionally, LegGUI provides the option to start and stop a secondary log file with a user-defined filename. This capability can be used to help organize the data for synchronization with motion-capture data. The LegGUI also provides a realtime graphical display of a subset of the data received from the TAP.

In addition to data logging, LegGUI also provides configuration of the TAP over Wi-Fi. The force-deflection curve of the actuator can be set, as well as the operating mode, control-system gains, torque and rotation offsets, and gait event detection parameters. All configuration changes are automatically logged so that the entire configuration is known at

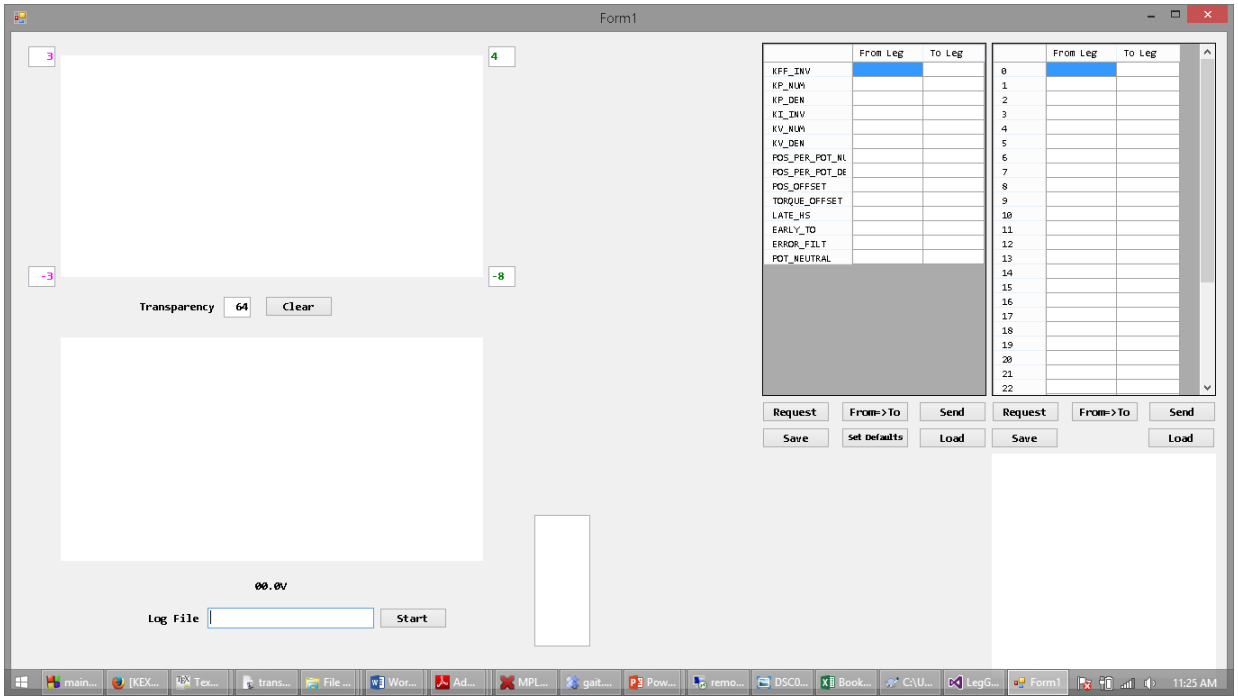

Figure 3.2: Screenshot of LegGUI user interface

all points of time. Sets of configuration parameters can be saved and recalled. There is also a "Set Defaults" command that restores the TAP to its default configuration.

LegGUI also provides voice enunciation of important events during TAP testing. The notification events are:

- TCP connection made
- TCP connection lost
- Low battery
- Torque sensor saturation

Audible notifications are reserved for important events that have implications for test operation. Data logging does not occur until the TCP connection is made. Loss of the TCP connection indicates loss of power or another problem with the TAP. The battery must be changed on a low battery condition. Torque sensor saturation may indicate failure of the torque sensor.

3.3 Inner-Loop Control

3.3.1 Control System Design

We desire a control system that will simulate a passive spring according to the equation

$$T_s = -K^*(\theta_s - \theta_d) \tag{3.1}$$

Because we can directly measure θ_m but not θ_s, we would like to satisfy equation 3.1 without referencing θ_s. Since the elastic element already behaves as a passive spring obeying the equation $T_s = -k(\theta_s - \theta_m)$, the desired relationship can be rewritten as

$$T_s = -K(\theta_m - \theta_d) \tag{3.2}$$

where $K^* = \frac{kK}{k+K}$. Here K represents the stiffness of the spring that results in the desired overall actuator stiffness when placed in series with the elastic element. The motor should simulate this spring. The stiffness of the elastic element provides an upper bound for the stiffness of the overall actuator, if K is to be non-negative. We propose a control law of the form

$$I = K_Q\{-K_{ff}K(\theta_m-\theta_d)+K_p[-K(\theta_m-\theta_d)-T_s]+K_i\int[-K(\theta_m-\theta_d)-T_s]dt-K_{v,m}\dot{\theta_m}+K_{v,s}\dot{\theta_s}\} \tag{3.3}$$

where T_s is the torque measured by the strain gauges, $T_s = k(\theta_m - \theta_s)$. The factor of K_Q in the front allows the control gains K_{ff}, K_p, K_i, $K_{v,m}$, and $K_{v,s}$ to have the convenient units of N-m/N-m, N-m/N-m, N-m/N-m-s, N-m/(deg/s), and N-m/(deg/s), respectively. If the feedforward gain K_{ff} is equal to 1, then the socket torque is perfect at DC without feedback.

If the integral gain is set to zero and the feedforward gain is set to 1, then the system matrix becomes

$$A = \frac{1}{J}\begin{bmatrix} 0 & J & 0 \\ -(1+K_p)(k+K) & -(K_{v,m}+c_g) & (1+K_p)k \\ 0 & 0 & 0 \end{bmatrix} \tag{3.4}$$

This system matrix has the same poles as a spring-mass-damper system with natural frequency $\omega_n = \sqrt{(1+K_p)(k+K)/J}$ and damping ratio $\zeta = (c_g + K_{v,m})/2\sqrt{J(1+K_p)(k+K)}$. The transfer function from θ_s to T_s has a pair of zeros with natural frequency $\omega_n = \sqrt{(1+K_p)K/J}$ and damping ratio $\zeta = (c_g + K_{v,m} - K_{v,s})/2\sqrt{J(1+K_p)K}$. These zeros are always at a lower frequency than the poles. Thus the torque response to socket rotation always has a lower bandwidth than the torque response to a change in equilibrium position, which does not have a zero in its transfer function.

3.3.2 Parameter Identification

The unknown parameters in the system dynamics model are the spring stiffness k, the gearbox damping c_g, and the lumped rotational inertia J. The stiffness k was determined to be 16.3 N-m/deg by measuring the slope of the torque-rotation curve obtained using a mechanical test machine(MTS Systems, Eden Prairie, MN). In order to estimate the gearbox damping c_g, the test machine performed rotational sine waves to determine the damping moment as a function of rotation speed. The damping moment is shown in Figure 3.3.

The gearbox damping is nonlinear, with a significant Coulomb-friction effect on direction changes. In order to identify a good value for c_g to be used in control system design, the response of the closed-loop system to a step change in θ_s was analyzed. For this test, both $K_{v,m}$ and $K_{v,s}$ were set to zero. In this case, the step response exhibits significant oscillation in T_s, the period and decay rate of which can be used to determine the value of the parameters J and c_g. Table 3.2 shows the identified model parameters and Figure 3.4 compares the measured step response with the simulated step response using the identified parameters. The initial response matches well, but small oscillations die out much faster in the physical system than in simulation due to high effective damping near zero speed. The open-loop

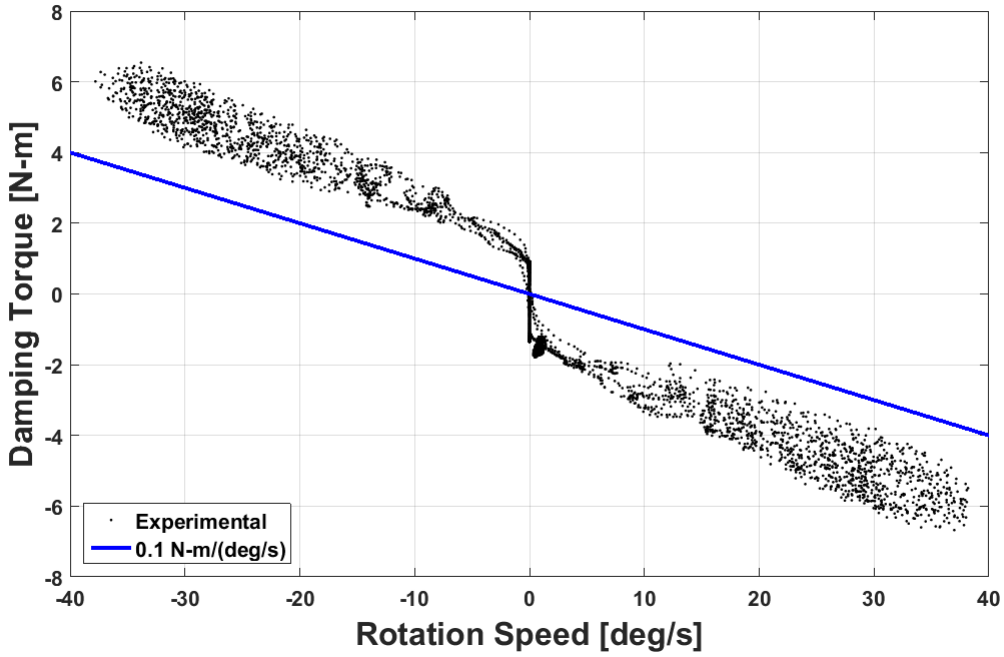

Figure 3.3: Measured gearbox damping. The solid line shows linear damping at 0.1 N-m/(deg/s).

system has a natural frequency $\omega_n = \sqrt{k/m}$ =17.9 Hz.

Parameter	Value
k	16.3 N-m/deg
c_g	0.1 N-m/(deg/s)
J	0.074 kg-m^2

Table 3.2: Identified model parameters

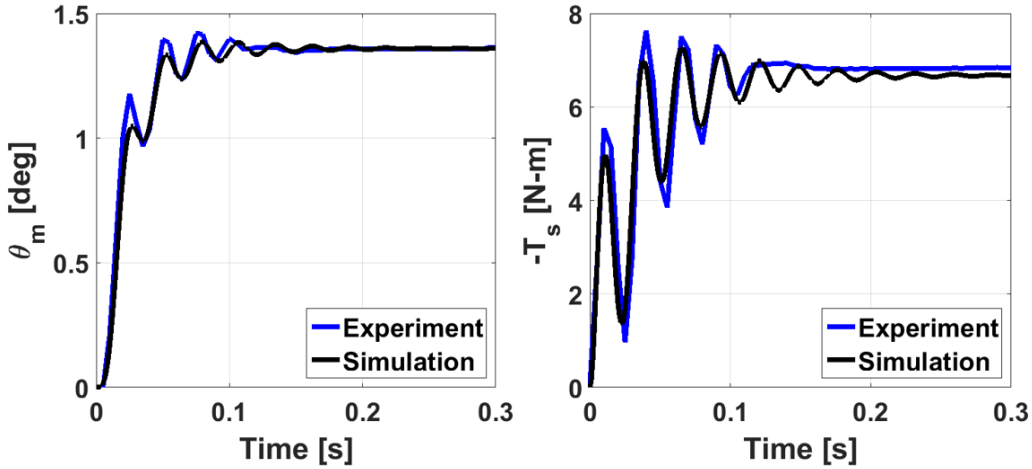

Figure 3.4: Comparison of simulated and experimental closed-loop response to a step change in θ_s with $K = 4.89$, $K_p = 2.28$ N-m/N-m, $K_{v,m} = 0$, $K_{v,s} = 0$, $K_i = 100$ N-m/N-m-s.

3.3.3 Control System Tuning

In the simple model, any desired bandwidth can be obtained by appropriate selection of K_p, $K_{v,m}$ and $K_{v,s}$. However, the model ignores the destabilizing effects of the integral gain, velocity estimation lag, and inner-loop delay. To account for these effects, we need to add six states to the system: $\int \theta_m$, $\int \theta_s$, $\int \theta_d$, the motor current I, the motor speed estimate $\hat{\dot{\theta}}_m$, and the socket speed estimate $\hat{\dot{\theta}}_s$. The motor current will by related to the current command given by equation 3.3 by a simple lag:

$$\frac{d}{dt}I = (I_c - I)/\tau_I \tag{3.5}$$

where the time constant τ_I is chosen to be 0.17 ms to model the 0.17 ms delay in the inner-loop controller. The delay in the speed estimate varies with motor speed because it is updated on each encoder pulse edge. The actual average motor speed estimation delay is

$$\tau_m = \begin{cases} 3.3\,\text{ms} & : \quad |\dot{\theta_m}| \leq 0.5364°/\text{s} \\ \frac{0.001758°}{|\dot{\theta_m}|} & : \quad |\dot{\theta_m}| > 0.5364°/\text{s} \end{cases} \tag{3.6}$$

A constant time constant $\tau_m = 1\,\text{ms}$ is used to simulate the motor speed estimation delay according to the equation

$$\frac{d}{dt}\hat{\dot{\theta}_m} = (\dot{\theta_m} - \hat{\dot{\theta}_m})/\tau_m \tag{3.7}$$

The socket speed estimation is modeled the same way. In the control system implementation, the quantity $-K_{v,m}\dot{\theta_m} + K_{v,s}\dot{\theta_s}$ is calculated as

$$-K_{v,m}\dot{\theta_m} + K_{v,s}\dot{\theta_s} = (K_{v,s} - K_{v,m})\hat{\dot{\theta}_m} + K_{v,s}(\hat{\dot{\theta}_s} - \hat{\dot{\theta}_m}) = (K_{v,s} - K_{v,m})\hat{\dot{\theta}_m} - \frac{K_{v,s}}{k}\hat{\dot{T}_s} \tag{3.8}$$

The torque rate estimate $\hat{\dot{T}_s}$ is calculated using finite differences and filtered with a fourth order filter.

The selection of K_p, $K_{v,m}$ and $K_{v,s}$ must be a compromise between high bandwidth and alleviation of the high frequency resonance. Figure 3.5 shows the effect on the system poles and zeros of changing K_p, $K_{v,m}$ and $K_{v,s}$ from nominal values of 8 N-m/N-m, 0.6 Nm/(deg/s), and 0.3 Nm/(deg/s).

Figure 3.6 shows the frequency response of the system. The feedback controller increases the system bandwidth from 13 Hz to 41 Hz. This bandwidth is sufficient for use with human walking, where most of the ankle power occurs at less than 6 Hz [101]. Fiqure 3.7 shows the stability boundary of the control system. Control system stability is insensitive to the

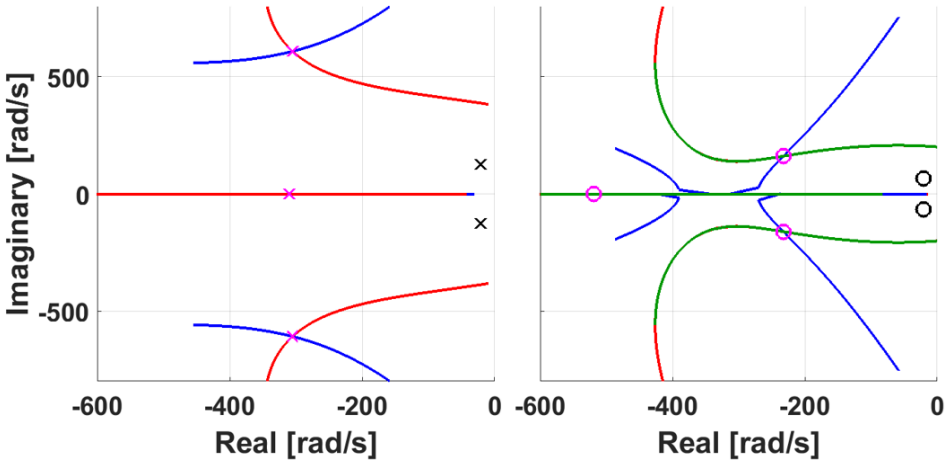

Figure 3.5: Response of system poles and zeros to changes in K_p, $K_{v,s}$ and $K_{v,s}$ at $K^* = 4$ N-m/deg. Black: open-loop. Blue: K_p varying with $K_{v,m} = 0.6$ N-m/(deg/s), $K_{v,s} = 0.3$ N-m/(deg/s). Red: $K_{v,m}$ varying with $K_p = 8$ N-m/N-m, $K_{v,s} = 0.3$ N-m/(deg/s). Green: $K_{v,s}$ varying with $K_p = 8$ N-m/N-m, $K_{v,m} = 0.6$ N-m/(deg/s). Magenta: $K_p = 8$ N-m/N-m, $K_{v,m} = 0.6$ N-m/(deg/s), $K_{v,s} = 0.3$ N-m/(deg/s).

integral gain and has good margins in both $K_{v,m}$ and K_p. Fiqure 3.8 shows how the stability boundary moves as a time delay t_d is added to the inner-loop delay τ_m. The delay margin of the control system is 2 ms, which is an order of magnitude higher than the existing inner-loop delay. $K_{v,s}$ does not affect system stability.

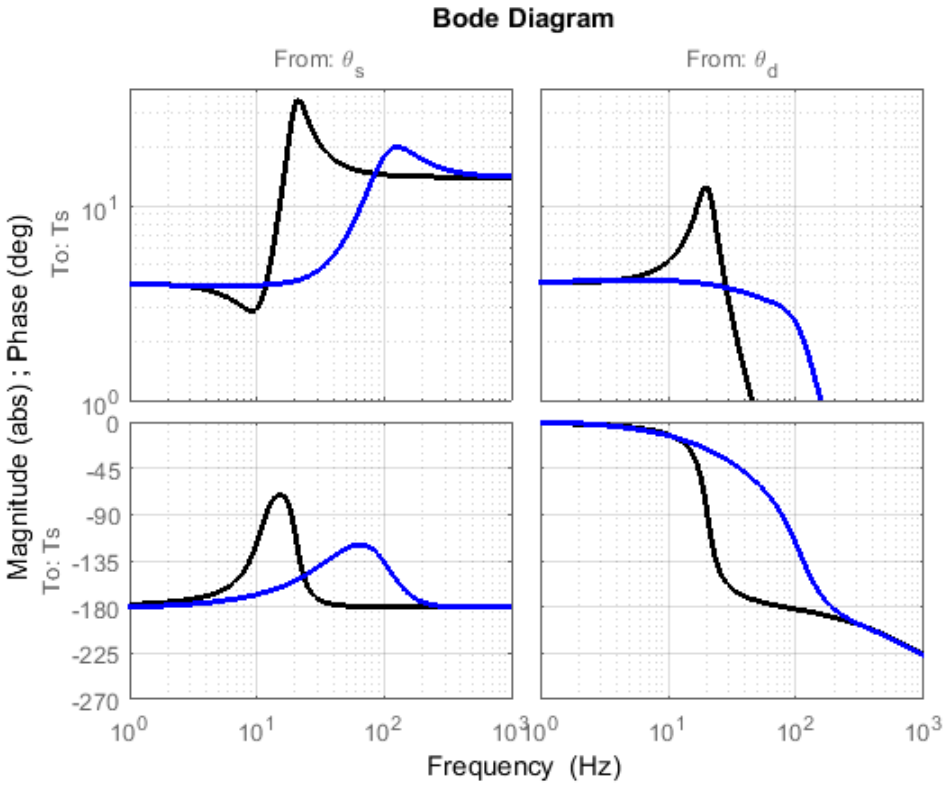

Figure 3.6: System frequency response at $K^* = 4$ N-m/deg. Black: open-loop. Blue: closed-loop with $K_p = 8$ N-m/N-m, $K_{v,m} = 0.6$ N-m/(deg/s), $K_{v,s} = 0.3$ N-m/(deg/s), $K_i = 100$ N-m/N-m-s.

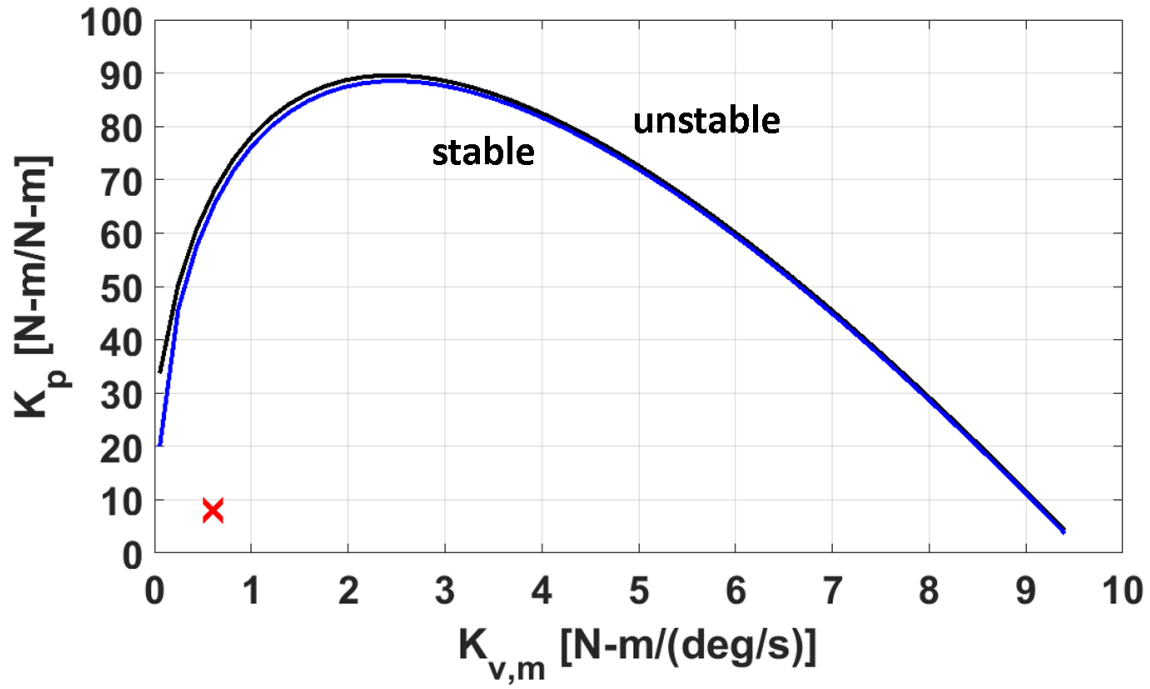

Figure 3.7: Control system stability boundaries at $K^* = 4$ N-m/deg with $K_i = 100$ N-m/N-m-s (black) and $K_i = 1000$ N-m/N-m-s (blue). The red x shows the selected gains.

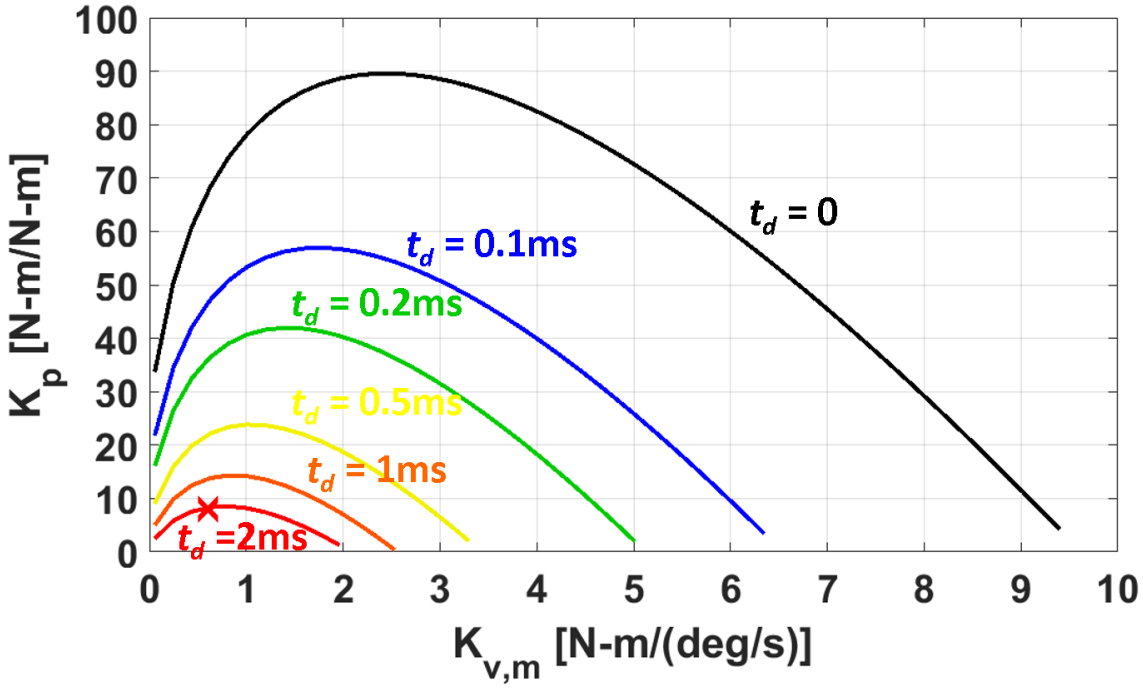

Figure 3.8: Control system stability boundaries at $K^* = 4$ N-m/deg with $K_i = 100$ N-m/N-m-s at various values of t_d. The red x shows the selected gains.

3.3.4 Control System Behavior during Swing

The system dynamics change discretely on the transition from stance to swing. Figure 3.9 shows the system model during swing. Instead of being fixed to the ground, the foot is modeled as a freely rotating mass with rotational inertia J_f attached to the output shaft.

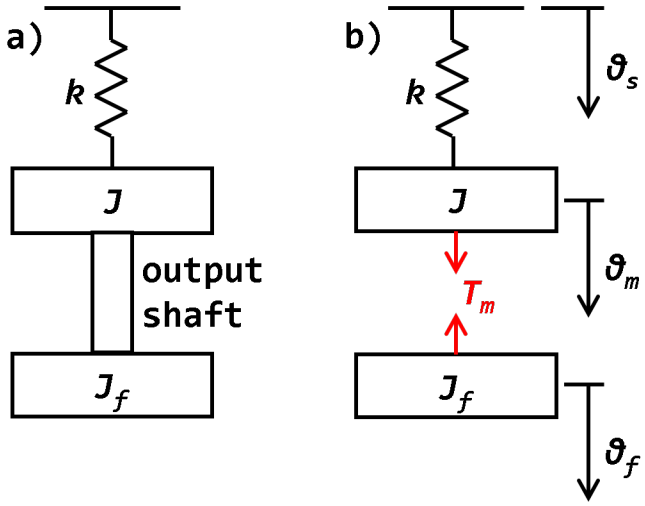

Figure 3.9: a) Diagram of simple system model during swing. b) Model with the output shaft connected to a freely rotating mass, as in swing phase of walking.

If the equations of motion are rewritten relative to the foot, equation 2.1 is valid if the rotational inertia J is replaced by $\frac{JJ_f}{J+J_f}$. The system natural frequencies and damping ratios are increased by a factor of $\sqrt{(J+J_f)/J_f}$ relative to stance phase. For a foot inertia of 0.012 kg-m^2, this factor is approximately 2.6. This reduction in effective inertia means that system stability is improved in swing phase relative to stance phase.

3.3.5 Control System for a Flexible Configuration

When emulating very flexible springs, the control system design is more challenging. If the effective stiffness is reduced by an order of magnitude to 0.4 N-m/deg, the open-loop bandwidth is only 1.6 Hz. This stiffness corresponds to the most flexible torsion adapter

tested by Flick et al. [26]. Figures 3.10, 3.11, and 3.12 show a control system design that increases the bandwidth to 18 Hz. The delay margin of the system is 0.5 ms.

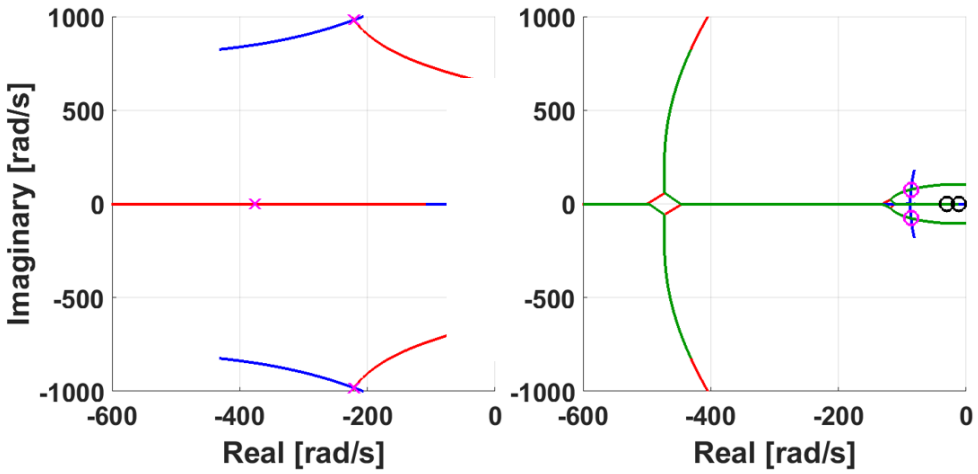

Figure 3.10: Response of system poles and zeros to changes in K_p, $K_{v,s}$ and $K_{v,s}$ at $K^* = 0.4$ N-m/deg. Black: open-loop. Blue: K_p varying with $K_{v,m} = 1.0$ N-m/(deg/s), $K_{v,s} = 0.9$ N-m/(deg/s). Red: $K_{v,m}$ varying with $K_p = 32$ N-m/N-m, $K_{v,s} = 0.9$ N-m/(deg/s). Green: $K_{v,s}$ varying with $K_p = 32$ N-m/N-m, $K_{v,m} = 1.0$ N-m/(deg/s). Magenta: $K_p = 32$ N-m/N-m, $K_{v,m} = 1.0$ N-m/(deg/s), $K_{v,s} = 0.9$ N-m/(deg/s).

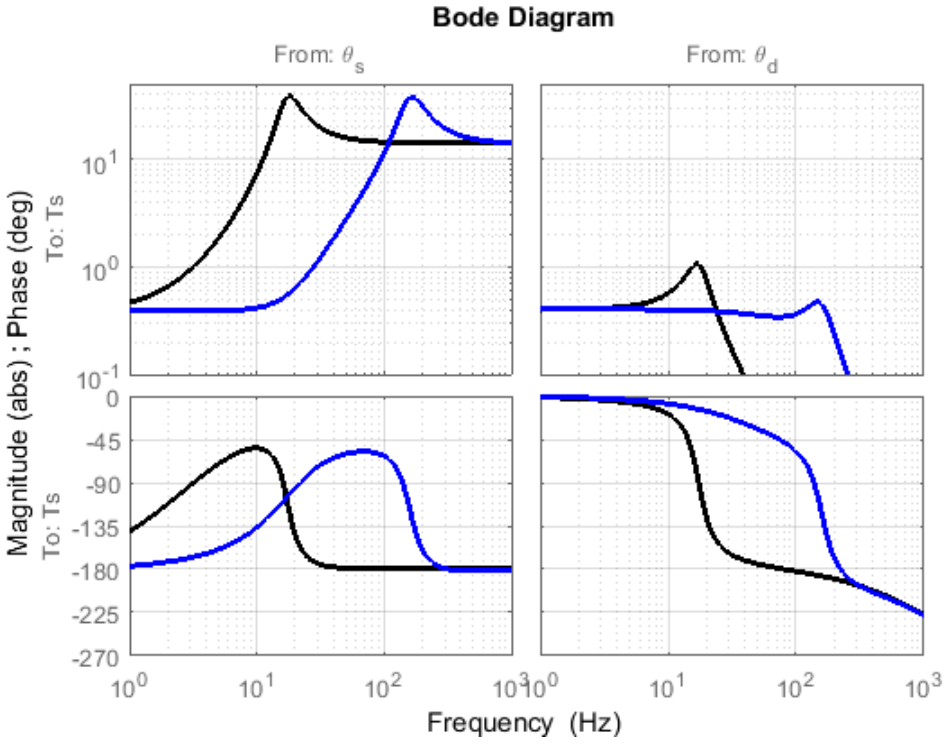

Figure 3.11: System frequency response at $K^* = 0.4$ N-m/deg. Black: open-loop. Blue: closed-loop with $K_p = 32$ N-m/N-m, $K_{v,m} = 1.0$ N-m/(deg/s), $K_{v,s} = 0.9$ N-m/(deg/s), $K_i = 100$ N-m/N-m-s.

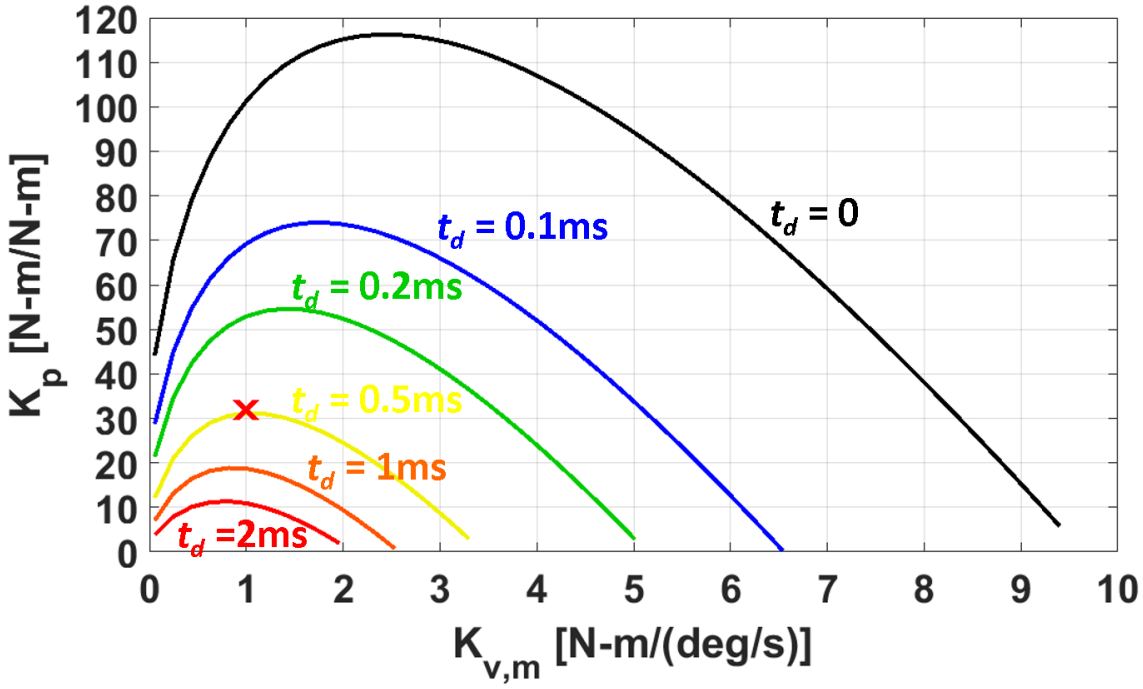

Figure 3.12: Control system stability boundaries at $K^* = 4$ N-m/deg with $K_i = 100$ N-m/N-m-s at various values of t_d. The red x shows the selected gains.

3.4 Iterative Controller

An iterative controller was developed to find a rotational equilibrium position as a function of sagittal-plane ankle rotation. The inputs to the iterative controller are the socket torque $T_s(t)$ and the sagittal-plane ankle rotation $\beta(t)$ during stance phase. The output is the equilibrium position function $\theta_d(\beta)$. The equilibrium position function is updated at the end of each step on the transition from stance to swing. To update $\theta_d(\beta)$, the time average of the socket torque during stance, $\overline{T_s}$ is calculated. This is the target socket torque throughout stance phase. A torque "error" is then calculated as

$$e_T(t) = \overline{T_s} - T_s(t) \tag{3.9}$$

The first and last timepoints of e_T are set to zero to produce a smooth transition from swing to stance. The torque error is then filtered with forward and reverse first order filters at 6 Hz to produce $e_{T,f}(t)$. The next step is to curve-fit the torque error to the sagittal-plane ankle rotation to give $\widetilde{e_{T,f}}(\beta)$. The implementation in LegPilot uses a lookup table with linear interpolation sagittal-plane ankle rotation points separated by about 1°to represent $\widetilde{e_{T,f}}(\beta)$. The equilibrium function is then updated according to

$$\theta_d(\beta)_{i+1} = \theta_d(\beta)_i + L\widetilde{e_{T,f}}(\beta), \tag{3.10}$$

where L is the iterative controller gain.

The iterative controller was designed for use in preliminary human testing to help find an equilibrium position function that could flatten the socket torque profile. The end goal was not to use an iterative controller at all, but to use a fixed equilibrium position function that could eventually be realized using passive components.

Chapter 4
TAP BENCH TESTING

Bench test were performed with a mechanical testing machine to determine model parameters, evaluate controller performance, and prepare for human subject testing. Quasi-static torque-rotation curves are presented, followed by the response of the TAP to a step input. Finally, results of iterative controller operation during simulated gait are presented.

4.1 Quasi-static Stiffness Profiles

In order to test the ability of the TAP to emulate a variety of stiffnesses, quasi-static testing was performed with the TAP emulating five different stiffnesses obeying the equation

$$T_s = -K_1\theta_m - (K_3\theta_m)^3 \tag{4.1}$$

The values of K_1 and K_3 for each of the five stiffness profiles is given in Table 4.1. These stiffness profiles were chosen to give two stiff linear profiles as well as linear, stiffening, and softening profiles at an average value of 1 N-m/deg, which is typical of commercially available torsion adapters [26].

The TAP was mounted in a mechanical testing machine(MTS Systems, Eden Prairie, MN) in series with a tele-torsion adapter(Total Shock 4410; Century XXII Innovations, Jackson, Michigan). The actuator head of the testing machine performed slow ramps of axial rotation. The axial torque was measured by both the testing machine and the TAP. The RMS difference between the torque measured by the testing machine and by the TAP was 0.11 N-m over the range of -20 to 20 N-m. The RMS differences between the commanded torque and the torque measured by the TAP were 0.029, 0.046, 0.031, 0.027, and 0.048 N-m for the five different stiffness profiles. Figure 4.1 shows T_s vs. θ_m for each of the five stiffness

Profile	K_1 [N-m/deg]	K_3 [(N-m)$^{1/3}$/deg]
1	0.348	0.117
2	1	0
3	1.859	-0.109
4	5	0
5	20	0

Table 4.1: Stiffness values for qausistatic testing

profiles. For profiles 4 and 5, the TAP was taken to its design torque of 28.5 N-m.

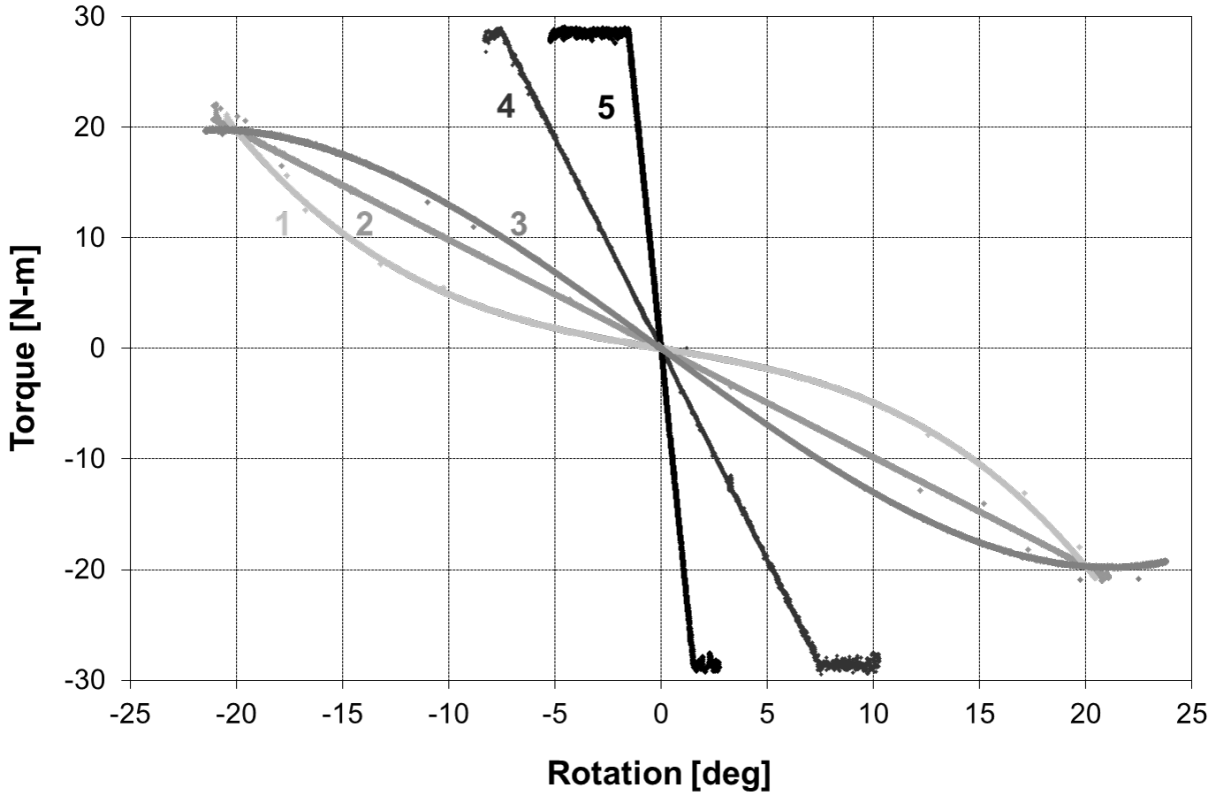

Figure 4.1: Quasi-static stiffness curves.

4.2 Step Response

In order to validate the system dynamics model and controller tuning, step responses were obtained using the mechanical testing machine. The TAP was placed in the machine and the actuator head was commanded to perform step changes in rotation. The response as measured by the TAP is shown in Figure 4.2. The actuator has a bandwidth of about 7 Hz, while the TAP in this configuration is modeled to have a bandwidth of 41 Hz. This means that the rise time of the response is almost entirely determined by the rise time of the input. The simulated motor rotation matches the measured motor rotation quite well. The measured socket torque in one direction has an early peak at about 15 ms that is not

captured by the simulation. This suggests that the model may have slightly more damping than the actual system at high rotation rates.

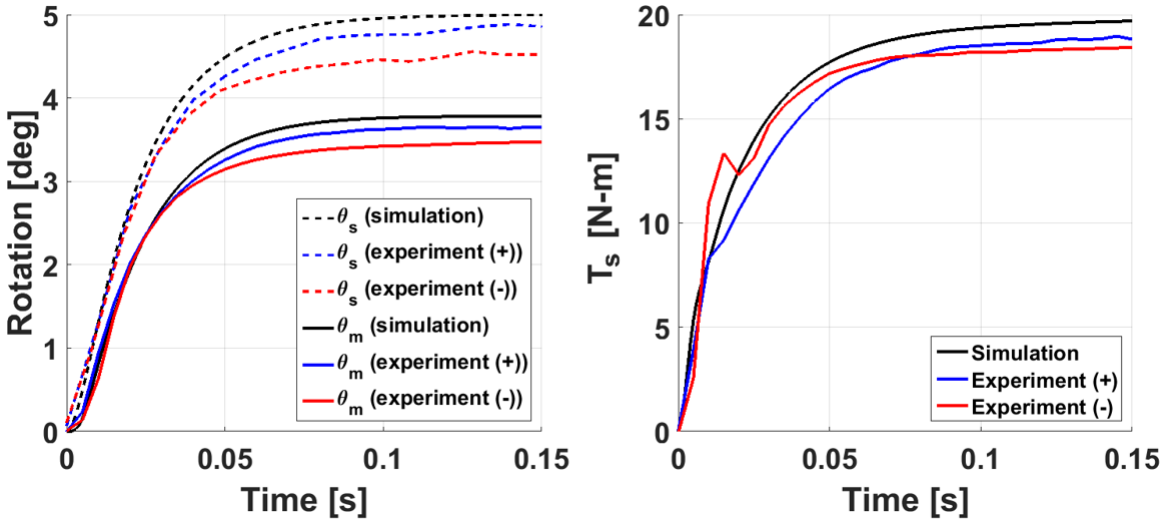

Figure 4.2: Simulated and experimental response to a 5°step change in θ_s in either direction.

4.3 Gait Simulation

In order to evaluate the iterative controller in a setting similar to human walking, a test was devised using the mechanical testing machine. The TAP was mounted in series with a tele-torsion adapter(Total Shock 4410; Century XXII Innovations, Jackson, Michigan) that included axial and torsion springs. The string potentiometer was connected to the test machine actuator head through an eye-bolt at the base of the test machine so that the string traveled twice the distance of the actuator head. Thus axial motion of the actuator head was interpreted as sagittal-plane ankle rotation by the TAP. The test setup is shown in figure 4.3.

The TAP was placed in the RGS_TEST mode described in section 3.2.1. In this mode, the IMU sensor data used to detect gait cycle events was obtained from a pre-recorded file. The playback of the sensor data file was triggered by a pulse from the mechanical test

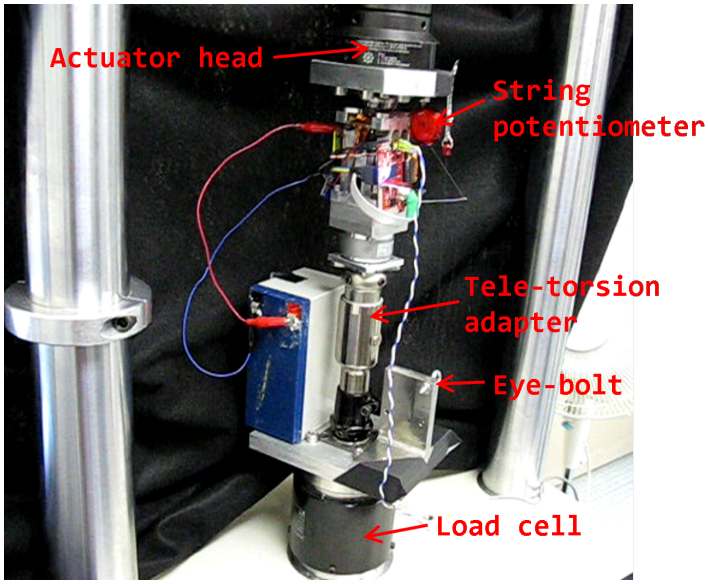

Figure 4.3: Simulated gait test setup on the mechanical testing machine.

machine. During simulated stance phase, the test machine performed a position ramp from 0 to 1 cm compression in the axial direction and a rotation haversine in the transverse plane. The amplitude of the haversines was a repeating pattern of 2°, 4°, and 6°. This simulated "low torque steps" (outside of a turn), "nominal torque steps" (straight walking), and "high torque steps" (inside of a turn). The test machine test profiles are shown in Figure 4.4.

The iterative controller described in section 3.4 was enabled during this test. The equilibrium position function $\theta_d(\beta)$ was updated on each stance-to-swing transition. Figure 4.5 shows the stance torque aver the course of operation of the iterative controller. As expected, the iterative controller flattens the torque profile during the nominal step. The torque peaks in the high torque and low torque steps are also reduced.

This test demonstrated the ability of the iterative controller to reduce peak socket torque when the socket followed a fixed trajectory. In human subject testing, the socket does not follow a fixed trajectory. Instead, subjects adapt their gait as the equilibrium position function changes. The iterative controller should adapt slower than the subject so that subjects do not have to make conscious changes to their gait. Bench testing does not give

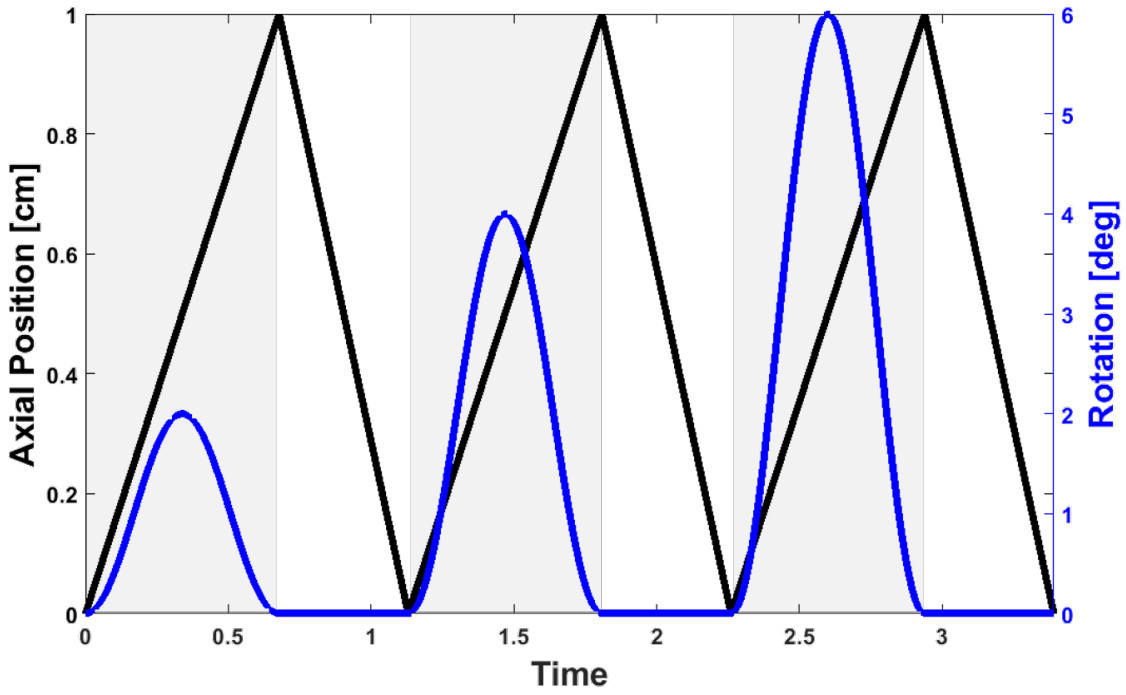

Figure 4.4: Actuator head motion profiles for simulated gait test. Grey background: simulated stance, white background: simulated swing.

insight into how high the iterative controller gain can be during human subject testing.

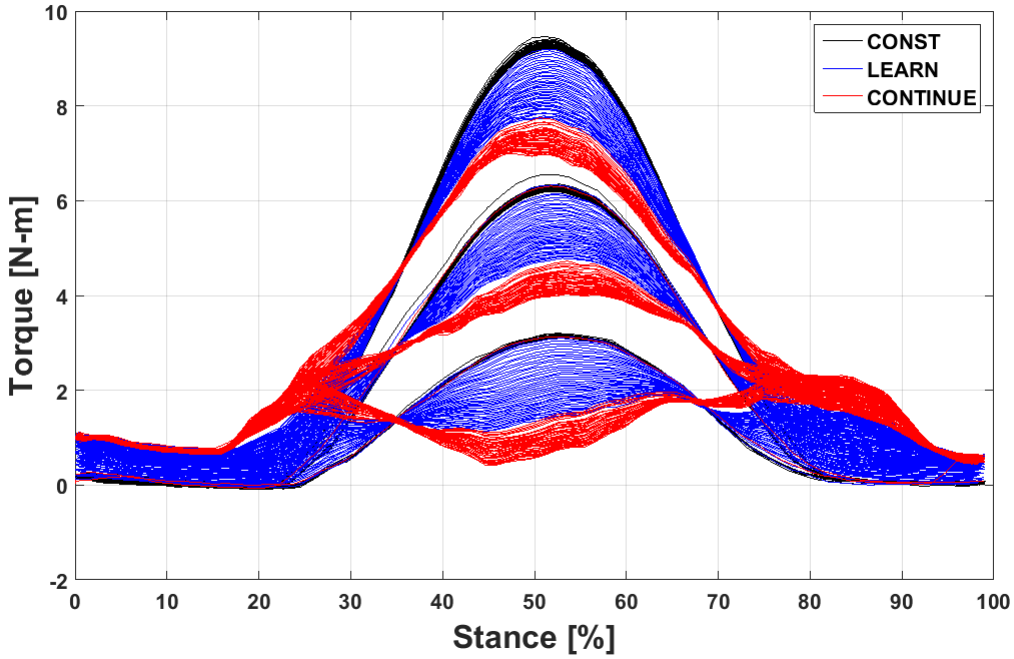

Figure 4.5: Stance torque during iterative controller operation during simulated gait. Black: iterative controller off, blue: iterative controller on, first 120 steps, red: iterative controller on, next 120 steps.

Chapter 5
HUMAN SUBJECT PROTOCOL DEVELOPMENT

Preliminary human subject testing was performed on two subjects. The goals of the preliminary tests were to evaluate the device performance and test procedures, to develop the test protocol, and to develop a strategy for controlling the transverse-plane equilibrium angle. Because the test protocol for the two subjects was different, the test method is presented separately for Subject 1 and Subject 2.

5.1 Methods

5.1.1 Subject 1

The primary objective of the first human subject test was to determine whether the TAP would be able to handle the rigors of human subject testing. The TAP performed well, inspiring enough confidence in the subject that he wore it on an unscheduled trip outside the gait lab. One problem observed with the TAP is that it rotated a small amount (about 2°) each time it was powered up. This led to a software change allowing adjustment of the neutral position before the second test.

The secondary objective of the test was to develop test procedures. For this test, TAP configuration changes were performed using an SD card. Changing mode or settings required removing the SD card from its slot on the TAP, inserting it into a laptop, opening, editing, and saving the settings file, ejecting the card, powering down the TAP, installing the SD card in the TAP, and repowering the TAP. Data was also logged to the SD card. While the SD card interface was successfully used in this test, it was cumbersome and time consuming. This led to the addition of Wi-Fi communication and a graphical user interface (LegGUI) before the second test.

The tertiary objectives of the test were to develop the test protocol and evaluate the strategy of using sagittal-plane ankle rotation to drive the transverse-plane equilibrium angle. For this test, the iterative controller described in 3.4 was used. Initially, the iterative controller was disabled and the TAP was configured to provide a rotational stiffness of 4 N-m/deg. After the subject was fitted with the TAP by a prosthetist, the subject was given five minutes of walking on the treadmill at his self-selected speed to become accustomed to the TAP and the treadmill. The iterative controller was then enabled and the subject walked on the treadmill for an additional five minutes. The equilibrium position function was saved at the end of the five minutes. After this, reflective markers were placed on the subject's body for use with the motion capture system. The subject then walked over force plates embedded in the floor. The subject performed 5 trials each of straight-line walking and clockwise and counterclockwise walking on a circle with a radius of 1 m. These tasks were repeated with the saved equilibrium position function and with a constant equilibrium position, as well as with the subject's prescribed prosthesis.

5.1.2 Subject 2

The primary objectives of the second human subject test were to explore the effects of different walking conditions and iterative controller gains on the equilibrium position function. The subject was fitted with the TAP by a prosthetist. The subject was then given five minutes of walking on the treadmill at his self-selected speed to become accustomed to the TAP and the treadmill. The subject then walked on the treadmill with the iterative controller enabled with three different gains. The subject then walked on a 1-m radius circle and a 1.6-m radius circle with the prosthetic limb on the inside with the iterative controller enabled.

The secondary objective of the test was to evaluate the new Wi-Fi interface and LegGUI. The wireless interface worked well, recorded all data, and made configuration changes much more convenient than the SD card interface. Future testing will use LegGUI and Wi-Fi.

5.2 Results

5.2.1 Torque Reduction by Iterative Control during Straight-Line Walking

Both subjects experienced a decrease in the transverse-plane socket torque measured by the TAP during straight-line walking with the iterative controller operating. Figure 5.1 shows the socket torque over the stance phase of gait during treadmill walking. Both subjects experienced a peak torque reduction greater than 30% from the initial steps to the final steps.

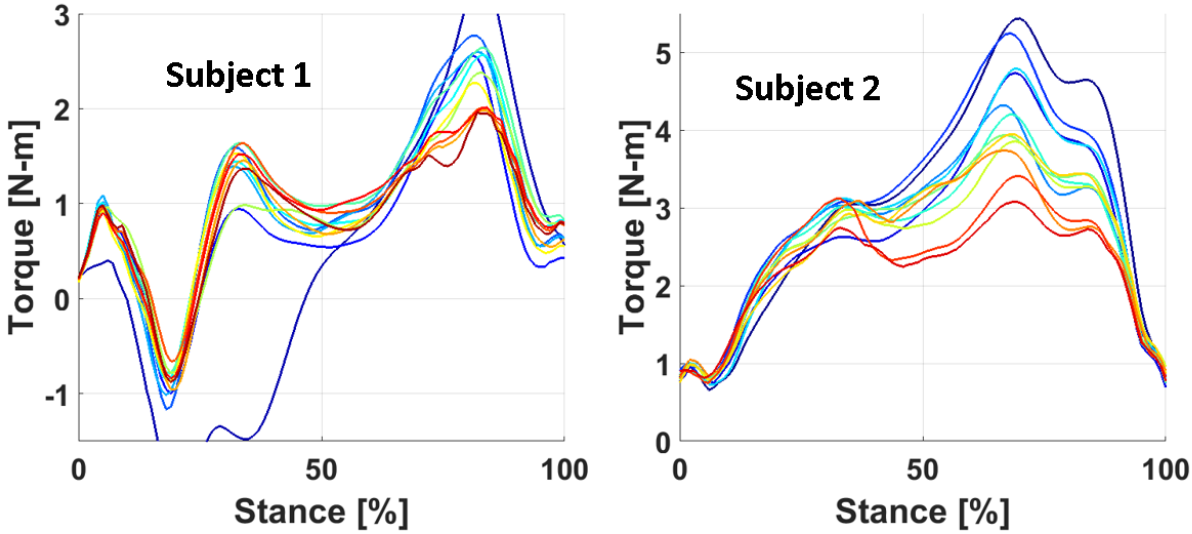

Figure 5.1: Ten-step average stance-phase TAP torque during operation of the iterative controller in treadmill walking at self-selected speed. Time progresses from the dark blue curve to the dark red curve.

This torque reduction was accompanied by increase transverse-plane rotation in both subjects. Figure 5.2 shows the rotation over the stance phase of gait during treadmill walking. Figure 5.3 shows the torque plotted against the rotation. The slope of this curve is the quasi-stiffness of the joint. Both subjects show a large decrease in the quasi-stiffness of the joint over the operation of the iterative controller. This decrease in quasi-stiffness comes without any change to the stiffness of the joint. Interestingly, while Subject 1's torque-rotation

curves show little hysteresis, Subject 2's curves enclose significant area, which increases as the quasi-stiffness decreases. This means that energy is being dissipated in the joint during walking.

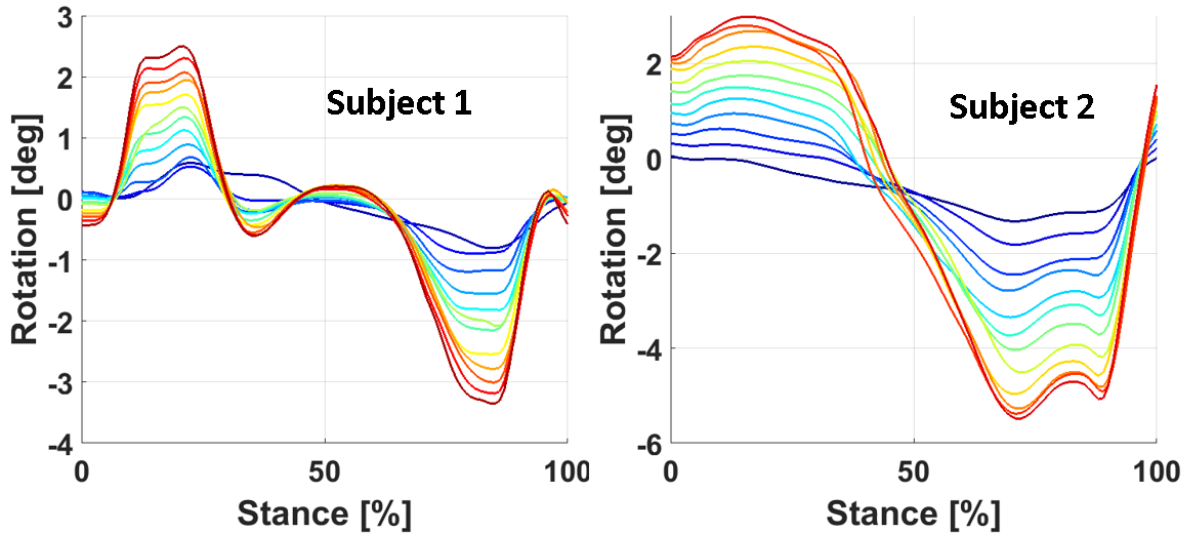

Figure 5.2: Ten-step average stance-phase TAP rotation during operation of the iterative controller in treadmill walking at self-selected speed. Time progresses from the dark blue curve to the dark red curve.

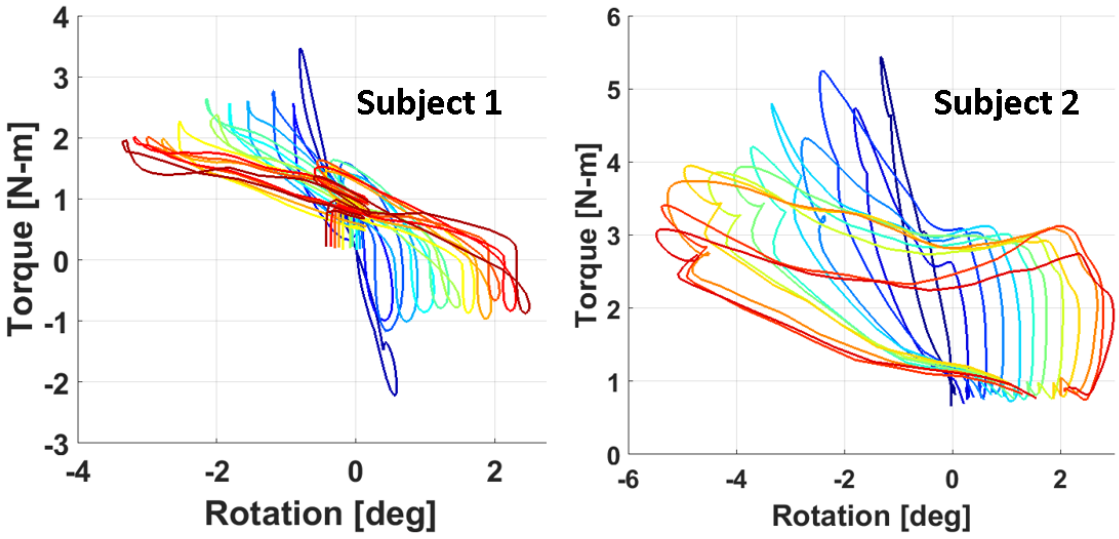

Figure 5.3: Ten-step average stance-phase TAP torque vs. rotation during operation of the iterative controller in treadmill walking at self-selected speed. Time progresses from the dark blue curve to the dark red curve.

5.2.2 Torque Reduction during Circular Walking

Subject 1 performed circular walking with the equilibrium function obtained from training during treadmill walking. No substantial difference in socket torque was seen between the trials using this equilibrium position function and those using a constant equilibrium position. Subject 2 performed circular walking with the iterative controller active and the prosthetic limb on the inside of the turn, and showed a decrease in socket torque as training progressed. However, Subject 2 did not perform circular walking with any steady-state equilibrium position function. Overall, the results for circular walking are inconclusive, but suggest that iterative controller training should occur during circular rather than straight-line walking if the equilibrium position function is to reduce socket torque during circular walking.

5.2.3 Effect of Iterative Controller Gain

During the second human subject test, identical walking tasks were repeated with different iterative control gains. Figure 5.4 shows the equilibrium position functions obtained during treadmill walking with three different iterative controller gains spanning an order of magnitude. The equilibrium position functions are nearly the same, demonstrating insensitivity to iterative controller gain in this range.

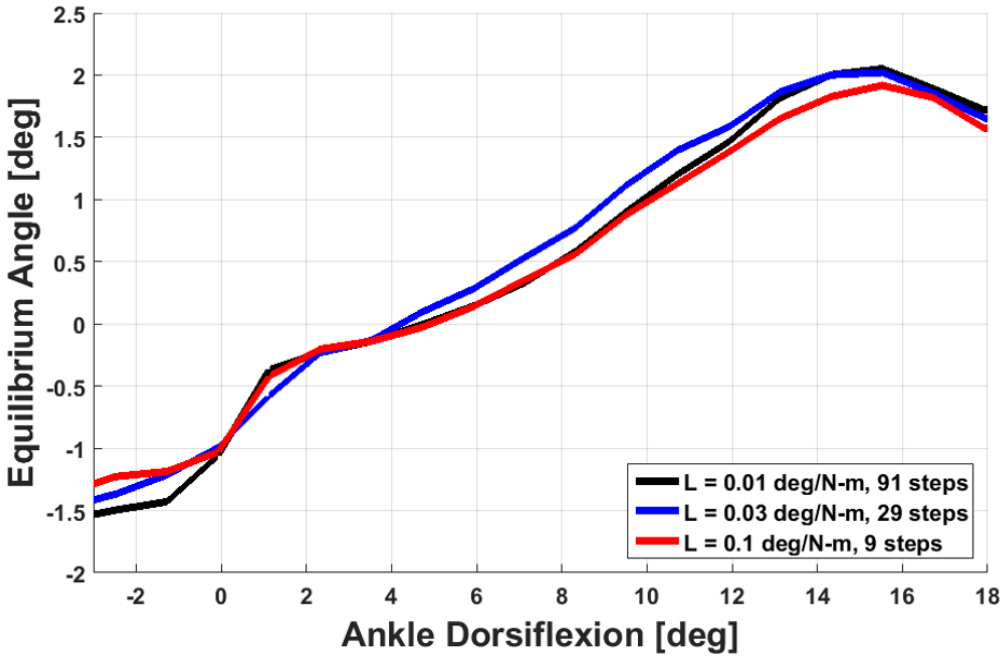

Figure 5.4: Comparison of equilibrium position functions obtained with different values of iterative controller gain L during treadmill walking

5.2.4 Iterative Controller Convergence

The target of the iterative controller was a uniform torque distribution over stance phase. If this target were achieved, the equilibrium position function would stop changing and convergence would be obtained. Figure 5.5 shows that this did not occur for any of the

training conditions. Instead, the ankle rotation kept increasing to very high values (over 16°) approaching the amount of ankle rotation in the sagittal plane. This caused the subject to comment that it "wasn't how he walked" and felt like there was a banana peel under his foot. The failure to converge can also be seen in Figure 5.1, which shows that the torque distribution does not become uniform over the course of training.

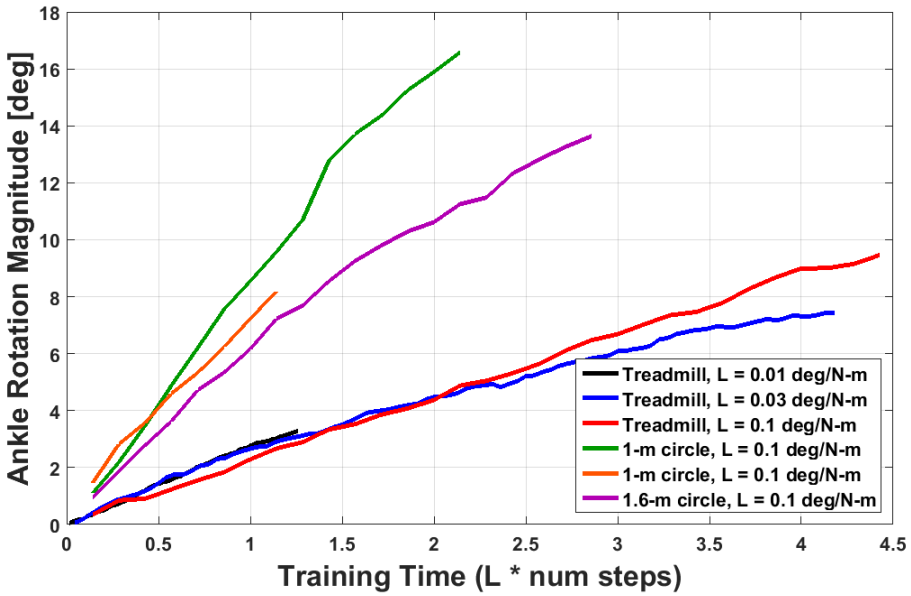

Figure 5.5: Overall magnitude of ankle rotation over the course of training for Subject 2. None of the conditions achieved convergence.

5.2.5 Equilibrium Position Functions

The output of each training session with the iterative controller was the rotational equilibrium position as a function of sagittal-plane ankle rotation. Figure 5.6 shows the shape of the equilibrium position function for both subjects. Because convergence was never obtained, the equilibrium position functions have been normalized by their total range. Iterative controller training was not performed during circular walking for Subject 1. However, Subject 1 did perform circular walking with a constant equilibrium position. The data from this trial were

used to produce the "simulated" curve shown in Figure 5.6.

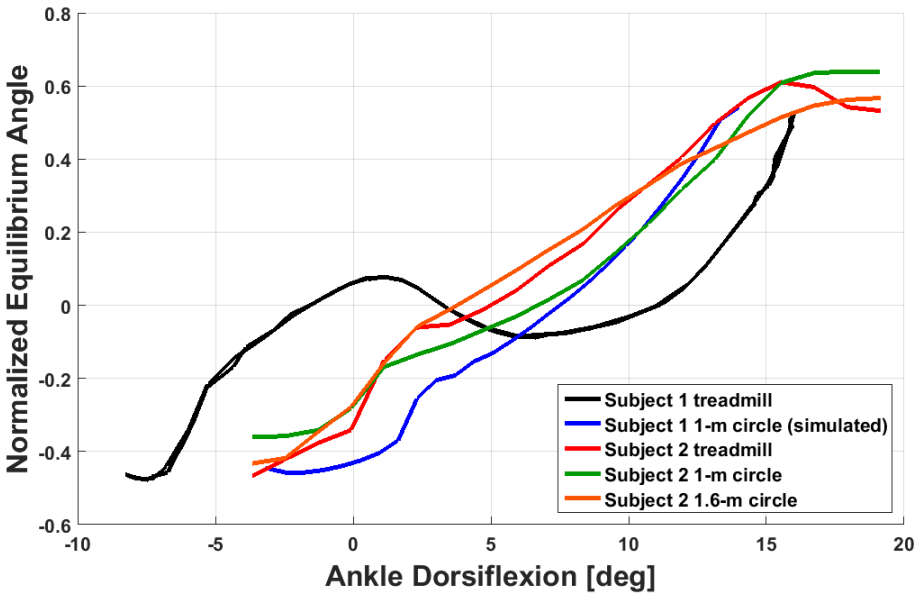

Figure 5.6: Normalized equilibrium position functions at the end of training for two human subjects. With one exception, the curve shapes are similar across subjects and training conditions.

5.3 Discussion

Preliminary testing demonstrated the feasibility of conducting human subject testing with the TAP and reducing socket torque during walking using a rotational equilibrium position that varies as a function of sagittal-plane ankle rotation. It also provided an opportunity to adjust testing procedures and improve the configuration and data communication interface.

The iterative controller used in the first two human subject tests attempted to produce an uniform torque distribution during stance in conjunction with the mechanics of the subject. The failure of the iterative controller to converge suggests that the uniform torque distribution target is not achievable. As Figure 5.1 shows, the iterative controller successfully reduced and flattened the torque peak that occurred in late stance for both subjects, but

had little effect on the torque during early stance. This may be because in early stance, there is little weight on the foot, and what weight there is is concentrated at the heel. Because of this, TAP rotation may result in rotation of the foot relative to the floor rather than rotation of the socket relative to the foot. In order for the TAP to modify the torque curve, the foot must remain fixed to the floor to provide a reaction torque.

Convergence could possibly be achieved by adding a term to penalize excessive rotation, but such a term would not have a physical basis and would require ad hoc tuning. Perhaps a better approach to achieving convergence would be to have the iterative controller attempt to flatten the torque curve in only the last 60 or 70 percent of stance phase. This might present an achievable target for the iterative controller.

Despite the lack of convergence, torque reduction was achieved using the iterative controller. In addition, the equilibrium position functions obtained during training had similar shapes across two subjects and three training conditions, as shown in Figure 5.6. The one equilibrium position function that does not match the others is Subject 1's straight-line walking function. Subject 1 showed an unusual negative torque peak in early stance and an overall low torque magnitude. Even so, the overall trend of transverse-plane rotation angle increasing with ankle dorsiflexion was still present.

The similarity and simplicity of the equilibrium position function curves in Figure 5.6 suggest that a single equilibrium function could work for multiple subjects. The shape of the curves suggest that a simple linear relationship between transverse-plane equilibrium position and sagittal-plane rotation could be used so that $\theta_d = CR \times \beta$, where CR is the "coupling ratio". Conventional prosthetic feet already exhibit this behavior with $CR = 0$ and a high transverse-plane stiffness K^*. In the limit of infinite transverse-plane stiffness, the transverse-plane rotation becomes equal to the equilibrium position and $\theta_s = CR \times \beta$. In this case, ankle rotation occurs about an axis that has components normal to both the sagittal plane and the transverse plane and transverse-plane rotation is said to be "coupled" with sagittal-plane rotation. In the case of finite transverse-plane stiffness, it is actually the transverse-plane equilibrium position that is coupled with sagittal-plane rotation. This

axis coupling could be implemented relatively easily in a passive device, and can easily be emulated by the TAP. This technique was evaluated in subsequent human subject tests.

Chapter 6

HUMAN SUBJECT TESTING OF AXIS COUPLING

The results of preliminary human subject testing were used to develop the test protocol for further testing. This chapter includes presentation and discussion of the test methods and results.

6.1 Methods

6.1.1 Participants

The 3 transtibial amputees (0 females) who gave informed consent to participate in this Investigational Review Board-approved study had a mean age of 54 years (range: 47-66) with a mean body mass of 91.6 kg (range: 85.5-98.4) and mean height of 185 cm (range: 182-188). None of the subjects wore a torsion adapter with their usual prosthesis. All subjects met the following criteria:

- wore a prosthesis for at least 2 years before the study and 8 hours each day
- considered themselves moderately active community ambulators
- did not use upper-limb aids
- were free from neurological deficits that might have affected gait characteristics by self-report

All subjects wore their own socket, liner and socks. The TAP was attached to the subject's socket and to a low-profile Vari-Flex foot whose size and stiffness category were selected by a research prosthetist. Table 6.1 shows the details of each subject's amputation type and prosthetic components.

Subject	Amputation Cause	Socket	Liner	Suspension	Foot	Socks
1	Infection from a traumatic MVA	TSB carbon fiber Socket	Ohio Willow Wood Alpha gel liner	Pin-lock	LP Vari-Flex Cat 6, size 27	1/2 1 ply sock
2	Traumatic	Carbon fiber	Ossur Iceross Sport	Pin-lock	LP Vari-Flex Cat 5, size 28 w/ red shim	2-ply + 3-ply
3	Traumatic	Test socket	Ohio Willow Wood silicone gel liner	Pin-lock	LP Vari-Flex Cat 6, size 27 w/ blue shim	6-ply

Table 6.1: Transtibial amputee parameters and prosthetic components used. MVA = motor vehicle accident, TSB = total surface bearing, LP = Low-profile, Cat = Category.

6.1.2 Prosthesis Fitting

The TAP was configured to act as a torsion spring with a 4 N-m/deg stiffness for prosthesis fitting. A research prosthetist installed and adjusted the TAP. Subjects were asked to walk back and forth while the prosthetist evaluated their gait. The prosthetist adjusted the height and orientation of the TAP and the prosthetic foot based on his observations and the subject's comments until both the prosthetist and the subject were satisfied with the alignment.

6.1.3 Experimental Procedures

Sixty-three 14 mm reflective markers were placed on each subject in locations consistent with a modified version of Vicon's Plug-In-Gait Model (Vicon, Centennial, CO). The Plug-In-Gait Model was modified by adding reflective markers at the medial malleolus, medial elbow, and first and fifth metatarsal heads of the feet. The thigh and upper arm segments were tracked with marker clusters as in [10] instead of wands. The shank segments were tracked with markers placed on the fibular head and tibial tuberosity instead of tibial wands. Height,

mass, and anatomical measurements were made according the Vicon requirements for static and dynamic modeling. Hip joint centers were calculated using regression equations using the inter-ASIS distance of the pelvis [5, 6]. Three additional 14 mm markers were used to track the portion of the TAP that rotates with the foot, and four additional markers were used to track the portion of the TAP that rotates with the shank. Gait kinematics were collected using a 12-camera Vicon system operating at 120 Hz. Ground reaction forces were collected using 8 force plates (AMTI, Watertown, MA) recorded at 1200 Hz.

Participants walked across force plates embedded in the laboratory floor in a straight line and both directions around a circle with a 1-m radius. Figure 6.1 shows the force plate configuration for straight-line and circular walking. The 1-m radius circle was marked with a dashed line on the floor. Participants were told that it did not matter whether they stepped on the line. Participants performed at least five trials each of straight, clockwise, and counterclockwise walking with each configuration of the TAP. Before beginning data collection trials with each configuration of the TAP, participants practiced each of the three walking tasks five times. Trials which did not contain at least one good force plate strike with each foot were repeated. Good force plate strikes were defined as steps during which a foot was placed entirely on a force plate that was not struck at all by the other foot.

Five configurations were used for the TAP. In each configuration the overall stiffness was set to 4 N-m/deg. Rotation of the transverse-plane equilibrium position was coupled to sagittal-plane ankle rotation with ratios of 0, 1:3, and 1:2. Two subjects also performed the walking tasks with a coupling ratio of 1:6, and one of these also tested a coupling ratio of 1:4. The order of the configurations was randomized for each subject. All data for a single TAP configuration was collected before changing to the next configuration.

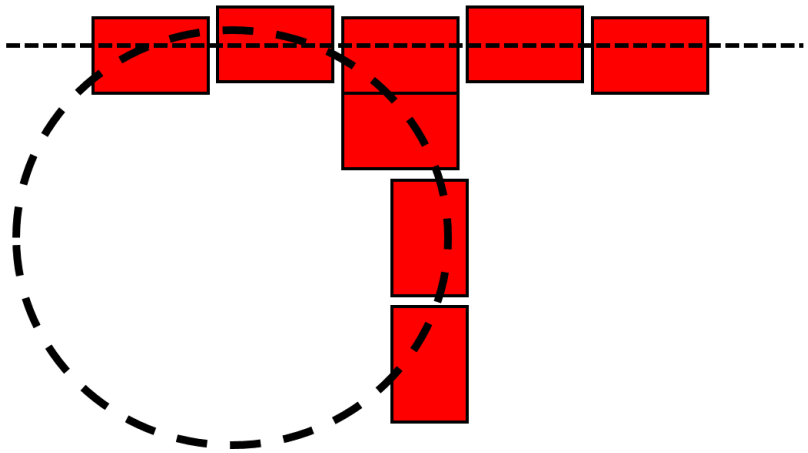

Figure 6.1: Force plate configuration. The red rectangles represent the force plates as seen from above. The dashed lines represent the paths for the straight-line and circular walking tasks.

6.1.4 Data Analysis

Gait kinematics, kinetics, and gait event timings were calculated using Visual3D software (C-Motion, Inc., Germantown, MD). Marker positions were filtered with a bidirectional Butterworth filter with a 6 Hz cutoff frequency. Ground reaction forces were filtered with a bidirectional Butterworth filter with a 25 Hz cutoff frequency. Data were exported to MATLAB (MathWorks, Natick, MA) for further processing, such as coordinate transformation, time normalization, and peak extraction. Shank torque in the prosthetic leg was measured using the TAP torque transducer. This measurement was available on all prosthetic leg steps, including those that did not have a good force plate strike. Other joint moments were only available during good force plate strikes.

Instantaneous walking speed was calculated by finite differences of the horizontal position of the center of mass. For straight walking trials, the average walking speed was calculated over a 6 m distance in the center of the walking path. For circular walking, the average walking speed was calculated over a 180 degree angle in the center of the walking path. Data from sensors on the TAP were analyzed independently from motion-capture data, except

that the average walking speed calculated from motion-capture data was applied to all TAP data obtained from the same trial.

6.1.5 Inertial Modeling

Body segment inertial parameters (BSIPs) are needed to propagate ground reaction forces up the kinematic chain to determine joint moments. A sixteen-segment human body model was used with segments chosen to match the body segments used by Zatsiorsky and Seluyanov [103]. The prosthetic-side shank was modeled as a rigid segment, so that TAP rotation was resolved at the ankle joint. BSIPs for intact body segments were estimated using de Leva's adjustments [15] to Zatsiorsky and Seluyanov's anthropometric data [103, 104] of college-age Caucasians. de Leva modifed the BSIPs to reference them to joint centers as opposed to bony landmarks and to make the mass of the segments proportional to total body mass.

de Leva's BSIPs are referenced to total body mass with both legs intact. Since the measured mass of amputee subjects includes the mass of the prosthetic leg instead of an intact leg, body segment masses were calculated using an adjusted mass, A, which is the estimated mass of the subject with both legs intact. The adjusted mass is calculated by subtracting the weight of shoes and the prosthetic-side shank and foot from the measured body mass and adding the estimated mass of the intact shank and foot. Figure 6.2 shows the concept behind the calculation of the adjusted mass. The prosthetic-side shank mass was estimated as 0.65 times the mass of the intact-side shank [88] plus the additional mass of the TAP. Shoe mass was estimated as 300g each, based on a typical running shoe. Thus

$$A = M - 2M_{shoe} - M_{pros\,foot} - M_{pros\,shank} + f_{foot}A + f_{shank}A \tag{6.1}$$

where M is measured body mass, M with a subscript is component mass, and f is the fraction of body mass in the subscripted body segment, obtained from anthropometric data. The mass of the prosthetic shank is estimated as

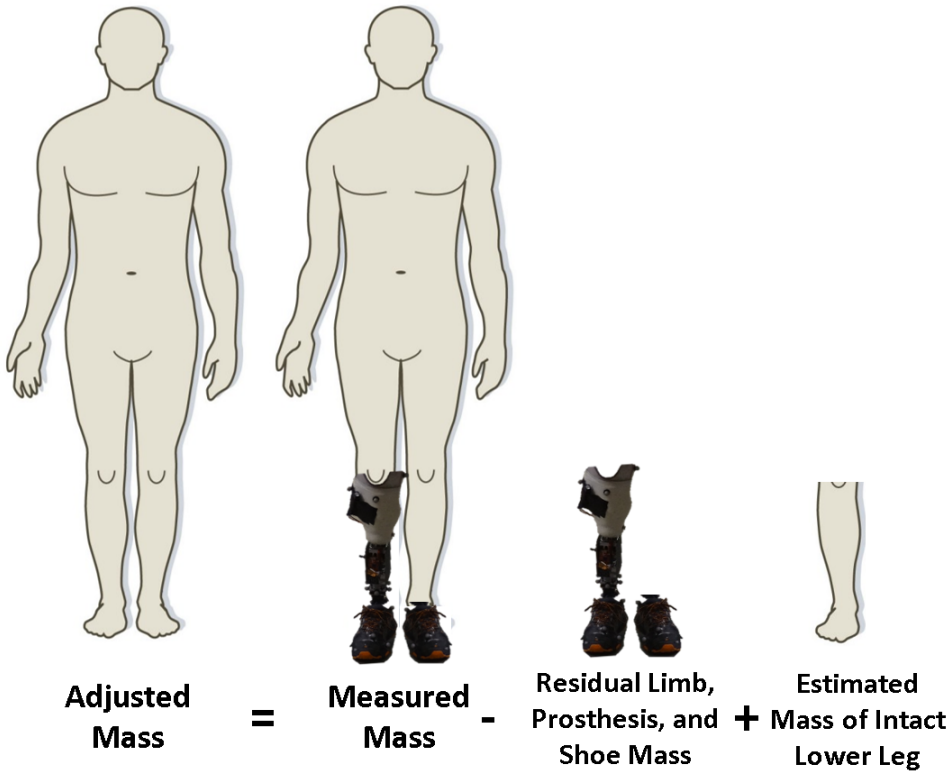

Figure 6.2: Conceptual diagram of the calculation of adjusted mass A.

$$M_{pros\ shank} = 0.65 f_{shank} A + \Delta M_{TAP} \tag{6.2}$$

where ΔM_{TAP} is the additional weight of the TAP compared to a conventional prosthetic shank. Combining equations 6.1 and 6.2 gives

$$A = \frac{M - 2M_{shoe} - M_{pros\ foot} - \Delta M_{TAP}}{1 - f_{foot} - 0.35 f_{shank}} \tag{6.3}$$

Subject 3 had an above-elbow arm amputation and did not wear an arm prosthesis. A similar procedure was used to include the effect of the missing arm in the calculation of A. The mass of the residual arm was estimated to be 30% of the mass of the intact upper arm segment. A custom fourteen-segment model was created for this subject, for whom

$$A = \frac{M - 2M_{shoe} - M_{pros\,foot} - \Delta M_{TAP}}{1 - f_{foot} - 0.35f_{shank} - f_{hand} - f_{forearm} - 0.7f_{upper\,arm}} \tag{6.4}$$

6.1.6 Statistical Analysis

Data were analyzed using linear mixed effect models. Analyses were performed using MATLAB R2015b with the Statistics and Machine Learning Toolbox version 10.1. Analysis of the straight(ST), prosthesis inside(PI), and prosthesis outside(PO) trials were performed independently, and no analyses were performed across trial types. To assess whether coupling ratio affected gait parameters, the alpha level of statistical significance was set at $p \leq 0.05$.

The effect of coupling ratio on walking speed was analyzed using a linear model with walking speed as the dependent variable, a fixed effect for coupling ratio, and a random effect for coupling ratio grouped by subject. Because of the strong influence of walking speed on other gait parameters [45, 50, 63], all other gait parameters were analyzed using a linear model with fixed effects for walking speed and coupling ratio, and a random effect for coupling ratio grouped by subject. Kinetic measures were normalized by body mass prior to statistical analysis.

6.2 Results

6.2.1 Walking Speed

All walking trials were performed at the subject's self-selected speed. It was hypothesized that higher values of coupling ratio would cause an increase in self-selected walking speed in the PI and ST trials due to a more comfortable gait pattern for the amputee. However, all subjects showed a trend toward lower walking speed with increased coupling ratio in the PI condition. Figure 6.3 shows the effect of coupling ratio on walking speed. Subject data are shown as a box and whiskers, with data each subject plotted with a subject-unique color. The box and whiskers represent the four quartiles of the data, and outliers are shown as individual circles. The thick black line represents the model estimate of the fixed effect of

coupling ratio on walking speed, and the grey region around it represents the 95% confidence interval. The p-values given in the title bar are in reference to the null hypothesis that the slope of the line is zero. The decrease in walking speed with increasing coupling speed is strongest in the PI trial type.

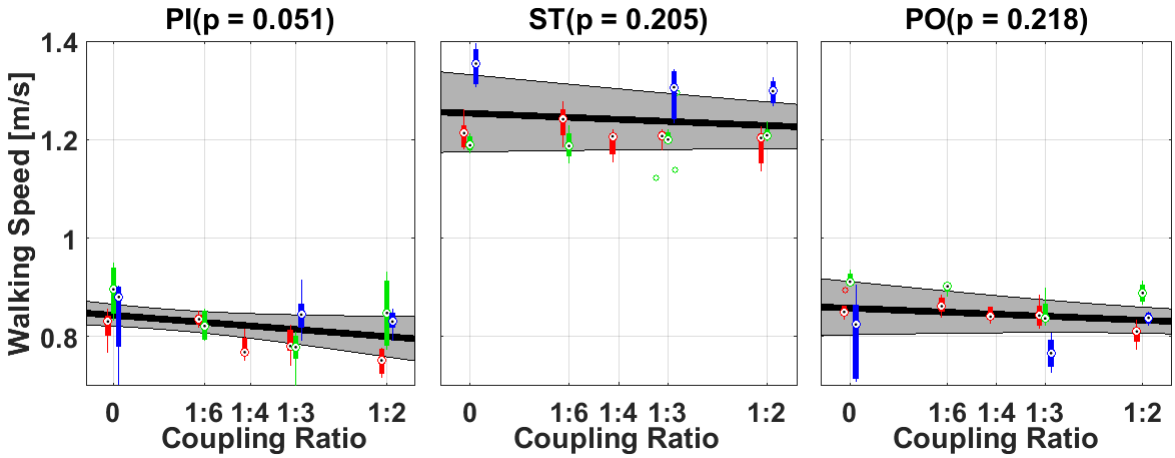

Figure 6.3: Effect of coupling ratio on walking speed. The boxes and whiskers show quartiles of per-trial data, with each subject shown with a unique color. The black line shows the estimated fixed effect and the grey region shows the 95% confidence interval for the estimate. PI = prosthesis inside, ST = straight, PO = prosthesis outside. The p-values are for nonzero slope of walking speed vs. coupling ratio.

6.2.2 Transverse- and Sagittal-Plane Ankle Rotation

The coupling ratio strongly influences the amount of ankle rotation about an axis aligned with the shank. Figure 6.4 shows the ankle rotation of the prosthetic and intact limb during the three walking trial types. Only trials using the minimum (0) and maximum (1:2) coupling ratios are shown for clarity. Positive rotation is defined as external rotation of the shank relative to the foot. The shape of the rotation curve is similar across trial types. For the intact ankle, neutral rotation is defined as the rotation at heel strike. The intact ankle exhibits little rotation until a large external rotation occurs at pushoff. The prosthetic ankle exhibits internal rotation immediately after pushoff, followed by a gradual external rotation

during midstance and a return to neutral rotation during pushoff. Figure 6.5 shows the effect of coupling ratio on ankle rotation. The magnitude of prosthetic ankle rotation increases dramatically with increasing coupling ratio. The rotation of the intact ankle is unaffected by coupling ratio.

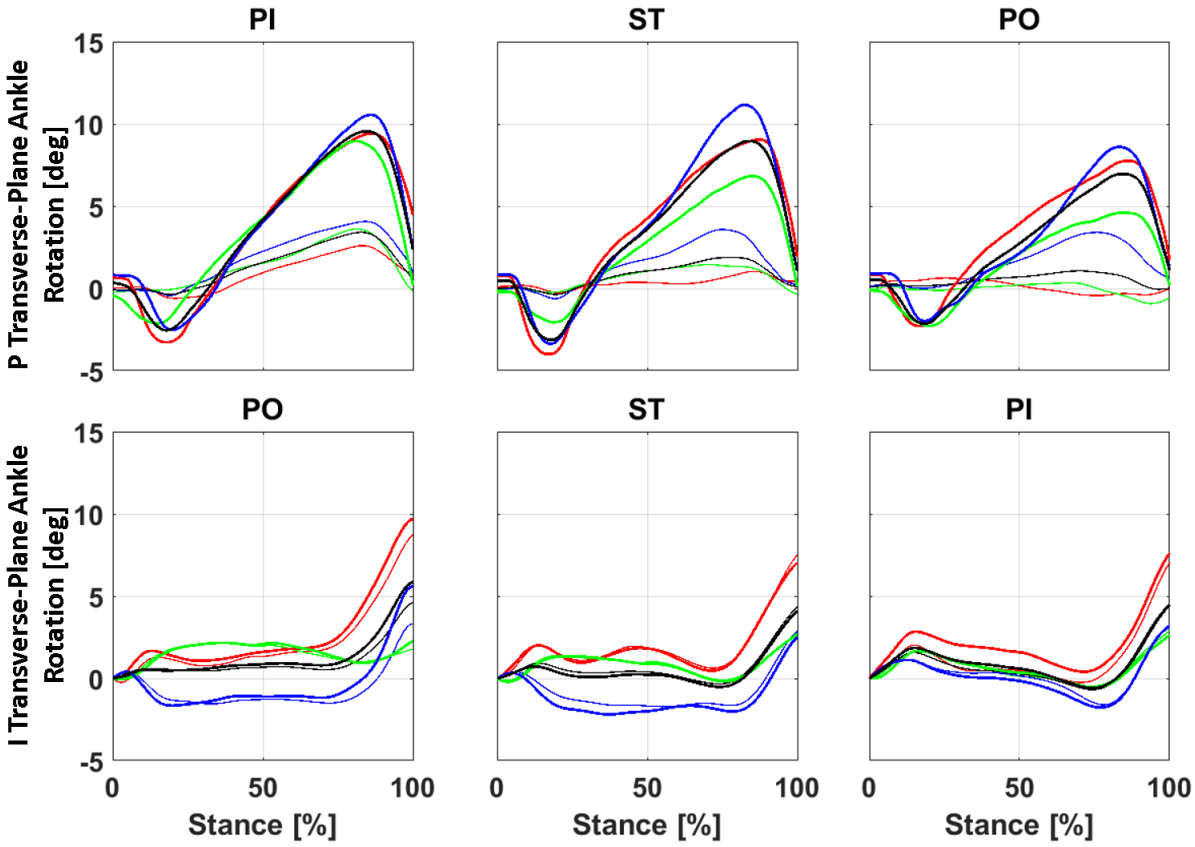

Figure 6.4: Transverse-plane ankle rotation during stance. Each color shows the mean for a particular subject. Black is the mean across all subjects. Thin lines show the mean at coupling ratio zero, thick lines show the mean at coupling ratio 1:2. Other coupling ratios are not shown for clarity. P = prosthetic side, I = intact side, PI = prosthesis inside, ST = straight, PO = prosthesis outside.

The ankle rotation and ankle moment are both typically substantially higher in the sagittal plane than in the transverse plane. For this reason, the TAP uses sagittal-plane ankle rotation to effectively drive axial rotation. However, coupling sagittal-plane ankle rotation

to axial rotation may also affect sagittal-plane rotation. Figure 6.6 shows the sagittal-plane ankle rotation during stance for the prosthetic and intact limbs. Neutral sagittal-plane ankle rotation is defined as the sagittal-plane ankle rotation at heel strike for both prosthetic and intact ankles. Both prosthetic and intact ankles show initial plantarflexion just after heel strike. In the prosthetic ankle, dorsiflexion rises at a nearly constant rate until late stance when the foot returns to the neutral position. In the intact ankle, dorsiflexion generally rises during midstance, but has a local maximum at about 35% of stance. At the end of stance, there is a fast motion from dorsiflexion to plantarflexion during pushoff. Figure 6.7 shows the effect of coupling ratio on sagittal-plane ankle rotation. The range of sagittal-plane ankle rotation is more variable in the intact ankle than the prosthetic ankle, both across subjects and across trials for a given subject. Coupling ratio does not show a statistically significant effect on sagittal-plane ankle rotation in either ankle.

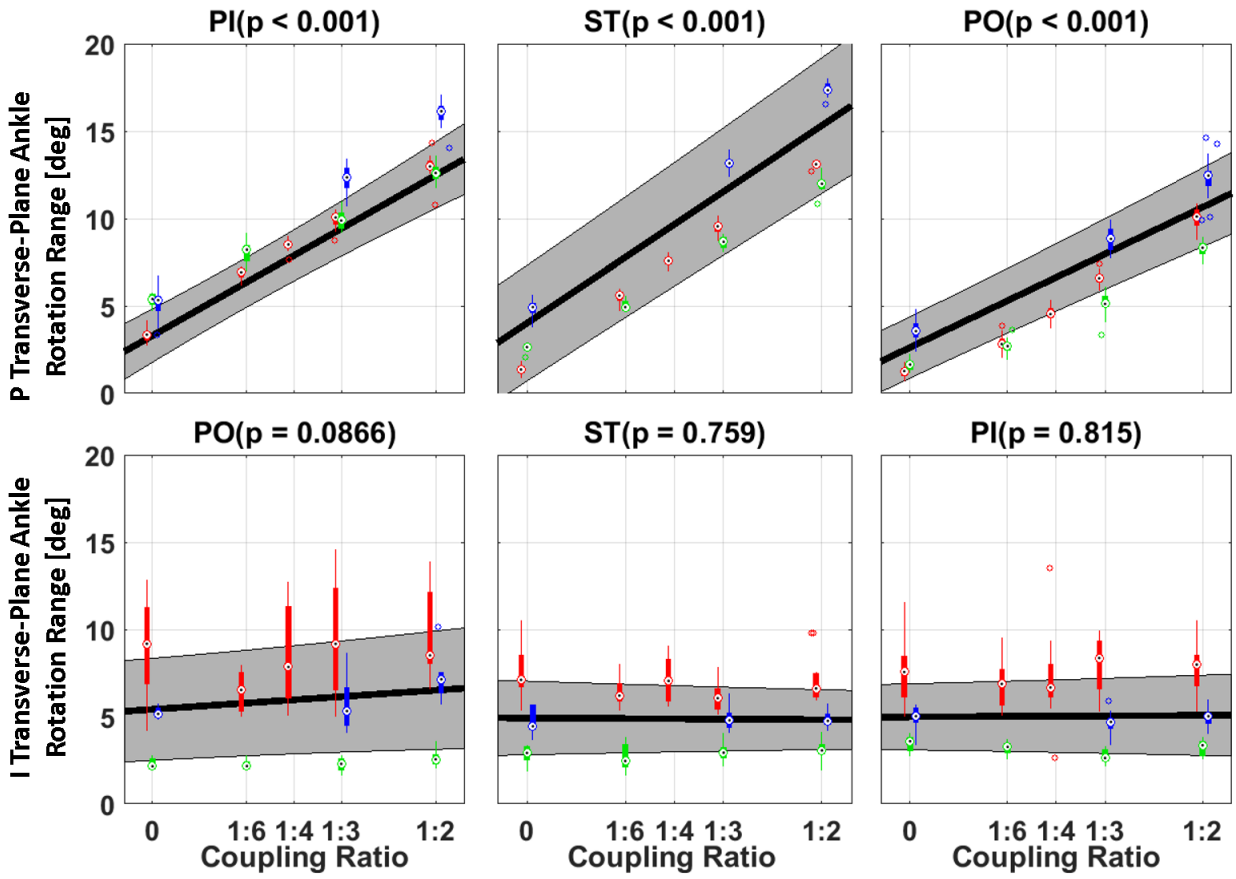

Figure 6.5: Effect of coupling ratio on total range of ankle transverse-plane rotation during stance. The boxes and whiskers show quartiles of per-trial data, with each subject shown with a unique color. The black line shows the estimated fixed effect and the grey region shows the 95% confidence interval for the estimate. P = prosthetic side, I = intact side, PI = prosthesis inside, ST = straight, PO = prosthesis outside. The p-values are for nonzero slope of transverse-plane ankle rotation range vs. coupling ratio.

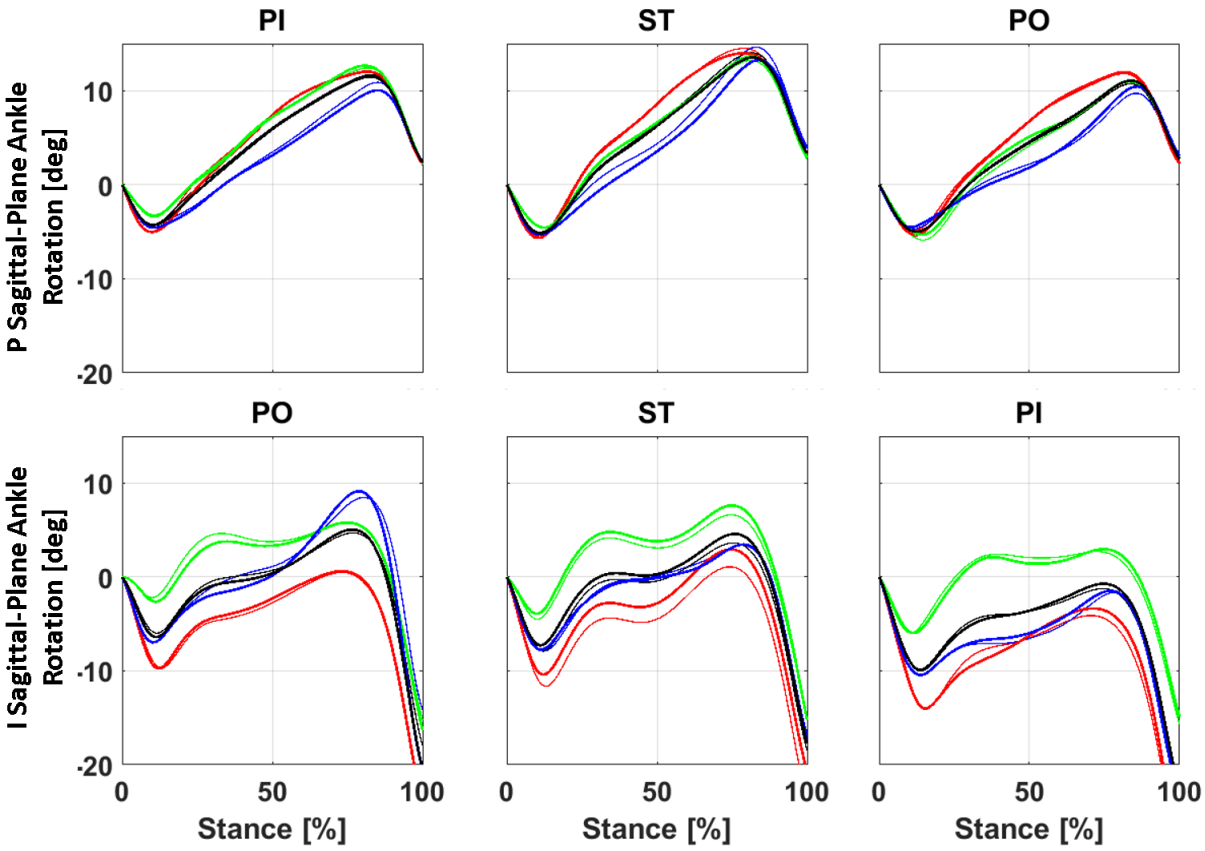

Figure 6.6: Sagittal-plane ankle rotation during stance. Each color shows the mean for a particular subject. Black is the mean across all subjects. Thin lines show the mean at coupling ratio zero, thick lines show the mean at coupling ratio 1:2. Other coupling ratios are not shown for clarity. P = prosthetic side, I = intact side, PI = prosthesis inside, ST = straight, PO = prosthesis outside.

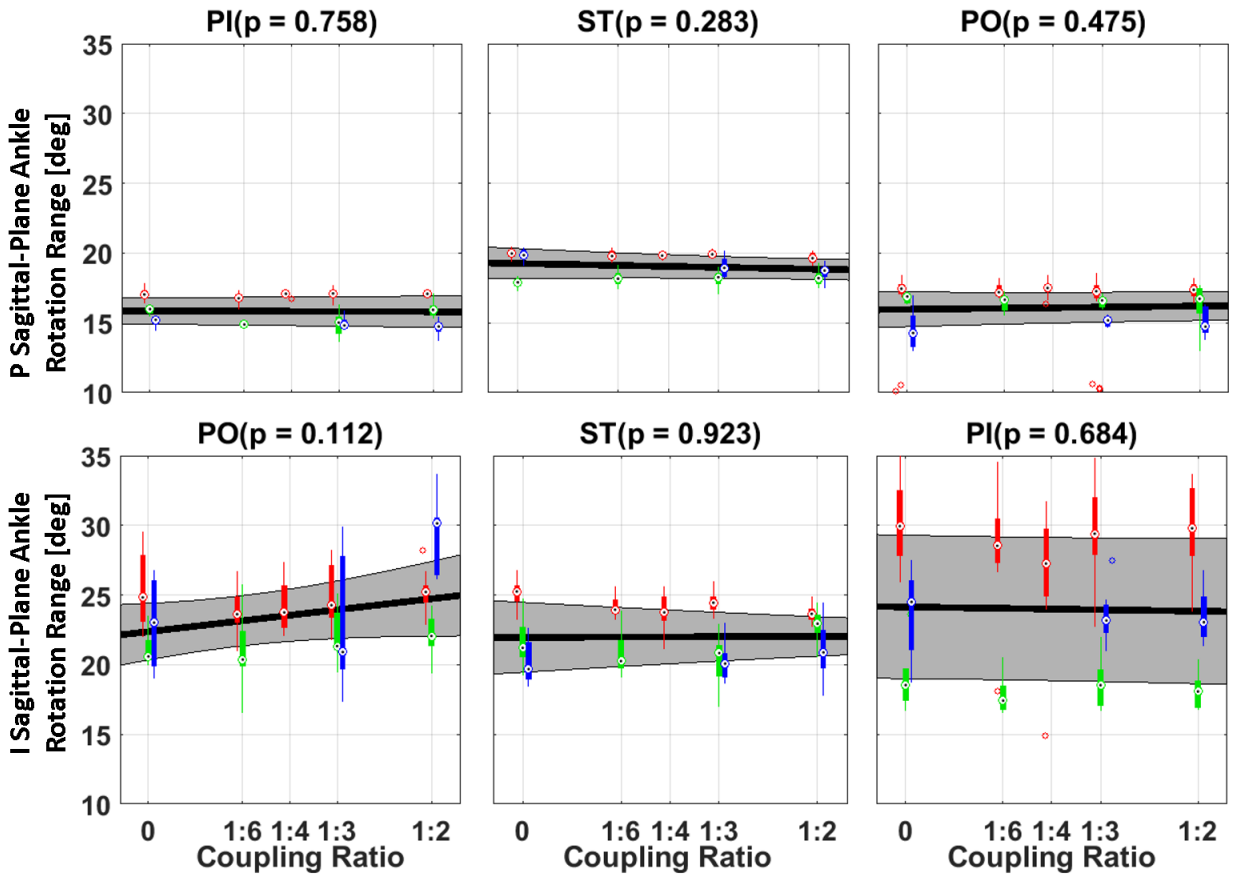

Figure 6.7: Effect of coupling ratio on total range of sagittal-plane ankle rotation during stance. The boxes and whiskers show quartiles of per-trial data, with each subject shown with a unique color. The black line shows the estimated fixed effect and the grey region shows the 95% confidence interval for the estimate. P = prosthetic side, I = intact side, PI = prosthesis inside, ST = straight, PO = prosthesis outside. The p-values are for nonzero slope of sagittal-plane ankle rotation range vs. coupling ratio.

6.2.3 Shank Torque

The iterative controller from which the axis-coupling scheme originated was designed to reduce peak shank torque, particularly during PI trials. Figure 6.8 shows the axial shank torque int the prosthetic ankle. Positive shank torque is defined as an internal rotation moment applied on the shank by the foot. In all three types of walking trials, the effect of coupling ratio on shank torque is minor during the first 30% or stance. In the final 70% of stance, the shank torque is reduced with increasing coupling ratio. Figure 6.9 shows the effect of coupling ratio on the minimum and maximum shank torque during stance. The first p-value given in the title bar is in reference to the null hypothesis that the slope of the trend line for the minimum shank torque is zero. The second p-value given in the title bar is in reference to the null hypothesis that the slope of the trend line for the maximum shank torque is zero. The reduction in maximum shank torque with increasing coupling ratio is statistically significant for the ST and PI trial types.

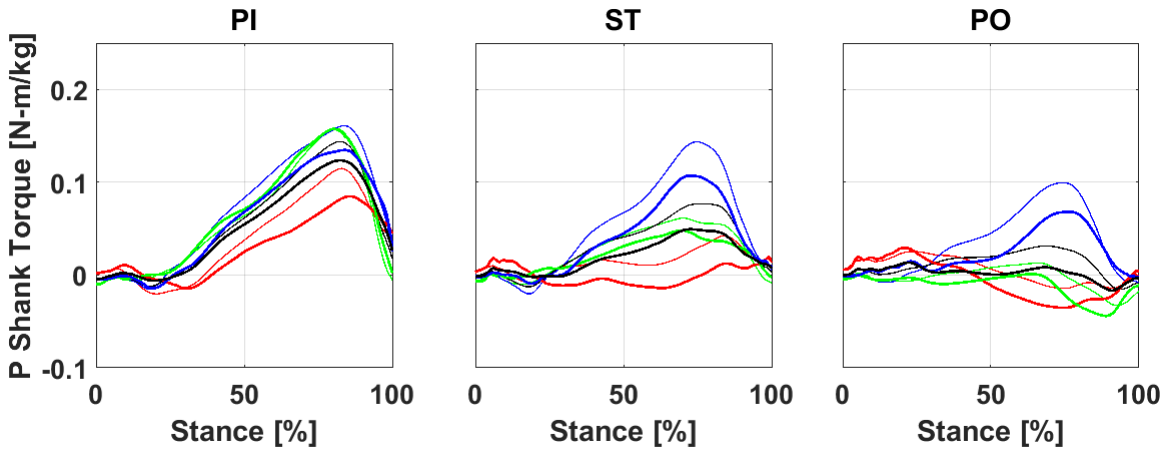

Figure 6.8: Axial shank torque in the prosthesis during stance. Each color shows the mean for a particular subject. Black is the mean across all subjects. Thin lines show the mean at coupling ratio zero, thick lines show the mean at coupling ratio 1:2. Other coupling ratios are not shown for clarity. P = prosthetic side, PI = prosthesis inside, ST = straight, PO = prosthesis outside.

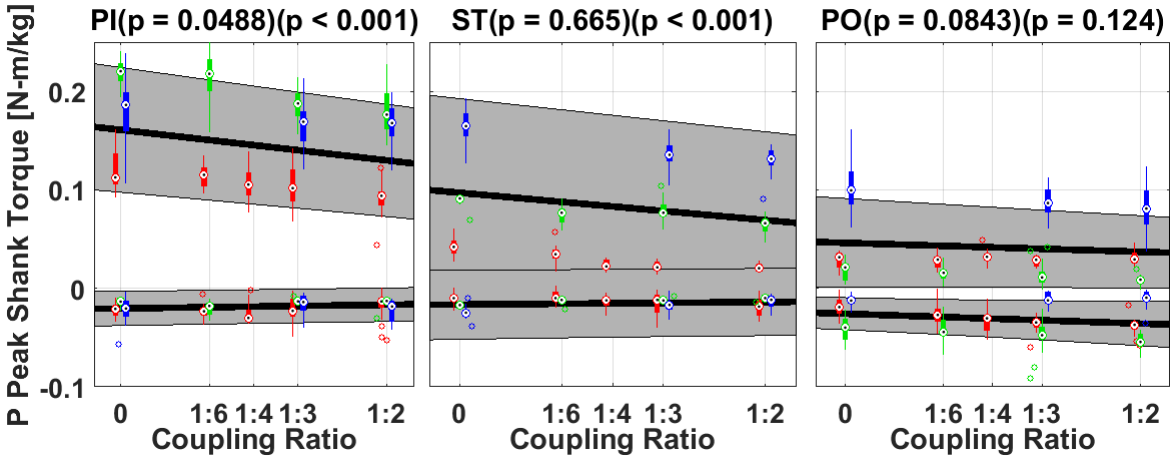

Figure 6.9: Effect of coupling ratio on minimum and maximum prosthetic-side shank torque. The boxes and whiskers show quartiles of per-trial data, with each subject shown with a unique color. The black line shows the estimated fixed effect and the grey region shows the 95% confidence interval for the estimate. P = prosthetic side, PI = prosthesis inside, ST = straight, PO = prosthesis outside. The first p-value is for nonzero slope of the minimum shank torque vs. coupling ratio; the second p-value is for nonzero slope of the maximum shank torque vs. coupling ratio.

Figure 6.10 shows the shank torque plotted against the axial ankle rotation. The slope of this curve is the quasi-stiffness of the ankle in the transverse plane. When the coupling ratio is zero, the quasi-stiffness of the ankle is equal to the stiffness, which was $K^* = 4$ N-m/deg. At higher values of coupling ratio, the quasi-stiffness becomes lower than the stiffness, even becoming negative for two subjects in the PO trial type. The quasi-stiffness changes between trial types, decreasing going from PI→ST→PO as the peak shank torque also decreases. This behavior is in contrast to the behavior of a torsion adapter, whose quasi-stiffness is always equal to its stiffness and cannot change between walking tasks.

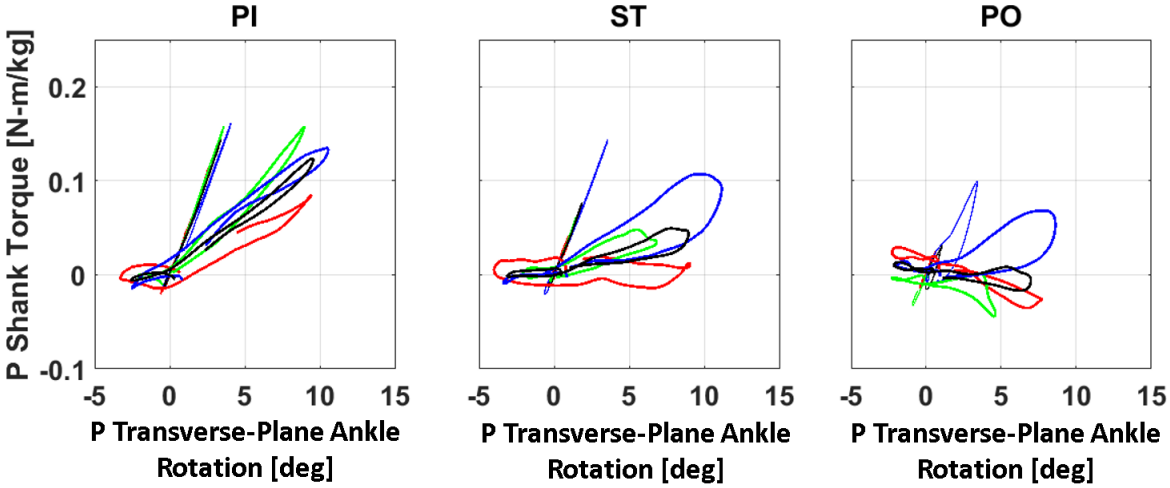

Figure 6.10: Torque-rotation behavior of the TAP. Each color shows the mean for a particular subject. Black is the mean across all subjects. Thin lines show the mean at coupling ratio zero, thick lines show the mean at coupling ratio 1:2. Other coupling ratios are not shown for clarity. P = prosthetic side, PI = prosthesis inside, ST = straight, PO = prosthesis outside.

6.2.4 Hip Power

Figure 6.11 shows the mean hip power for each subject during the three types of walking trials. While the subjects' hip strategies vary in early and midstance, all subjects show a large positive hip power near the end of stance. This positive hip power is exhibited on both prosthetic and intact legs, and is smallest in the inside leg of a turn. The maximum value of hip power that occurs near toe-off shows some decrease with increasing coupling ratio. Figure 6.12 shows the effect of coupling ratio on the positive and negative hip work during the gait cycle. The decrease in positive hip work is statistically significant for the prosthetic limb in the ST and PO trial types.

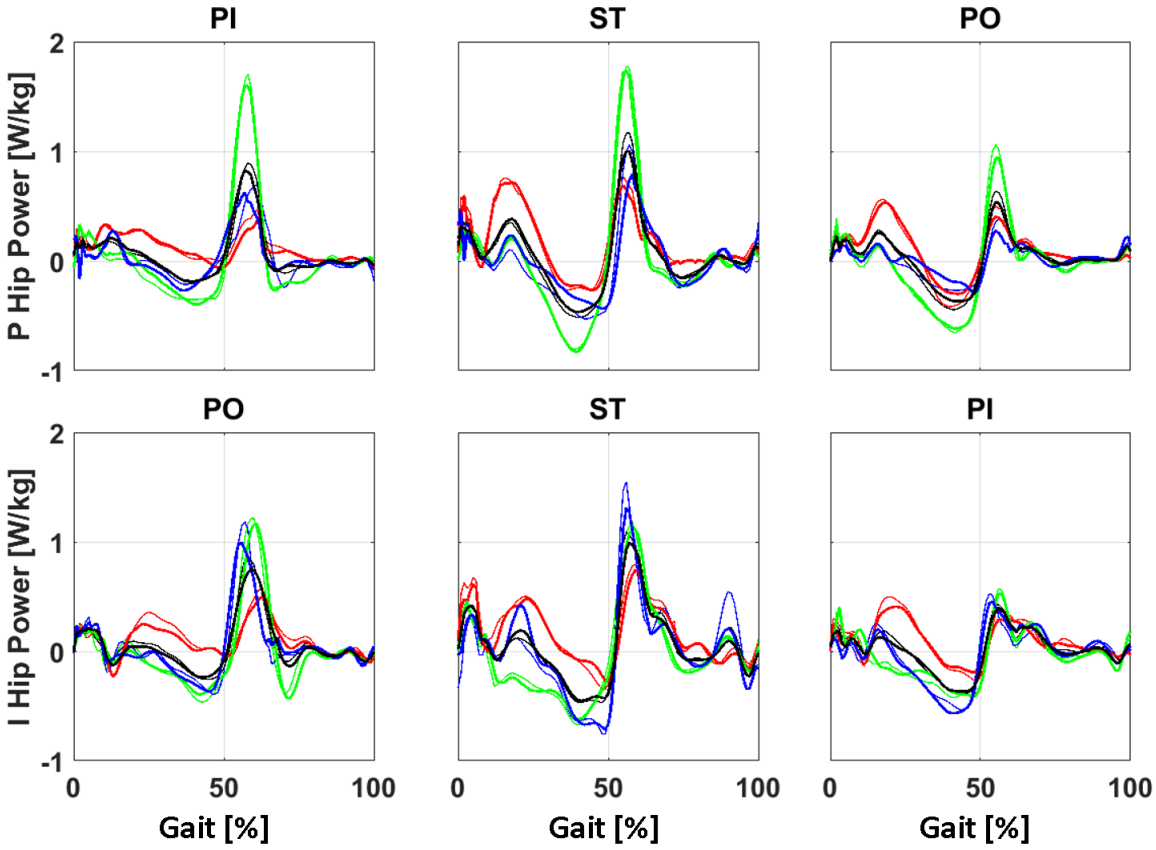

Figure 6.11: Hip power during the gait cycle. Each color shows the mean for a particular subject. Black is the mean across all subjects. Thin lines show the mean at coupling ratio zero, thick lines show the mean at coupling ratio 1:2. Other coupling ratios are not shown for clarity. P = prosthetic side, I = intact side, PI = prosthesis inside, ST = straight, PO = prosthesis outside.

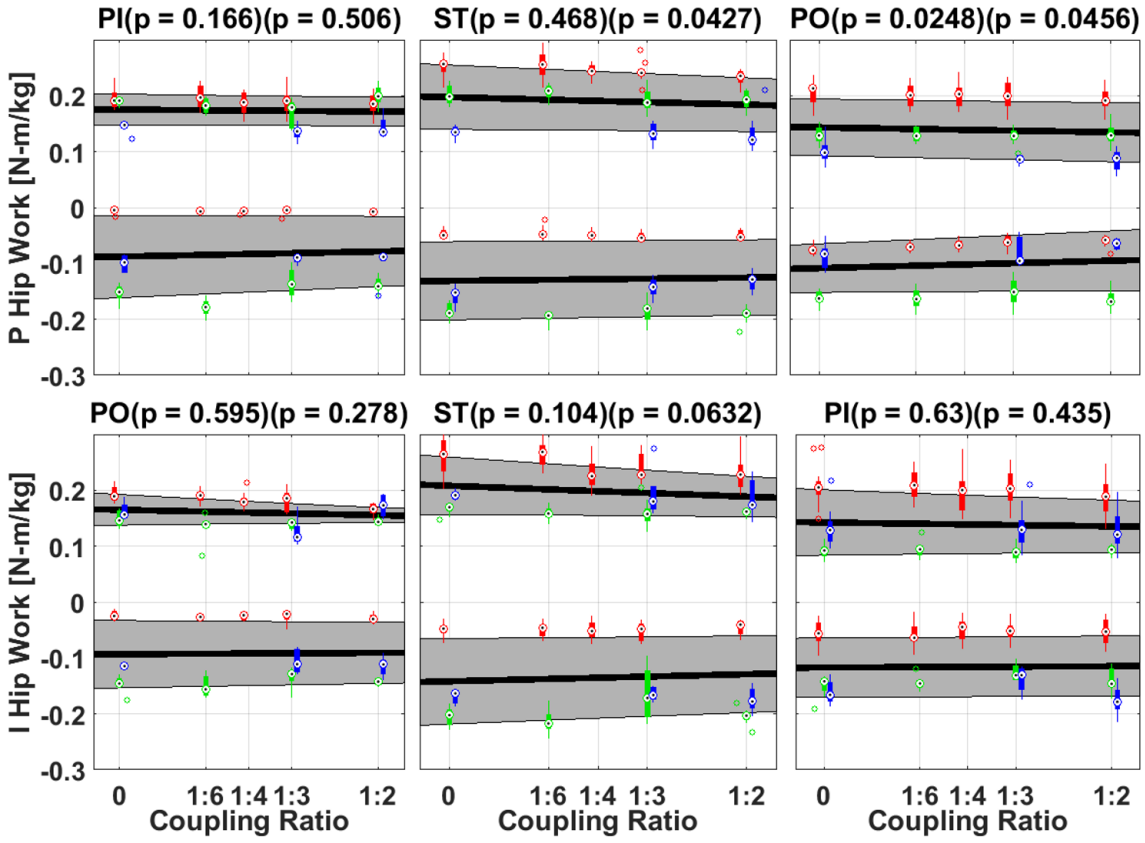

Figure 6.12: Effect of coupling ratio on positive and negative hip work during a gait cycle. The boxes and whiskers show quartiles of per-trial data, with each subject shown with a unique color. The black line shows the estimated fixed effect and the grey region shows the 95% confidence interval for the estimate. P = prosthetic side, I = intact side, PI = prosthesis inside, ST = straight, PO = prosthesis outside. The first p-value is for nonzero slope of negative hip work vs. coupling ratio; the second p-value is for nonzero slope of positive hip work vs. coupling ratio.

6.3 Discussion

6.3.1 Generalizability of Results

The statistical conclusions that can be drawn from this study are limited by the size and makeup of the study sample. The small number of subjects inherently limits the power of the statistics so that a large effect size is required for statistical significance. This limitation can be removed by increasing the sample size. However, it is unlikely that the sample size can be large enough in practice to discover all of the small effects that may be present.

Additionally, the study sample included only male subjects. Females have a lower rate of lower limb amputation [25, 96], and are also underrepresented in the veteran population from which study participants were taken. While several studies have found gender differences in walking gait [44, 89, 12, 40], the differences are primarily in hip and knee kinematics. Ankle kinetics and kinematics are very similar between men and women, and gait differences are unlikely to affect the behavior or utility of the axis-coupling scheme.

Perhaps more importantly, the study sample included only subjects whose amputation etiology was traumatic. In the United States, amputations due to vascular disease are much more frequent than amputations due to trauma [96, 17, 106]. People with amputations caused by trauma tend to be healthier in general than people with amputations caused by vascular disease. There are also gait differences between these two groups of amputees [37, 91]. In particular, people with amputations caused by trauma tend to walk faster than people with amputations caused by vascular disease. However, kinematic patterns are generally similar between these two groups [91]. People with amputations caused by vascular disease are also likely to benefit from a reduction in shank torque during walking, and are likely to experience similar effects of axis coupling in their prosthetic ankle.

Although the TAP was only tested on transtibial amputees, the axis-coupling behavior of the TAP may also be of benefit to transfemoral amputees, whose gait differs more from nonamputee gait than does transtibial amputee gait [62]. Transfemoral amputees were the targeted users for early torsion adapters [47]. Further research is needed to discover whether

an axis-coupling prosthetic ankle can benefit transfemoral amputees.

6.3.2 Self-Selected Walking Speed

Self-selected walking speed showed a decreasing trend with increasing coupling ratio for all three walking tasks, and the trend appears to be strongest for the PI walking task. This is surprising because the axis coupling scheme was targeted at the PI walking task in particular. If axis coupling improved walking comfort during the PI task, an increase in walking speed with increasing coupling ratio would be expected. Indeed, one subject commented that at a coupling ratio of 1:3, the PI walking task felt "almost too easy".

It may be that the lower walking speeds observed at higher coupling ratios were due to the short acclimation period subjects had at each coupling ratio. The zero coupling ratio condition was most similar to the subjects' usual prostheses, which may have made this condition require less acclimation than the more novel, higher coupling ratio conditions. Previous research suggests that at least a week of acclimation to new prosthetic components is required to achieve a consistent gait, and three weeks of acclimation is sufficient [24]. This acclimation period is not possible with the TAP, which is not designed to withstand the rigors of everyday use outside of the laboratory. However, future studies could achieve a three-week acclimation period by using a passive prosthesis that provides axis coupling. A prototype for such a device is described in chapter 7. Additionally, the alignment of the prosthesis was set with zero coupling ratio. Using a passive device would allow the alignment to be optimized independently for each coupling ratio.

6.3.3 Ankle Kinematics

While the human ankle exhibits coupled motion between the sagittal and transverse planes [56], its behavior is quite different from the axis-coupling behavior of the TAP in this study. In fact, the sign of the coupling ratio is reversed in the human ankle compared to the TAP. This is not surprising given the the axis-coupling behavior of the TAP was designed to reduce shank torque, while amputees already experience reduced shank torque compared

with nonamputees [80, 78]. In the human ankle, the shank rotates externally relative to the foot during plantarflexion. Most of the motion occurs during pushoff, when the ankle is in plantarflexion and generating positive power. In the TAP, the shank rotates externally relative to the foot during dorsifexion, which occurs at a roughly constant rate through midstance. The passive prosthetic foot does not generate net power, and so pushoff is much weaker and only returns the ankle to the neutral position.

The mechanical behavior of the prosthetic foot is very consistent between subjects and between trials for a given subject. All subjects used the same make and model of prosthetic foot, with the appropriate size and stiffness category. The intact ankle shows more variation between subjects and between trials. This is partially because the intact ankle is still rotating at toe-off, while the prosthetic ankle has returned to the neutral position at toe-off.

6.3.4 Shank Torque

At a moderate value of coupling ratio(1:4), the TAP provides a reduction in peak internal shank torque similar to the torque reduction provided by a torsion adapter [80]. However, the mechanical behavior of the TAP is quite different from the behavior of a torsion adapter. Figure 6.13 compares the torque-rotation behavior for the intact ankle, the axis-coupling TAP, a torsion adapter, and a rigid pylon. While both the TAP and the torsion adapter increase ankle rotation and decrease the peak internal torque, the quasi-stiffness of the TAP changes with the type of walking task. Like the intact ankle, the torque-rotation curve for the TAP encloses a nonzero area, meaning that work is done by the rotating ankle. This is possible even with a passive axis-coupling device, because energy can be transferred between the sagittal and transverse planes.

Unlike a torsion adapter, the TAP achieves its reduced quasi-stiffness compared to a rigid pylon at a high stiffness. This may help reduce feelings of instability compared to torsion adapters [71] by providing a large resistance to rotational disturbances. This possibility could be examined with future studies looking at the local dynamic stability of leg joint kinematics during straight-line and circular walking. Similar studies have found reduced local dynamic

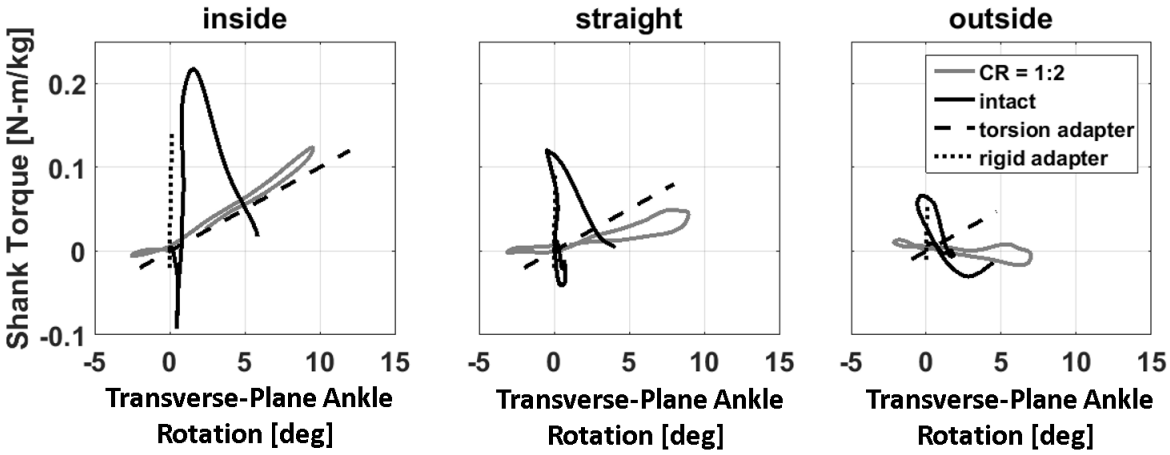

Figure 6.13: Torque-rotation behavior during stance of the TAP, the intact ankle, a torsion adapter, and a rigid adapter.

stability during circular walking compared to straight-line walking [79] and a trend($p = 0.09$) toward reduced local dynamic stability during straight-line walking with a torsion adapter compared to without a torsion adapter [81].

6.3.5 Hip Power

Nonamputees typically generate positive net ankle power during walking at their self-selected speed and faster [100, 35]. Passive prosthetic ankles are only able to return a fraction of energy stores prior to pushoff, making positive power generation at the ankle impossible. Amputees compensate for this reduction in ankle power by increasing positive hip work in both limbs, particularly the prosthetic limb [85]. While the TAP in its axis-coupling configuration does not provide any power generation capability, it is possible that it could reduce the compensatory hip work by improving gait efficiency in other ways. Both hips show a trend toward decreasing positive hip work, and this trend is significant on the prosthetic side for the PO and ST walking tasks. This suggests that an axis-coupling ankle could allow amputees to achieve a more natural gait than a conventional prosthetic ankle.

Chapter 7

PASSIVE IMPLEMENTATION OF AXIS COUPLING

This chapter describes preliminary work on developing a passive prosthesis that couples ankle sagittal-plane rotation with transverse plane rotation. The theory of operation of the device is presented, followed by a description of the prototype device and results from preliminary bench testing.

7.1 Theory of Operation

Modern prosthetic feet are typically composed of a carbon-fiber composite leaf spring (called the keel) enclosed in a cosmetic silicone foot shell. The cosmetic foot shell is very flexible and the mechanical behavior of the foot is determined by the shape of the composite leaf spring. The typical keel has a nonuniform rectangular cross-section with a large width-to-thickness ratio ranging from 2:1 to 10:1. Because the leaf spring is much more flexible in the sagittal plane than in the other planes, the rotation of the foot is effectively confined to the sagittal plane. Figure 7.1 shows a schematic representation of the sagittal-plane rotation of the foot. Because the stiffness of the leaf spring is distributed, there is no single axis of rotation. Instead, the effective axis of rotation moves forward during the gait cycle as the center of pressure progresses from the heel to the toe. Additionally, many keels are split along the sagittal plane. This allows differential deflection between the medial and lateral leaf springs, which emulates coronal-plane rotation.

A cantilever leaf spring can provide coupling between flexure in the sagittal and transverse planes by tailoring the cross-section of the leaf spring. This can be seen by considering a rectangular cross-section subject to a bending moment M_y in the sagittal plane. If the principal moments of inertia are aligned with the sagittal plane moment, the deflection of

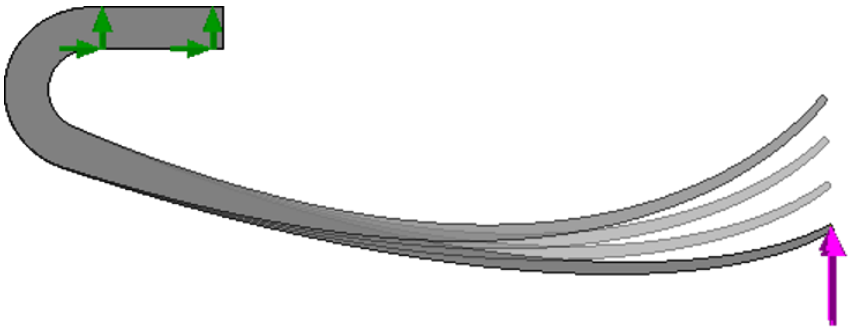

Figure 7.1: Deformation of a prosthetic foot keel with a vertical force at the toe.

the beam obeys

$$\frac{\partial^2 w_z}{\partial x^2} = \frac{M_y}{EI_{zz}}, \quad \frac{\partial^2 w_y}{\partial x^2} = -\frac{M_z}{EI_{yy}} = 0 \tag{7.1}$$

where E is the modulus of elasticity of the material, w_y and w_z are the deflections in the y and$z$ directions, respectively, and I_{yy} and I_{zz} are the second moments of area of the cross-section.

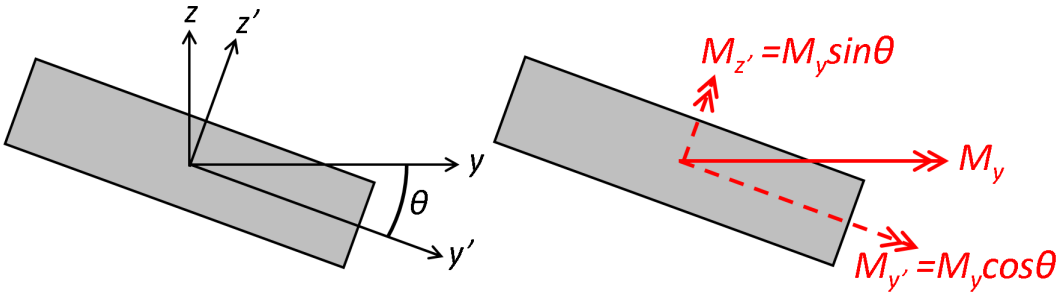

Figure 7.2: Axes and moment components for a typical cross-section of a cantilever beam with a rectangular cross-section that is misaligned with the applied sagittal-plane moment by an angle θ.

If the cross-section is rotated as in Figure 7.2, a sagittal plane bending moment results in deflections in both the y and z directions:

$$\frac{\partial^2 w_z}{\partial x^2} = \frac{M_y \cos^2\theta}{EI_{zz}} + \frac{M_y \sin^2\theta}{EI_{yy}},\ \frac{\partial^2 w_y}{\partial x^2} = \frac{M_y \cos\theta \sin\theta}{EI_{zz}} - \frac{M_y \cos\theta \sin\theta}{EI_{yy}} \tag{7.2}$$

The ratio of the deflections is

$$\frac{\frac{\partial^2 w_y}{\partial x^2}}{\frac{\partial^2 w_z}{\partial x^2}} = \frac{\cos\theta \sin\theta(1 - \frac{I_{zz}}{I_{yy}})}{\cos^2\theta + \sin^2\theta \frac{I_{zz}}{I_{yy}}} = \frac{\tan\theta(1 - \frac{I_{zz}}{I_{yy}})}{1 + \tan^2\theta \frac{I_{zz}}{I_{yy}}} \tag{7.3}$$

For a rectangular cross-section, $\frac{I_{zz}}{I_{yy}} = \frac{t^2}{w^2}$, where t is the thickness and w is the width of the cross-section. If the rotation angle is constant and the thickness is small relative to the width, then $\frac{I_{zz}}{I_{yy}} \ll 1$ and $\frac{w_y}{w_z} \approx \tan\theta$. Thus coupling between sagittal-plane and transverse-plane rotation can be achieved in a cantilever beam with a rectangular cross-section if the cross-section is misaligned with the sagittal plane.

Coupling between sagittal-plane and transverse-plane rotation could also be achieved in a cantilever beam with an L-shaped or triangular cross-section. However, these cross-sections would have higher peak stresses for a given stiffness because the bending stress is shared less equally across the cross-section.

7.2 Prototype Device: the Pivot-Flex Foot

In order to demonstrate the technical feasibility and manufacturability of a passive axis-coupling prosthesis, a prototype device called the Pivot-Flex Foot (PFF) was manufactured. The PFF was made out of a carbon fiber-epoxy composite material to match commercially available prosthetic feet.

A flat test panel was made from 8 plies of epoxy-impregnated carbon fiber oriented at 0° to determine the thickness per ply and the modulus of elasticity of the composite material. The test panel was cured in an autoclave at 250°F and 85 psi for 2 hours. After it was cured, the test panel was cut into 5 beams that were measured and subjected to a 3-point bend test according to ASTM D7264: Standard Test Method for Flexural Properties of Polymer Matrix Composite Materials [42]. Figure 7.3 shows the test samples and the result of the 3-point bend test. The thickness was measured to be 1.35±0.04 mm and the flexural modulus

was measured to be 63±3 GPa.

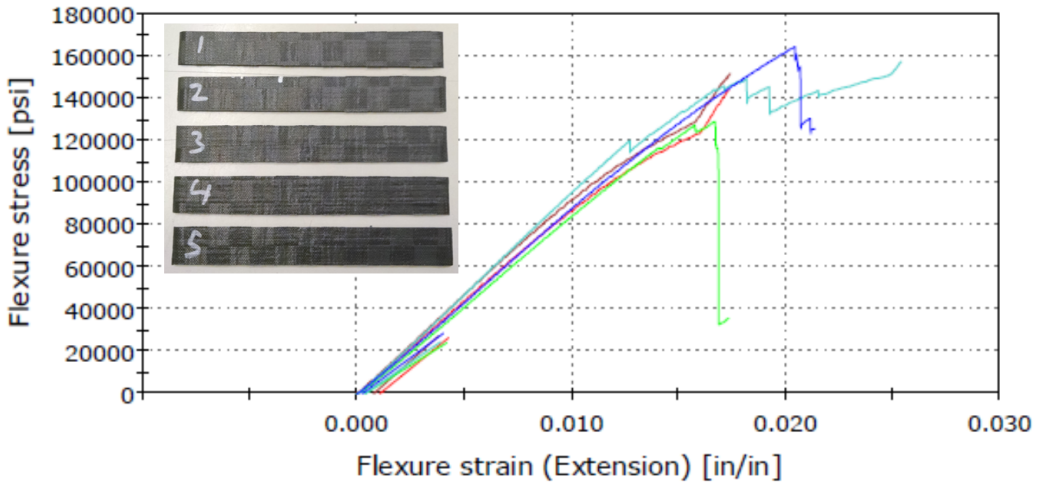

Figure 7.3: Carbon fiber test samples and 3-point bend test data.

Using these measurements, a prosthetic foot shape and thickness distribution were designed to achieve a stiffness similar to commercially available "Category 5" feet (e.g. Ossur Variflex, Freedom Innovations Sierra, Endolite Elite2). These feet are designed for moderately active amputees weighing 170-195 lb. The thickness distribution was loosely modeled after a commercially available prosthetic foot (Freedom Innovations Highlander, Irvine, CA). The thickness distribution is important because it determines where the effective center of rotation is and how it moves during the gait cycle. The PFF was designed to have a low profile to provide room for a pylon-mounted load cell or other diagnostic equipment. The cross-section of the PFF design is shown in Figure 7.4.

To manufacture the foot pieces in the desired shape, two one-sided molds were made from sheet metal formed and screwed to mounts that were cut into the shape of the desired profile. Rectangular sheets of carbon fiber with orientation alternating between 0° and 45° were cut to lay over the surface of the mold. The length of the carbon fiber rectangles varied to achieve the desired thickness distribution. The rectangular plies were laid on a sheet of

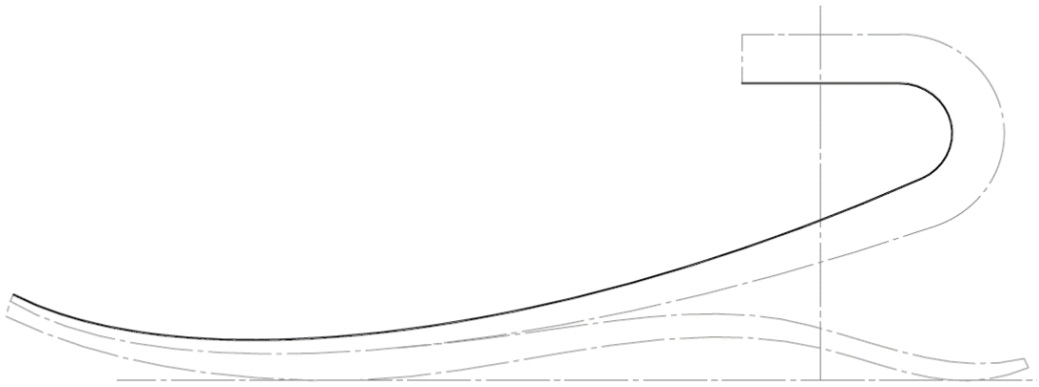

Figure 7.4: Cross-section of the PFF design, showing the shape and thickness distribution of the leaf springs.

release film on the surface of the mold. For the upper piece of the foot only, a piece of thin sheet metal covered with release film was placed directly over the outer plies of carbon fiber after being bent to fit. This was to keep wrinkles from forming in the high-curvature portion of the part during the curing process. A piece of permeable release film was placed outside of this, followed by a layer of polyester breather cloth and a high-temperature vacuum bag. The two heel springs were cured in an autoclave at 250°F and 85 psi for 2 hours. Figure 7.5 shows the steps in the layup and cure processes. The products of these processes were curved carbon fiber panels ready to be cut into the shape of the foot.

The thickness of the carbon fiber panels was measured in order to compare to the design thickness. The actual thickness was thicker than the design thickness by 20-40%. This is likely because the flow path for the resin was more restricted than it was for the test panels, causing excess resin to be retained in the part. Because the stiffness of the foot scales with the number of plies times the square of the cross-sectional thickness, the actual stiffness is between 1.4 and 2.0 times as high as the designed stiffness.

After the carbon fiber panels were cured and removed from the molds, they were cut into the shape of the foot using a desktop bandsaw with a diamond-grit blade. The panels were cut at an 18.5° angle to give approximately a 1:3 coupling ratio, using the approximation

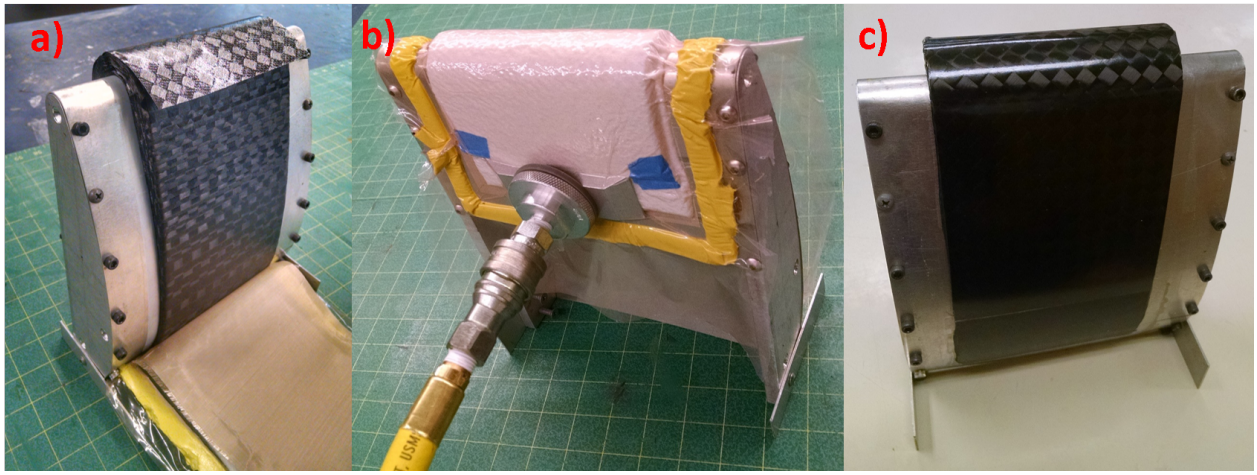

Figure 7.5: Steps in the layup and cure of the composite panels for the PFF: a) laying the carbon fiber plies on the mold, b) the completed layup under vacuum, and c) the cured panel on the mold.

$\frac{w_y}{w_z} \approx \tan\theta$. Each panel was cut into two pieces to give a foot with a split toe and heel. The upper and lower leaf springs were glued together at the toe and then bolted together near the toe. An aluminum bracket was made to hold the left and right half of the foot together and provide an interface for a standard pyramid adapter. Heel and toe wedges were cut out of polycarbonate and glued to the bottom of the foot. This gives the foot a flat surface to contact the ground, so that the lower leaf spring does not only contact the ground along an edge. Finally, strips of urethane foam were placed between the upper and lower leaf springs to prevent the carbon fiber surfaces from abrading each other. The assembled PFF is shown in Figure 7.6.

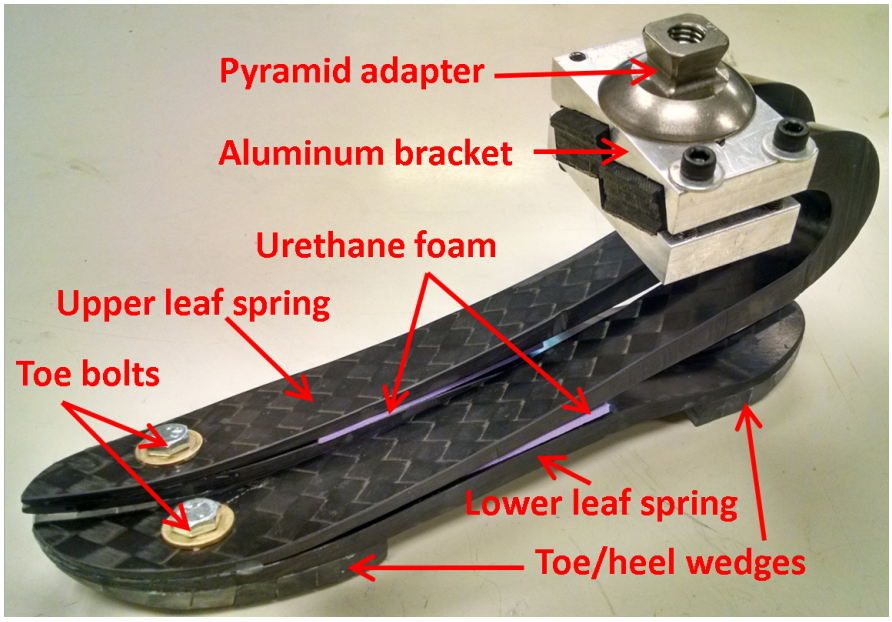

Figure 7.6: The assembled Pivot-Flex Foot.

7.3 Bench Testing

The axis-coupling functionality of the PFF was tested using the Robotic Gait Simulator (RGS). The RGS consists of a forceplate mounted on a 6 degree-of freedom rotopod robot (Mikrolar, Inc., Hampton, NH) and a rigid mount to which a prosthetic foot can be mounted [3]. For this test, a custom mount with a bearing to allow free rotation about the axis of the shank was created. Figure 7.7 shows the PFF mounted in the RGS on the bearing mount. Reflective markers were placed on the force plate, the PFF, and the mount to track their motions using a motion capture system. Reflective surfaces of the PFF and the mount were covered with matte black tape to prevent interference with the motion capture system.

In order to determine the deformation of the PFF during the gait cycle, a bodyweight load of 1500N (337 lb) was applied to the PFF in a direction normal to the forceplate. The forceplate was set at a range of pitch angles from -15°(plantarflexion) to 22°(dorsiflexion). This range of motion was intended to cover the range of motion of the intact human ankle

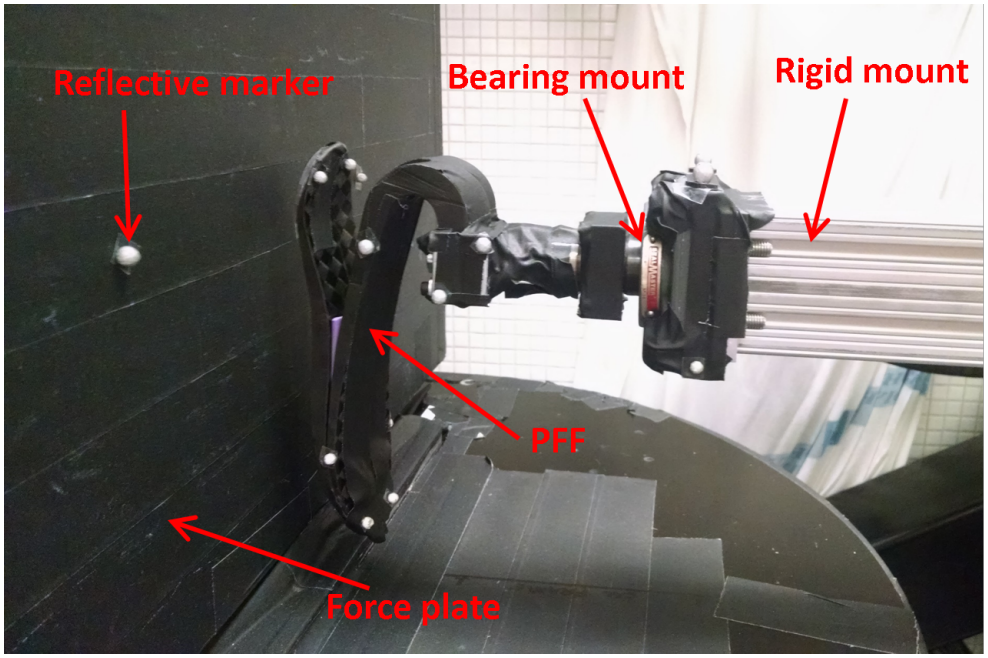

Figure 7.7: The Pivot-Flex Foot mounted in the Robotic Gait Simulator.

during walking, which is approximately 28°[100, 43] and to encompass the prosthetic ankle deflections typically seen in amputee gait [32]. Because the RGS uses position control and does not have a force control option, the forceplate was set at the desired pitch angle and then manually moved toward the foot along the shank axis until the desired force was reached. The force plate position was recorded, and then the force plate was backed off until it was just contacting the foot. At this point the motion capture system and force plate were configured to record data, and the position of the force plate was commanded to follow a 4 second ramp to the recorded position, followed by a 1 second hold and a return to the initial position. The test was also performed at 500N and 1000N of normal force.

Both of the leaf springs that make up the PFF deform under load. To measure the effective sagittal-plane and transverse-plane rotation of the PFF, a line joining the heel and the toe was expressed in a coordinate system fixed at the shank ("shank coordinates"). Figure 7.8 shows the shank coordinate system. The heel-toe line was tracked using heel and

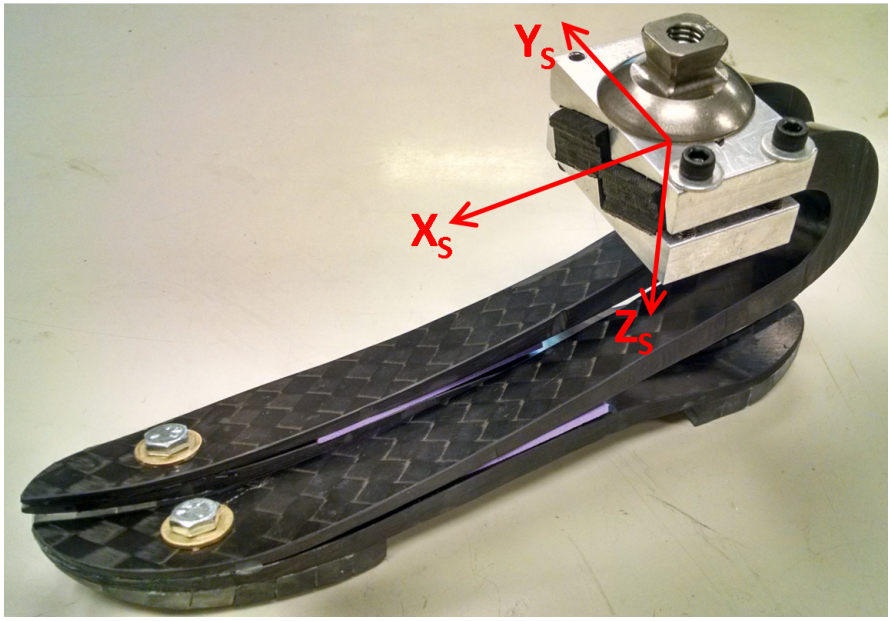

Figure 7.8: The shank coordinate system.

toe markers on left and right sides of the foot. Sagittal-plane rotation and transverse-plane rotation were defined so that at zero rotation, the heel-toe line was parallel to the X axis of the shank coordinate system. In order to calculate the rotation angles, define

$$\vec{p} = \vec{h} \times \vec{X_S} \tag{7.4}$$

where $\vec{h}$ is a unit vector along the heel-toe line. The total rotation angle is $\theta_T = \text{asin}\|\vec{p}\|$. Sagittal-plane rotation and transverse-plane rotation are defined as the components of θ_T in the Y_S and Z_S directions, respectively; that is

$$\theta_y = \frac{\vec{p} \cdot Y_S}{\|\vec{p}\|}\theta_T, \ \theta_z = \frac{\vec{p} \cdot Z_S}{\|\vec{p}\|}\theta_T \tag{7.5}$$

Figure 7.9 shows the measured transverse-plane rotation θ_z vs. the measured sagittal-plane rotation θ_y. It also shows the best-fit line for the 1500N trials and the 1:3 design line. The measured coupling ratio is 1:3.7.

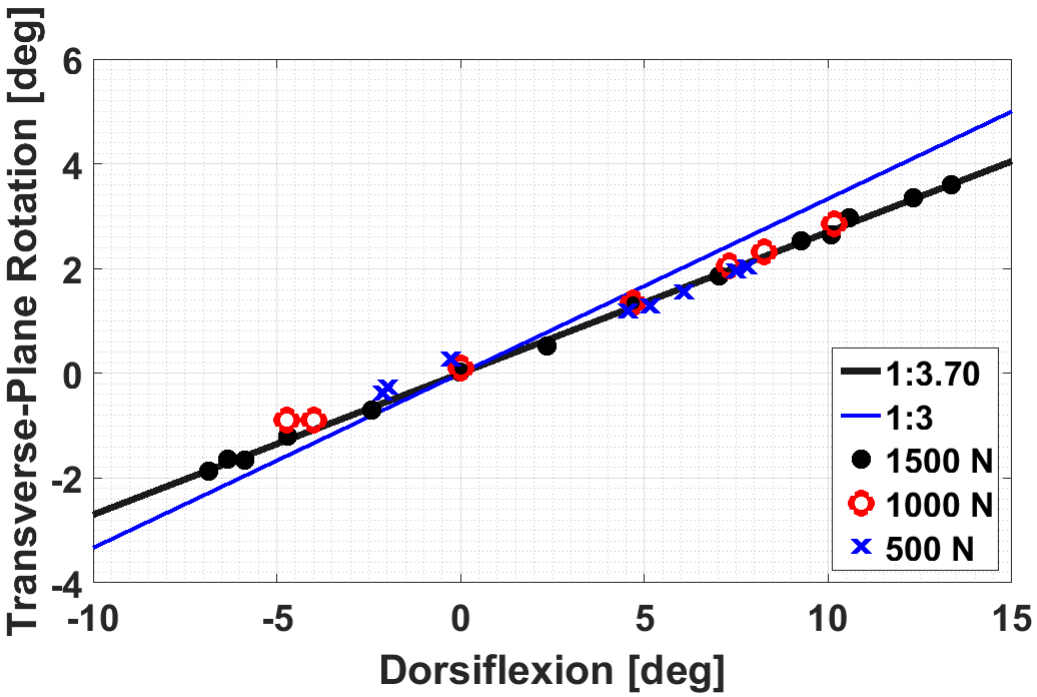

Figure 7.9: Measured transverse-plane rotation vs. measured sagittal-plane rotation from RGS test of the PFF.

7.4 Discussion

The manufacture of the Pivot-Flex Foot demonstrates the feasibility of implementing coupling between ankle sagittal-plane rotation and transverse-plane rotation using a passive mechanical device. The PFF was manufactured using materials and processes already in use in the prosthetic foot industry, and could be made commercially for approximately the same cost as existing prosthetic feet.

The PFF does not fit into existing cosmetic foot shells because the heel and toe wedges increase the height of the forefoot. A custom foot shell could be made to house the PFF, or the height of the forefoot could be reduced by adding twist to the leaf springs near the toe or using three or four leaf springs instead of two.

The PFF is thicker and therefore much stiffer than designed. This makes it unsuitable for human subject testing. Future versions of the PFF could be made less stiff by using fewer

plies of carbon fiber to compensate for the apparent thickness increase. The thickness issue could be resolved using a two-sided mold to give accurate control over the thickness.

The PFF exhibits a linear relationship between sagittal-plane rotation and transverse-plane rotation, as designed. The coupling ratio is 1:3.7 compared to the design coupling ratio of 1:3. There are several factors that reduce the coupling ratio compared to the design. First, the leaf spring design couples sagittal-plane rotation and transverse-plane rotation at the desired ratio only when the cross-section is normal to X_S. Where the leaf spring cross-section is normal to Z_S, the structure contributes to sagittal-plane rotation but not to transverse-plane rotation. Second, the approximation $\frac{w_y}{w_z} \approx \tan\theta$ is only valid when $\frac{I_{zz}}{I_{yy}} \ll 1$. In the PFF, the value of $\frac{I_{zz}}{I_{yy}}$ ranges from 0.014 near the toe to 0.5 near the heel. At the heel, equation 7.3 must be used and $\frac{\frac{\partial^2 w_y}{\partial x^2}}{\frac{\partial^2 w_z}{\partial x^2}}$ is reduced by half relative to the simple approximation. This effect is somewhat alleviated by the fact that the cross-section of the PFF is a canted parallelogram rather than a rectangle. Because the heel is near the root of the leaf spring, the effect is felt all the way to the toe. Finally, the heel and toe wedges stiffen the leaf springs more in the transverse plane than in the sagittal plane, further reducing the coupling ratio. This effect was made small by using a material for the wedges that is flexible compared with carbon fiber, and by using a "serrated" design with many small wedges instead of a single, continuous wedge. Future versions of the PFF should account for the observed reduction in coupling ratio compared with the ratio calculated using the simple approximation.

It should also be noted that the principle underlying the linear coupling between sagittal-plane rotation and transverse-plane rotation could be extended to provide nonlinear coupling between the axes. In the PFF, a constant cross-sectional rotation angle was used to provide linear coupling. Nonlinear coupling could be achieved by using a variable cross-sectional rotation angle, at the cost of adding significant design complexity.

Chapter 8

CONCLUSIONS AND FUTURE WORK

This chapter summarizes the work presented in this dissertation and provides suggestions for future work in this area. The four primary contributions of the dissertation are: 1) development of a general-purpose powered prosthetic device, the TAP, to control transverse-plane ankle rotation, 2) use of the TAP to develop a control strategy to reduce shank torque in transtibial amputees, 3) human subject testing of the axis-coupling scheme, and 4) development of a prototype passive prosthesis that provides coupling between ankle sagittal-plane rotation and transverse-plane rotation.

8.1 Development of the TAP

The TAP is an untethered series elastic actuator for conducting laboratory tests on the transverse-plane rotation of lower-limb prostheses. It provides several important features for laboratory tests: torque measurement and feedback, rotation measurement, sagittal-plane ankle rotation measurement, real-time wireless data display, and wireless configuration. These features allow smooth test operation, and include the possibility of testing outside the lab and even outdoors.

The TAP is able to provide a wide range of different behaviors for investigating transverse-plane rotation in prosthetic ankles. During the course of this work, the TAP has been configured to: 1) simulate both linear and nonlinear passive springs, 2) act like a stiff spring with an equilibrium rotation adjusted by an iterative controller attempting to flatten the torque profile during stance, and 3) act like a stiff spring with an equilibrium rotation proportional to sagittal-plane ankle rotation. For these configurations, sagittal-plane ankle rotation and stance/swing detection were the only inputs used to control the behavior of

the TAP. For other investigations, other inputs could be used, such as a pressure insole, an axial force transducer, or even a camera or ultrasound ranging system. These types of inputs would allow the TAP to respond dynamically to changes in the user's gait or environment, but would likely be more difficult to incorporate in a commercially viable device.

A design feature of the TAP with important implications is the backdriveable harmonic drive gearbox. The harmonic drive has zero backlash due to having many concurrently meshing teeth, and is more efficient than backdriveable gearboxes. The primary reason the harmonic drive was selected is because it has about one third the mass of a conventional gearbox rated to the same torque, and is also more compact. However, the backdrivability means that the device is free to rotate when it is unpowered, making walking on the unpowered device uncomfortable and dangerous. Active prostheses are typically design to be stiff when unpowered. Designing a hard stop for the TAP would improve safety of the device at the cost of extra weight. The TAP software used in the axis-coupling human subjects incorporated a software rotation limit (i.e. "soft stop"), but this is not active before the device is powered on or if the battery dies or the device has a power failure. Human subject testing has demonstrated that laboratory testing can be conducted safely with a backdriveable gearbox and no hard stop. However, if future versions of the TAP are designed, the tradeoff between weight and size and operational safety should be reevaluated when selecting a drive system.

8.2 Development of Torque Reduction Strategy

An iterative controller was developed and tested on two human subjects. The target of the iterative controller was to flatten the shank torque profile during stance so that the shank torque was constant during stance. The failure of the iterative controller to converge indicates that a constant shank torque profile during stance is not a feasible target. In particular, the shank torque during early stance is insensitive to transverse-plane rotation. However, the results of human subject testing with the iterative controller suggested that a linear coupling between transverse-plane rotation and sagittal-plane rotation could reduce

the peak shank torque. Further human subject testing confirmed the viability of this torque reduction strategy.

The iterative controller could also be used to explore other targets for the shank torque profile during stance. An obvious target is the average shank torque profile of nonamputees. Using this target would increase shank torque during stance. Although the shank torque would be more similar to that of a nonamputee, this target is probably not appropriate for amputees because of the unique interface between the socket and the residual limb that is not present in nonamputees.

8.3 Human Subject Testing

Three human subjects tested the TAP configured to couple ankle transverse-plane rotation to sagittal-plane rotation at ratios ranging from 0 to 1:2. A clear, statistically significant trend toward decreasing shank torque with increasing coupling ratio was shown despite the low number of subjects. The size of the torque reduction at a coupling ratio of 1:4 is comparable to the torque reduction caused by the use of torsion adapters. While peak torque is reduced at high coupling ratios, the torque during the first 30% of stance is not changed much. Voluntary subjective feedback from the three subjects indicates that the preferred coupling ratio is around 1:4 or 1:3, and that 1:2 is considered "too much".

Results indicate that amputees walk slower at higher values of coupling ratio, particularly when the prosthesis was on the inside of a turn. However, this may be because the subjects felt less comfortable with the unfamiliar behavior of the device. A longer acclimation period would be beneficial to determine whether the decrease in walking speed is present after the subject becomes accustomed to the axis coupling. Providing a longer acclimation peiod was not feasible with the TAP because it is limited to laboratory use. However, a passive device such as the PFF could be worn home by a subject during a multi-week acclimation period.

Some trends toward decreasing hip work with increasing coupling ratio were observed, but the low number of subjects makes these results inconclusive. Future testing should be performed on more subjects to allow small and medium-sized effects to be observed.

Additionally, future testing should include subjects with amputations caused by vascular disease, which is the primary cause of transtibial amputations in the United States. The axis-coupling scheme could also provide increased transverse-plane rotation and a reduction in socket torque for transfemoral amputees. The research should be extended to include transfemoral amputees.

8.4 Development of the PFF

The TAP is a useful tool for studying transverse-plane ankle rotation in amputees in a laboratory setting, but is poorly suited for commercialization or even for tests by amputees during daily living. Since the end goal of this research is a product that can improve the lives of amputees, the research was conducted with commercialization in mind. The structure of the iterative controller was designed to give a transverse-plane rotation profile that could be passively driven by sagittal-plane ankle rotation. The identified relationship between transverse-plane rotation and sagittal-plane rotation was linear, allowing it to be implemented with a prosthetic foot very similar to commercially available prosthetic feet but with a rotated cross-section.

The PFF was designed, built, and tested to demonstrate the technical feasibility and commercial viability of coupling transverse-plane rotation with sagittal-plane rotation in a passive prosthetic foot. The PFF was built using materials and processes that are already in use for commercially available prosthetic feet. A commercial foot based on the PFF could be manufactured for approximately the same cost as a conventional carbon-fiber prosthetic foot. There are two additional elements in the PFF that would raise the manufacturing cost slightly. The first is the more complex structure required at the interface to the pyramid adapter. Second, the PFF needs some provision to make the bottom of the foot rest flat on the ground. The PFF uses polycarbonate wedges glued to the bottom of the foot for this purpose.

The PFF that was built as a technology demonstrator is much stiffer than the design stiffness, making it unsuitable for human subject testing. This is in large part because of

poor thickness control due to using a one-sided mold. A full mold would better constrain the geometry but would be much more difficult and expensive to build. The single-sided mold has the advantages that it can be used to make feet of different thickness and therefore different stiffness categories, and that it can be used to make both left and right feet. It could also be used to make feet of different sizes in a small range, with minor differences in geometry. The one-sided mold is a suitable technique for making a small batch of 4-8 feet in both sides and different sizes and stiffness categories that would be required for a research study using the PFF. It may also be useful to create some "uncoupled" feet with no cross-section rotation using the same mold. These feet could be used as control feet with sagittal-plane behavior very similar to the PFF.

The two prostheses presented in this dissertation serve different and complimentary purposes. The TAP is a general-purpose testbed for exploring transverse-plane rotation schemes in the laboratory environment. Using the TAP to reduce shank torque led to the development of the PFF, a passive prosthetic foot that couples transverse-plane rotation with sagittal-plane rotation. The PFF is a proof-of-concept of a technology that could be incorporated into commercial prostheses to provide increased transverse-plane ankle rotation and decreased shank torque to lower-limb amputees.

BIBLIOGRAPHY

[1] Samuel K Au, Hugh Herr, Jeff Weber, and Ernesto Carlos Martinez-Villalpando. Powered ankle-foot prosthesis for the improvement of amputee ambulation. In *Engineering in Medicine and Biology Society, 2007. EMBS 2007. 29th Annual International Conference of the IEEE*, pages 3020–3026. IEEE, 2007.

[2] Samuel K Au, Jeff Weber, and Hugh Herr. Biomechanical design of a powered ankle-foot prosthesis. In *Rehabilitation Robotics, 2007. ICORR 2007. IEEE 10th International Conference on*, pages 298–303. IEEE, 2007.

[3] Patrick M Aubin, Matthew S Cowley, and William R Ledoux. Gait simulation via a 6-dof parallel robot with iterative learning control. *Biomedical Engineering, IEEE Transactions on*, 55(3):1237–1240, 2008.

[4] CH Barnett and JR Napier. The axis of rotation at the ankle joint in man. its influence upon the form of the talus and the mobility of the fibula. *Journal of anatomy*, 86(Pt 1):1, 1952.

[5] Alexander L Bell, Richard A Brand, and Douglas R Pedersen. Prediction of hip joint centre location from external landmarks. *Human Movement Science*, 8(1):3–16, 1989.

[6] Alexander L Bell, Douglas R Pedersen, and Richard A Brand. A comparison of the accuracy of several hip center location prediction methods. *Journal of biomechanics*, 23(6):617–621, 1990.

[7] Bryan J Bergelin and Philip A Voglewede. Design of an active ankle-foot prosthesis utilizing a four-bar mechanism. *Journal of Mechanical Design*, 134(6):061004, 2012.

[8] Joaquin A Blaya and Hugh Herr. Adaptive control of a variable-impedance ankle-foot orthosis to assist drop-foot gait. *Neural Systems and Rehabilitation Engineering, IEEE Transactions on*, 12(1):24–31, 2004.

[9] MJ Burke, V Roman, and V Wright. Bone and joint changes in lower limb amputees. *Annals of the rheumatic diseases*, 37(3):252–254, 1978.

[10] Aurelio Cappozzo, Angelo Cappello, Ugo Della Croce, and Francesco Pensalfini. Surface-marker cluster design criteria for 3-d bone movement reconstruction. *Biomedical Engineering, IEEE Transactions on*, 44(12):1165–1174, 1997.

[11] Pierre Cherelle, Arnout Matthys, Victor Grosu, Bram Vanderborght, and Dirk Lefeber. The amp-foot 2.0: Mimicking intact ankle behavior with a powered transtibial prosthesis. In *Biomedical Robotics and Biomechatronics (BioRob), 2012 4th IEEE RAS & EMBS International Conference on*, pages 544–549. IEEE, 2012.

[12] SH Cho, JM Park, and OY Kwon. Gender differences in three dimensional gait analysis data from 98 healthy korean adults. *Clinical biomechanics*, 19(2):145–152, 2004.

[13] JR Close, VT Inman, PM Poor, and FN Todd. The function of the subtalar joint. *Clinical orthopaedics and related research*, 50:159–180, 1967.

[14] Nationnal Research Council. *Terminal research reports on artificial limbs*. Neely Printing Company, Inc., 1947.

[15] Paolo De Leva. Adjustments to zatsiorsky-seluyanov's segment inertia parameters. *Journal of biomechanics*, 29(9):1223–1230, 1996.

[16] Myron A Diftler, JS Mehling, Muhammad E Abdallah, Nicolaus A Radford, Lyndon B Bridgwater, Adam M Sanders, Roger Scott Askew, D Marty Linn, John D Yamokoski, FA Permenter, et al. Robonaut 2-the first humanoid robot in space. In *Robotics and Automation (ICRA), 2011 IEEE International Conference on*, pages 2178–2183. IEEE, 2011.

[17] Timothy R Dillingham, Liliana E Pezzin, and Ellen J MacKenzie. Limb amputation and limb deficiency: epidemiology and recent trends in the united states. *Southern medical journal*, 95(8):875–884, 2002.

[18] Timothy R Dillingham, Liliana E Pezzin, Ellen J MacKenzie, and Andrew R Burgess. Use and satisfaction with prosthetic devices among persons with trauma-related amputations: a long-term outcome study. *American Journal of Physical Medicine & Rehabilitation*, 80(8):563–571, 2001.

[19] Ernest Doebelin. *System dynamics: Modeling, analysis, simulation, design*. CRC Press, 1998.

[20] Nancy L Dudek, Meridith B Marks, and Shawn C Marshall. Skin problems in an amputee clinic. *American journal of physical medicine & rehabilitation*, 85(5):424–429, 2006.

[21] J Dul and GE Johnson. A kinematic model of the human ankle. *Journal of biomedical engineering*, 7(2):137–143, 1985.

[22] Dawn M Ehde, Joseph M Czerniecki, Douglas G Smith, Kellye M Campbell, W Thomas Edwards, Mark P Jensen, and Lawrence R Robinson. Chronic phantom sensations, phantom pain, residual limb pain, and other regional pain after lower limb amputation. *Archives of physical medicine and rehabilitation*, 81(8):1039–1044, 2000.

[23] Dawn M Ehde, Douglas G Smith, Joseph M Czerniecki, Kellye M Campbell, Dee M Malchow, and Lawrence R Robinson. Back pain as a secondary disability in persons with lower limb amputations. *Archives of physical medicine and rehabilitation*, 82(6):731–734, 2001.

[24] Rowan D English, Wendy Hubbard, and G Keith McElroy. Establishment of consistent gait after fitting of new components. 1995.

[25] Joe Feinglass, Jacqueline L Brown, Anthony LoSasso, Min-Woong Sohn, Larry M Manheim, Sanjiv J Shah, and William H Pearce. Rates of lower-extremity amputation and arterial reconstruction in the united states, 1979 to 1996. *American Journal of Public Health*, 89(8):1222–1227, 1999.

[26] Kevin C Flick, Michael S Orendurff, Jocelyn S Berge, Ava D Segal, and Glenn K Klute. Comparison of human turning gait with the mechanical performance of lower limb prosthetic transverse rotation adapters. *Prosthetics and orthotics international*, 29(1):73–81, 2005.

[27] Cheryl D Fryar, Qiuping Gu, and Cynthia L Ogden. Anthropometric reference data for children and adults: United states, 2007-2010. *Vital and health statistics. Series 11, Data from the national health survey*, (252):1–48, 2012.

[28] RS Gailey, MS Nash, TA Atchley, RM Zilmer, GR Moline-Little, N Morris-Cresswell, and LI Siebert. The effects of prosthesis mass on metabolic cost of ambulation in non-vascular trans-tibial amputees. *Prosthetics and orthotics international*, 21(1):9–16, 1997.

[29] Brian C Glaister, Greta C Bernatz, Glenn K Klute, and Michael S Orendurff. Video task analysis of turning during activities of daily living. *Gait & posture*, 25(2):289–294, 2007.

[30] Brian C Glaister, Jason A Schoen, Michael S Orendurff, and Glenn K Klute. A mechanical model of the human ankle in the transverse plane during straight walking: implications for prosthetic design. *Journal of biomechanical engineering*, 131(3):034501, 2009.

[31] Jeffrey J Gorges. Controlled coronal stiffness prosthetic ankle for improving balance on uneven terrain. Master's thesis, University of Washington, 2013.

[32] H Goujon, X Bonnet, P Sautreuil, M Maurisset, L Darmon, P Fode, and F Lavaste. A functional evaluation of prosthetic foot kinematics during lower-limb amputee gait. *Prosthetics and orthotics international*, 30(2):213–223, 2006.

[33] Martin Grimmer and André Seyfarth. Stiffness adjustment of a series elastic actuator in a knee prosthesis for walking and running: the trade-off between energy and peak power optimization. In *Intelligent Robots and Systems (IROS), 2011 IEEE/RSJ International Conference on*, pages 1811–1816. IEEE, 2011.

[34] K Hagberg and R Brånemark. Consequences of non-vascular trans-femoral amputation: a survey of quality of life, prosthetic use and problems. *Prosthetics and Orthotics International*, 25(3):186–194, 2001.

[35] Andrew H Hansen, Dudley S Childress, Steve C Miff, Steven A Gard, and Kent P Mesplay. The human ankle during walking: implications for design of biomimetic ankle prostheses. *Journal of biomechanics*, 37(10):1467–1474, 2004.

[36] Andrew H Hansen and Charles C Wang. Effective rocker shapes used by able-bodied persons for walking and fore-aft swaying: Implications for design of ankle–foot prostheses. *Gait & posture*, 32(2):181–184, 2010.

[37] Y Hermodsson, C Ekdahl, BM Persson, and G Roxendal. Gait in male trans-tibial amputees: a comparative study with healthy subjects in relation to walking speed. *Prosthetics and orthotics international*, 18(2):68–77, 1994.

[38] JH Hicks. The mechanics of the foot: I. the joints. *Journal of Anatomy*, 87(Pt 4):345, 1953.

[39] Joseph K Hitt, Thomas G Sugar, Matthew Holgate, and Ryan Bellman. An active foot-ankle prosthesis with biomechanical energy regeneration. *Journal of medical devices*, 4(1):011003, 2010.

[40] Wendy J Hurd, Terese L Chmielewski, Michael J Axe, Irene Davis, and Lynn Snyder-Mackler. Differences in normal and perturbed walking kinematics between male and female athletes. *Clinical Biomechanics*, 19(5):465–472, 2004.

[41] Marco Hutter, C David Remy, Mark A Hoepflinger, and Roland Siegwart. High compliant series elastic actuation for the robotic leg scarleth. In *Proc. of the International Conference on Climbing and Walking Robots (CLAWAR)*, number EPFL-CONF-175826, 2011.

[42] ASTM International. Astm d7264 / d7264m-15, standard test method for flexural properties of polymer matrix composite materials, 2015.

[43] Mrn P Kadaba, HK Ramakrishnan, and ME Wootten. Measurement of lower extremity kinematics during level walking. *Journal of orthopaedic research*, 8(3):383–392, 1990.

[44] D Casey Kerrigan, Mary K Todd, and Ugo Delia Croce. Gender differences in joint biomechanics during walking normative study in young adults. *American journal of physical medicine & rehabilitation*, 77(1):2–7, 1998.

[45] Chris Kirtley, Michael W Whittle, and RJ Jefferson. Influence of walking speed on gait parameters. *Journal of biomedical engineering*, 7(4):282–288, 1985.

[46] J Kulkarni, WJ Gaine, JG Buckley, JJ Rankine, and J Adams. Chronic low back pain in traumatic lower limb amputees. *Clinical Rehabilitation*, 19(1):81–86, 2005.

[47] LW Lamoureux and CW Radcliffe. Functional analysis of the uc-bl shank axial rotation device. *Prosthetics and orthotics international*, 1(2):114–118, 1977.

[48] Marcia W Legro, Gayle Reiber, MD Aguila, Megan J Ajax, David A Boone, L Jerrie, Douglas G Smith, and Bruce Sangeorzan. Issues of importance reported by persons with lower limb amputations and prostheses. *Journal of rehabilitation research and development*, 36(3), 1999.

[49] Justus F Lehmann, Robert Price, Ramona Okumura, Kent Questad, Barbara J de Lateur, and Alain Négretot. Mass and mass distribution of below-knee prostheses: effect on gait efficacy and self-selected walking speed. *Archives of physical medicine and rehabilitation*, 79(2):162–168, 1998.

[50] Jennifer L Lelas, Gregory J Merriman, Patrick O Riley, and D Casey Kerrigan. Predicting peak kinematic and kinetic parameters from gait speed. *Gait & posture*, 17(2):106–112, 2003.

[51] Edward D Lemaire and F Ronald Fisher. Osteoarthritis and elderly amputee gait. *Archives of physical medicine and rehabilitation*, 75:1094–1099, 1994.

[52] AS Levens, Verne T Inman, and JA Blosser. Transverse rotation of the segments of the lower extremity in locomotion. *The Journal of Bone & Joint Surgery*, 30(4):859–872, 1948.

[53] S William Levy. Skin problems of the leg amputee. *Prosthetics and Orthotics International*, 4(1):37–44, 1980.

[54] SW Levy. Amputees: skin problems and prostheses. *Cutis*, 55(5):297–301, 1995.

[55] Suh-Jen Lin-Chan, David H Nielsen, H John Yack, Miao-Ju Hsu, and Donald G Shurr. The effects of added prosthetic mass on physiologic responses and stride frequency during multiple speeds of walking in persons with transtibial amputation. *Archives of physical medicine and rehabilitation*, 84(12):1865–1871, 2003.

[56] A Lundberg, OK Svensson, G Nemeth, and G Selvik. The axis of rotation of the ankle joint. *Journal of Bone & Joint Surgery, British Volume*, 71(1):94–99, 1989.

[57] Arne Lundberg, Ola K Svensson, Carin Bylund, and Göran Selvik. Kinematics of the ankle/foot complexpart 3: influence of leg rotation. *Foot & Ankle International*, 9(6):304–309, 1989.

[58] ITZHAK Melzer, MARGARET Yekutiel, and SHAUL Sukenik. Comparative study of osteoarthritis of the contralateral knee joint of male amputees who do and do not play volleyball. *The Journal of rheumatology*, 28(1):169–172, 2001.

[59] Henk EJ Meulenbelt, Jan HB Geertzen, Pieter U Dijkstra, and Marcel F Jonkman. Skin problems in lower limb amputees: an overview by case reports. *Journal of the European Academy of Dermatology and Venereology*, 21(2):147–155, 2007.

[60] PFD Naylor. Experimental friction blisters. *British Journal of Dermatology*, 67(10):327–342, 1955.

[61] Caroline C Nielsen. A survey of amputees: Functional level and life satisfaction, information needs, and the prosthetist's role. *JPO: Journal of Prosthetics and Orthotics*, 3(3):125–129, 1991.

[62] Lee Nolan and A Lees. The functional demands on the intact limb during walking for active trans-femoral and trans-tibial amputees. *Prosthetics and orthotics international*, 24(2):117–125, 2000.

[63] Lee Nolan, Andrzej Wit, Krzysztof Dudziñski, Adrian Lees, Mark Lake, and Michał Wychowañski. Adjustments in gait symmetry with walking speed in trans-femoral and trans-tibial amputees. *Gait & posture*, 17(2):142–151, 2003.

[64] Michael S Orendurff, Ava D Segal, Jocelyn S Berge, Kevin C Flick, David Spanier, and Glenn K Klute. The kinematics and kinetics of turning: limb asymmetries associated with walking a circular path. *Gait & posture*, 23(1):106–111, 2006.

[65] Jason T Panzenbeck and Glenn K Klute. A powered inverting and everting prosthetic foot for balance assistance in lower limb amputees. *JPO: Journal of Prosthetics and Orthotics*, 24(4):175–180, 2012.

[66] Corey Pew. Design and testing of a variable stiffness transverse plane adaptor for use in a lower limb prosthesis. Master's thesis, University of Washington, 2014.

[67] Liliana E Pezzin, Timothy R Dillingham, Ellen J MacKenzie, Patti Ephraim, and Paddy Rossbach. Use and satisfaction with prosthetic limb devices and related services. *Archives of physical medicine and rehabilitation*, 85(5):723–729, 2004.

[68] Malcolm H Pope, GBJ Andersson, JW Frymoyer, and Don B Chaffin. *Occupational Low Back Pain: Assessment, Treatment, and Prevention.* CRC Press, 1991.

[69] Gill A Pratt and Matthew M Williamson. Series elastic actuators. In *Intelligent Robots and Systems 95.'Human Robot Interaction and Cooperative Robots', Proceedings. 1995 IEEE/RSJ International Conference on*, volume 1, pages 399–406. IEEE, 1995.

[70] Jerry E Pratt, Benjamin T Krupp, Christopher J Morse, and Steven H Collins. The roboknee: an exoskeleton for enhancing strength and endurance during walking. In *Robotics and Automation, 2004. Proceedings. ICRA'04. 2004 IEEE International Conference on*, volume 3, pages 2430–2435. IEEE, 2004.

[71] Walt Racette and James W Breakey. Clinical experience and functional considerations of axial rotators for the amputee.

[72] Sreesha S Rao, Lara A Boyd, Sara J Mulroy, Ernest L Bontrager, JK Gronley, and Jacquelin Perry. Segment velocities in normal and transtibial amputees: prosthetic design implications. *Rehabilitation Engineering, IEEE Transactions on*, 6(2):219–226, 1998.

[73] David W Robinson, Jerry E Pratt, Daniel J Paluska, and Gill A Pratt. Series elastic actuator development for a biomimetic walking robot. In *Advanced Intelligent Mechatronics, 1999. Proceedings. 1999 IEEE/ASME International Conference on*, pages 561–568. IEEE, 1999.

[74] Elliott J Rouse, Robert D Gregg, Levi J Hargrove, and Jonathon W Sensinger. The difference between stiffness and quasi-stiffness in the context of biomechanical modeling. *Biomedical Engineering, IEEE Transactions on*, 60(2):562–568, 2013.

[75] Heydar Sadeghi, Paul Allard, and Morris Duhaime. Muscle power compensatory mechanisms in below-knee amputee gait. *American journal of physical medicine & rehabilitation*, 80(1):25–32, 2001.

[76] R Sedgman, P Goldie, and R Iansek. Development of a measure of turning during walking. In *Advancing rehabilitation: Proceedings of the inaugural conference of the faculty of health sciences. La Trobe University*, 1994.

[77] Ava D Segal, Rose Kracht, and Glenn K Klute. Does a torsion adapter improve functional mobility, pain, and fatigue in patients with transtibial amputation? *Clinical Orthopaedics and Related Research®*, 472(10):3085–3092, 2014.

[78] Ava D Segal, Michael S Orendurff, Joseph M Czerniecki, Jason Schoen, and Glenn K Klute. Comparison of transtibial amputee and non-amputee biomechanics during a common turning task. *Gait & posture*, 33(1):41–47, 2011.

[79] Ava D Segal, Michael S Orendurff, Joseph M Czerniecki, Jane B Shofer, and Glenn K Klute. Local dynamic stability in turning and straight-line gait. *Journal of biomechanics*, 41(7):1486–1493, 2008.

[80] Ava D Segal, Michael S Orendurff, Joseph M Czerniecki, Jane B Shofer, and Glenn K Klute. Transtibial amputee joint rotation moments during straight-line walking and a common turning task with and without a torsion adapter. *J Rehabil Res Dev*, 46(3):375–83, 2009.

[81] Ava D Segal, Michael S Orendurff, Joseph M Czerniecki, Jane B Shofer, and Glenn K Klute. Local dynamic stability of amputees wearing a torsion adapter compared to a rigid adapter during straight-line and turning gait. *Journal of biomechanics*, 43(14):2798–2803, 2010.

[82] Ruud W Selles, Johannes BJ Bussmann, Robert C Wagenaar, and Henk J Stam. Effects of prosthetic mass and mass distribution on kinematics and energetics of prosthetic gait: a systematic review. *Archives of physical medicine and rehabilitation*, 80(12):1593–1599, 1999.

[83] Richard E Seroussi, Andrew Gitter, Joseph M Czerniecki, and Kelly Weaver. Mechanical work adaptations of above-knee amputee ambulation. *Archives of physical medicine and rehabilitation*, 77(11):1209–1214, 1996.

[84] AK Silverman and RR Neptune. Differences in whole-body angular momentum between below-knee amputees and non-amputees across walking speeds. *Journal of biomechanics*, 44(3):379–385, 2011.

[85] Anne K Silverman, Nicholas P Fey, Albert Portillo, Judith G Walden, Gordon Bosker, and Richard R Neptune. Compensatory mechanisms in below-knee amputee gait in response to increasing steady-state walking speeds. *Gait & posture*, 28(4):602–609, 2008.

[86] Emily H Sinitski, Andrew H Hansen, and Jason M Wilken. Biomechanics of the ankle–foot system during stair ambulation: Implications for design of advanced ankle–foot prostheses. *Journal of biomechanics*, 45(3):588–594, 2012.

[87] Douglas G Smith, Dawn M Ehde, Marcia W Legro, Gayle E Reiber, Michael del Aguila, and David A Boone. Phantom limb, residual limb, and back pain after lower extremity amputations. *Clinical orthopaedics and related research*, 361:29–38, 1999.

[88] Jeremy D Smith, Abbie E Ferris, Gary D Heise, Richard N Hinrichs, and Philip E Martin. Oscillation and reaction board techniques for estimating inertial properties of a below-knee prosthesis. *Journal of visualized experiments: JoVE*, (87), 2014.

[89] Lynnelle K Smith, Jennifer L Lelas, and D Casey Kerrigan. Gender differences in pelvic motions and center of mass displacement during walking: stereotypes quantified. *Journal of women's health & gender-based medicine*, 11(5):453–458, 2002.

[90] WR Spence and MN Shields. Prevention of blisters, callosities and ulcers by absorption of shear forces. *Journal of the American Podiatry Association*, 58(10):428, 1968.

[91] Po-Fu Su, Steven A Gard, Robert D Lipschutz, and Todd A Kuiken. Differences in gait characteristics between persons with bilateral transtibial amputations, due to peripheral vascular disease and trauma, and able-bodied ambulators. *Archives of physical medicine and rehabilitation*, 89(7):1386–1394, 2008.

[92] Po-Fu Su, Steven A Gard, Robert D Lipschutz, and Todd A Kuiken. The effects of increased prosthetic ankle motions on the gait of persons with bilateral transtibial amputations. *American journal of physical medicine & rehabilitation/Association of Academic Physiatrists*, 89(1):34, 2010.

[93] Frank Sup, Amit Bohara, and Michael Goldfarb. Design and control of a powered transfemoral prosthesis. *The International journal of robotics research*, 27(2):263–273, 2008.

[94] Martin Twiste and Shyam Rithalia. Transverse rotation and longitudinal translation during prosthetic gait-a literature review. *Journal of rehabilitation research and development*, 40(1):9–18, 2003.

[95] Berkeley. College of Engineering. Prosthetic devices research project University of California. *Report to National Research Council, Committee on Artificial Limbs, on Fundamental Studies of Human Locomotion and Other Information Relating to Design of Artificial Limbs, Covering the Period from September 1945 Through June 1947*. University of California, 1947.

[96] N Unwin. Epidemiology of lower extremity amputation in centres in europe, north america and east asia. *British Journal of Surgery*, 87(3):328–337, 2000.

[97] ML Van der Linden, N Twiste, and SVS Rithalia. The biomechanical effects of the inclusion of a torque absorber on trans-femoral amputee gait, a pilot study. *Prosthetics and orthotics international*, 26(1):35–43, 2002.

[98] Jessica D Ventura, Ava D Segal, Glenn K Klute, and Richard R Neptune. Compensatory mechanisms of transtibial amputees during circular turning. *Gait & posture*, 34(3):307–312, 2011.

[99] Rino Versluys, Pieter Beyl, Michael Van Damme, Anja Desomer, Ronald Van Ham, and Dirk Lefeber. Prosthetic feet: State-of-the-art review and the importance of mimicking human ankle-foot biomechanics. *Disability & Rehabilitation: Assistive Technology*, 4(2):65–75, 2009.

[100] David A Winter. Biomechanical motor patterns in normal walking. *Journal of motor behavior*, 15(4):302–330, 1983.

[101] David A Winter, H Grant Sidwall, and Douglas A Hobson. Measurement and reduction of noise in kinematics of locomotion. *Journal of biomechanics*, 7(2):157–159, 1974.

[102] David A Winter and Susan E Sienko. Biomechanics of below-knee amputee gait. *Journal of biomechanics*, 21(5):361–367, 1988.

[103] V Zatsiorsky and V Seluyanov. The mass and inertia characteristics of the main segments of the human body. *Biomechanics viii-b*, 56(2):1152–1159, 1983.

[104] V Zatsiorsky, V Seluyanov, and L Chugunova. In vivo body segment inertial parameters determination using a gamma-scanner method. *Biomechanics of human movement: Applications in rehabilitation, sports and ergonomics*, pages 186–202, 1990.

[105] Jinying Zhu, Qining Wang, and Long Wang. On the design of a powered transtibial prosthesis with stiffness adaptable ankle and toe joints. *Industrial Electronics, IEEE Transactions on*, 61(9):4797–4807, 2014.

[106] Kathryn Ziegler-Graham, Ellen J MacKenzie, Patti L Ephraim, Thomas G Travison, and Ron Brookmeyer. Estimating the prevalence of limb loss in the united states: 2005 to 2050. *Archives of physical medicine and rehabilitation*, 89(3):422–429, 2008.

[107] Hans Zwipp and Thorsten Randt. Ankle joint biomechanics. *Foot and Ankle Surgery*, 1(1):21–27, 1994.